Berichte
zur Polar-
und Meeresforschung

633
2011

Reports
on Polar and Marine Research

Investigation of Katabatic winds and Polynyas during Summer – IKAPOS

Field Phase Report

Edited by
Günther Heinemann, Thomas Ernsdorf and Clemens Drüe

HELMHOLTZ GEMEINSCHAFT

ALFRED-WEGENER-INSTITUT FÜR
POLAR- UND MEERESFORSCHUNG
in der Helmholtz-Gemeinschaft
D-27570 BREMERHAVEN
Bundesrepublik Deutschland

ISSN 1866-3192

Hinweis

Die Berichte zur Polar- und Meeresforschung werden vom Alfred-Wegener-Institut für Polar-und Meeresforschung in Bremerhaven* in unregelmäßiger Abfolge herausgegeben.

Sie enthalten Beschreibungen und Ergebnisse der vom Institut (AWI) oder mit seiner Unterstützung durchgeführten Forschungsarbeiten in den Polargebieten und in den Meeren.

Es werden veröffentlicht:

- Expeditionsberichte (inkl. Stationslisten und Routenkarten)
- Expeditionsergebnisse (inkl. Dissertationen)
- wissenschaftliche Ergebnisse der Antarktis-Stationen und anderer Forschungs-Stationen des AWI
- Berichte wissenschaftlicher Tagungen

Die Beiträge geben nicht notwendigerweise die Auffassung des Instituts wieder.

Notice

The Reports on Polar and Marine Research are issued by the Alfred Wegener Institute for Polar and Marine Research in Bremerhaven*, Federal Republic of Germany. They appear in irregular intervals.

They contain descriptions and results of investigations in polar regions and in the seas either conducted by the Institute (AWI) or with its support.

The following items are published:

- expedition reports (incl. station lists and route maps)
- expedition results (incl. Ph.D. theses)
- scientific results of the Antarctic stations and of other AWI research stations
- reports on scientific meetings

The papers contained in the Reports do not necessarily reflect the opinion of the Institute.

The „Berichte zur Polar- und Meeresforschung” continue the former „Berichte zur Polarforschung”

* Anschrift / Address
Alfred-Wegener-Institut
für Polar- und Meeresforschung
D-27570 Bremerhaven
Germany
www.awi.de

Editor in charge:
Dr. Horst Bornemann

Assistant editor:
Birgit Chiaventone

Die "Berichte zur Polar- und Meeresforschung" (ISSN 1866-3192) werden ab 2008 ausschließlich als Open-Access-Publikation herausgegeben (URL: http://epic.awi.de).

Since 2008 the "Reports on Polar and Marine Research" (ISSN 1866-3192) are only available as web-based open-access publications (URL: http://epic.awi.de)

Investigation of Katabatic winds and Polynyas during Summer – IKAPOS

Field Phase Report

Edited by
Günther Heinemann, Thomas Ernsdorf and Clemens Drüe

Please cite or link this publication using the identifier
hdl:10013/epic.37929 or http://hdl.handle.net/10013/epic.37929

ISSN 1866-3192

Environmental Meteorology, Faculty of Geography/Geosciences, University of Trier, 2011

Corresponding authors address:
Günther Heinemann, Thomas Ernsdorf, Clemens Drüe
Environmental Meteorology
Faculty of Geography/Geosciences
University of Trier
Behringstr. 21
54296 Trier
Germany
email: heinemann@uni-trier.de, ernsdorf@uni-trier.de, druee@uni-trier.de

Contents

Abstract

Processes of the exchange of energy and momentum at the sea-ice/ocean/ atmosphere interface are key processes for the polar climate system. The experiment IKAPOS (**I**nvestigation of **Ka**tabatic winds and **Po**lynyas during **S**ummer) was performed in June 2010. The investigations comprised studies of the summertime katabatic wind system in the coastal area of north and northwest Greenland, and of atmosphere/sea-ice/ocean exchange processes over the North Water Polynya (NOW). The main tool of the experimental study was the polar aircraft POLAR 5 of the Alfred Wegener Institute (AWI), which was based at Qaanaaq (Northwest Greenland). The aircraft was instrumented with turbulence sensors, basic meteorological equipment, radiation and surface temperature sensors, laser altimeters, and video and digital cameras. A total of six research flights have been performed, two of them were katabatic wind flights (over the Humboldt and Steenstrup glacier, respectively). Katabatic wind flights capture conditions of weak and strong synoptically forced katabatic wind. During the NOW flights a fully turbulent stable boundary layer with strong winds of 15 to 20 m s^{-1} was measured, and channeling effects caused by Smith Sound and Nares Strait were documented. The data of IKAPOS are valuable for the validation of numerical models (including climate models) and will contribute to the understanding of the exchange processes over summertime Arctic polynyas and the Greenland ice sheet.

Figure i: Qaanaaq airport on 18 June 2010 (photo taken from POLAR 5).

Chapter 1

Introduction

1.1 Goals

The aircraft-based experiment IKAPOS (**I**nvestigation of **Ka**tabatic winds and **Po**lynyas during **S**ummer) was performed in June 2010. The polar aircraft POLAR 5 of the Alfred Wegener Institute (AWI) was based at Qaanaaq (Northwest Greenland, Figure 1.1). The investigations comprised studies of the summertime katabatic wind system in the coastal area of north and northwest Greenland, and of atmosphere/sea-ice/ocean exchange processes over the North Water Polynya (NOW). The main goals of IKAPOS are as follows:

1. Study of the katabatic wind system in the coastal area of Greenland during summer.
2. Study of atmosphere/sea-ice/ocean exchange processes over the North Water Polynya (NOW) during summer.
3. Verification of model simulations and parameterizations.

1.2 Scientific background

1.2.1 Summertime katabatic wind at Greenland

The katabatic-driven near-surface wind regime plays an important role in questions of the exchange of energy and momentum between the atmosphere and the underlying surface and also for the mass balance of the ice sheets of the Antarctic and Greenland. A stably stratified boundary layer (SBL) is a necessary condition for the development of katabatic winds, and the Coriolis force is important because of the relatively large horizontal scale of the wind system over the polar ice sheets. Observations show katabatic winds as a quasi-permanent phenomenon during wintertime with wind speeds up to gale force (*Putnins*, 1970; *Rasmussen*, 1989), and pronounced daily courses during seasons with significant insolation (*van den Broeke et al.*, 1994).

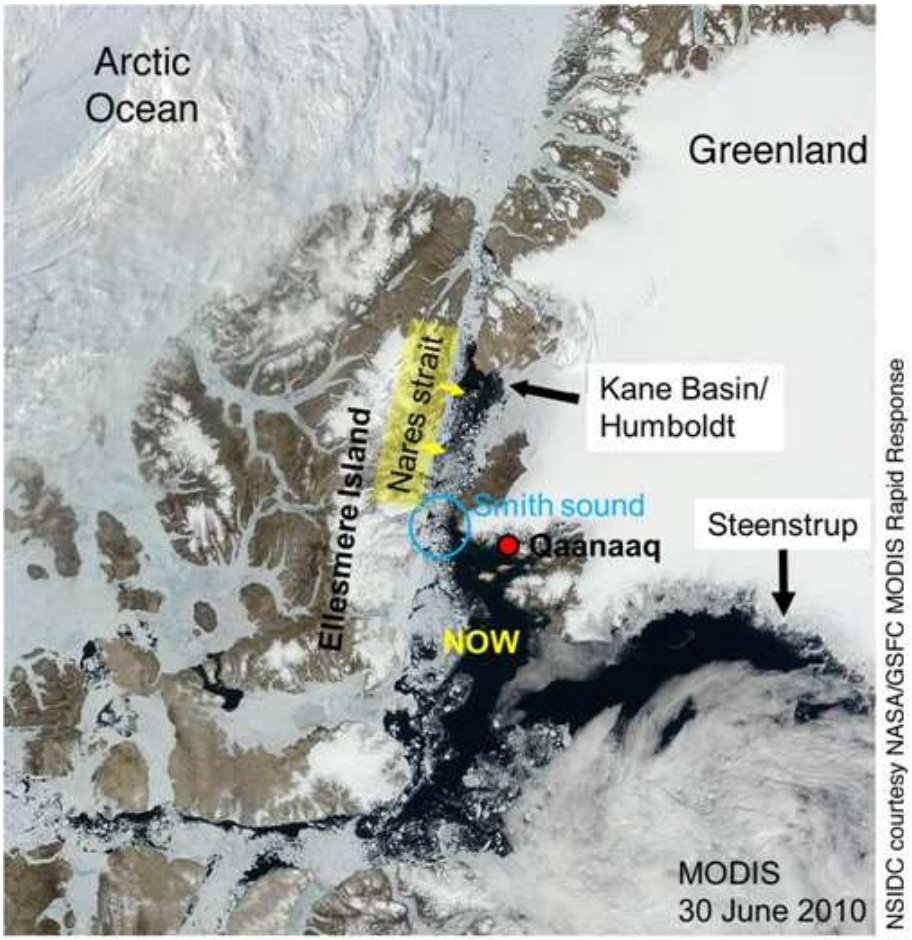

Figure 1.1: MODIS satellite image for 30 June 2010 (modified from *NSIDC*, 2010) indicating the measurement areas for the katabatic wind (Humboldt and Steenstrup glaciers) and the NOW programmes.

Prior to the melting season, the SBL over the ice sheet forms during nighttime due to cooling of the near-surface air by the divergences of sensible heat flux and net radiation, and katabatic winds occur during the early morning hours almost on every day (*Heinemann*, 1999; *Heinemann and Falk*, 2002). A comprehensive effort to study the winter to springtime katabatic wind system was made during the aircraft-based experiment KABEG (**Ka**tabatic Wind and **B**oundary Layer Front **E**xperiment around **G**reenland) in April/May 1997 in the area of southern Greenland (*Heinemann*, 1999). For the first time, direct turbulence measurements were performed in the whole boundary layer over the ice during strong katabatic wind situations, allowing for the determination of the three-dimensional (3D) boundary-layer structure and the turbulent fluxes of momentum, sensible and latent heat. Vertical profiles flown by the aircraft yielded boundary-layer heights over the ice slope between 70 and 200 m, and low-level jets (LLJs) with wind speeds of up to 25 m s^{-1} (Figure 1.2). Studies of the boundary-layer dynamics yielded that the katabatic force is the main driving mechanism for the flow regime. It could also be shown that for the strongest LLJs considerable influence of the large-scale synoptic forcing is present. Signatures of 'katabatic streaks' as seen on high-resolution thermal satellite images were investigated by *Heinemann* (2000) using KABEG data. Results using the KABEG surface

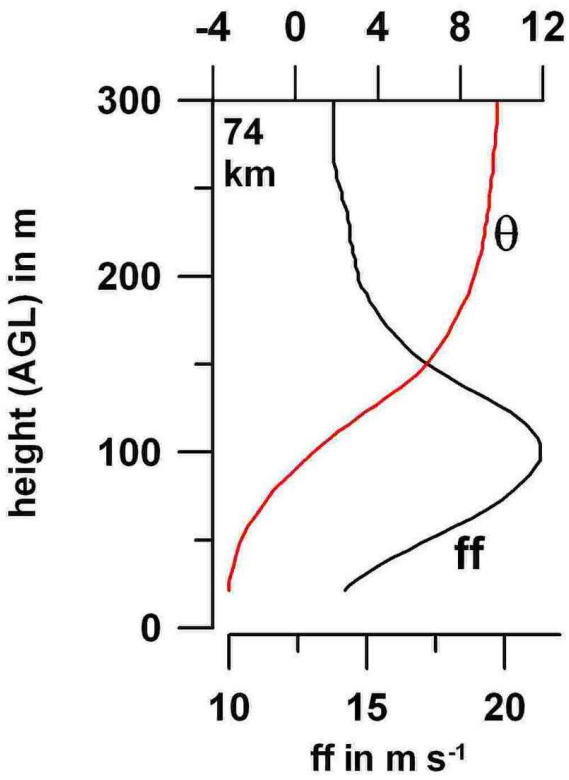

Figure 1.2: Vertical profiles of potential temperature and wind speed (ff) for katabatic wind under strong synoptic forcing on 22 April 1997 (modified from *Heinemann*, 2002).

stations, particularly the evaluation of surface fluxes over the ice and tundra, are shown in *Heinemann and Falk* (2002).

During summertime, melting occurs at the ice surface of the Greenland ice sheet. As a result, the katabatic wind system in the melting zone is not driven by the nighttime cooling of the snow surface, but instead by the daytime warming of the tundra boundary layer. Because of the dominating thermal forcing by the daily cycle of the tundra boundary layer, the maximum wind speeds are found to be present during the afternoon. This was demonstrated in the summertime investigation of the katabatic wind system over Greenland which was made during the Greenland Ice Margin Experiment (GIMEX; *Oerlemans and Vugts*, 1993). In addition to data from surface stations, the katabatic wind at the ice margin was studied using a tethered sonde for summertime conditions (*van den Broeke et al.*, 1994). Measurements and also numerical simulations of *Meesters* (1994) show the development of a shallow, weak katabatic flow in the absence of synoptic forcing. The mean downslope wind maximum near the ice edge has values of less than 5 m s^{-1} for July 1991 and lies at about 100 m above the surface (Figure 1.3). However, strong winds over the ice sheet can be expected also for summer conditions when strong synoptic pressure gradients are superimposed on the katabatic forcing and/or during conditions of strong warm air advection towards the ice sheet. The summertime katabatic wind system has also a strong impact in the redistribution of snow by snow drift (*Hebbinghaus and Heinemann*, 2006).

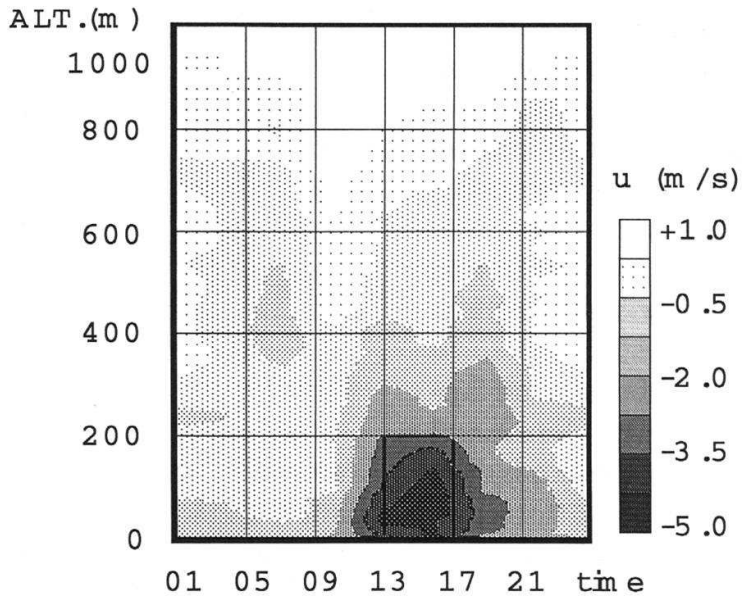

Figure 1.3: Mean daily cycle of the downslope wind component from GIMEX during 5 – 24 July 1991 (from *van den Broeke et al.*, 1994).

1.2.2 North Water Polynya (NOW)

Open water fractions associated with polynyas can cause intense exchange processes, and have important consequences for ocean processes, ice formation, brine release, gas exchange (e.g. CO_2) and biology. These interactions are highly complex and are still not sufficiently understood. Air/sea-ice/ocean dynamics in polar regions are influenced, e.g. by ocean currents, by synoptic cyclones and by mesoscale processes. Wind-induced advection of sea-ice leads to the formation of most coastal polynyas (at the coast) or flaw polynyas (at the fast ice edge). The sea-ice coverage in coastal areas can also be modulated by coastal katabatic winds. The formation of coastal polynyas by the katabatic wind and the associated strong air-sea interaction processes have been considered to be relevant for the oceanic thermohaline circulation (e.g. *Gordon and Comiso*, 1988). The evidence of a polynya associated with channeled katabatic wind in the area of East Greenland is shown in *Klein and Heinemann* (2002). Simulations for the same area using a mesoscale atmospheric model coupled with a dynamic-thermodynamic sea-ice model by *Heinemann* (2003) show that the polynya formation occurs at relatively short time scales (one day).

A summary of recurrent Arctic polynyas is shown in Figure 1.4. In the Greenland area, which represents the focus of the current study, two large polynyas can be found: The North Water Polynya (NOW), which forms at the north end of Baffin Bay and has shown to be stable, and the Northeast Water Polynya (NEW), which lies northeast of Greenland (*Schneider and Budéus*, 1997). The NEW has now disappeared and became a long marginal ice zone. The NOW is mainly wind-driven (*Barber and Massom*, 2007) and is the most biologically productive and stable polynya (`http://www.aosb.org/iapp/iapp.html`), but may also change due to the projected changes in the polar climate (*ACIA*, 2005).

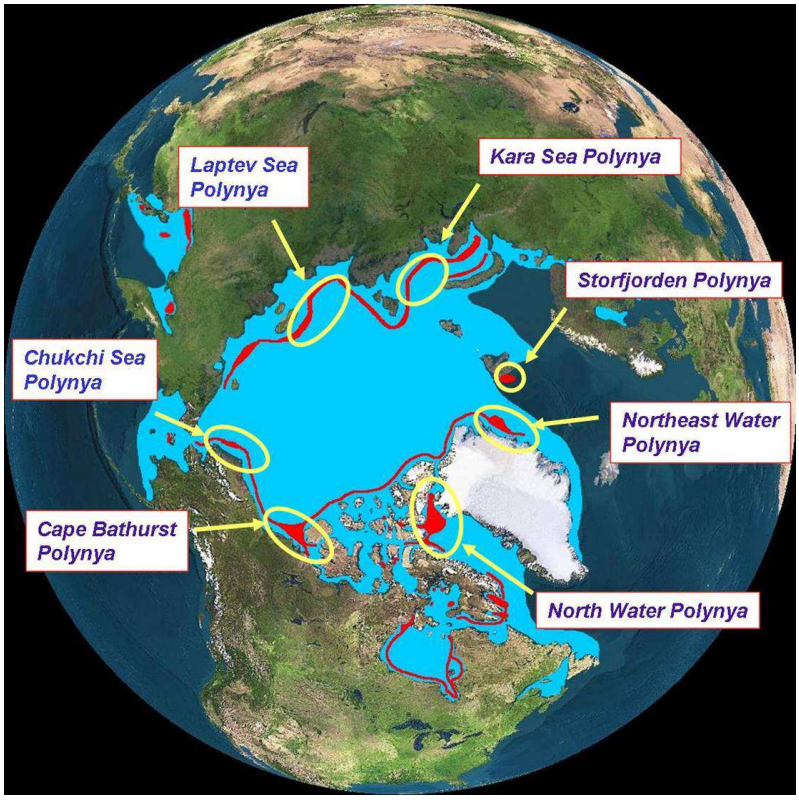

Figure 1.4: Recurrent polynyas in the Northern Hemisphere and their locations (modified from *Barber and Massom*, 2007).

The NOW is a latent heat polynya, since it forms in an area where the ocean temperature is at the freezing point and the sea-ice is transported away by winds or ocean currents directly after its formation. The Nares Strait and a corresponding ice bridge are responsible for the NOW, if northerly winds advect sea-ice southwards (see Figure 2.1). The NOW area is covered by sea-ice during winter, and the polynya starts to expand in April (Figure 1.5). The maximum open water area of the NOW reaches about 80,000 km^2 (*Preußer et al.*, 2011). The mechanisms being responsible for the generation of the NOW are still discussed, and a major study of the NOW has been carried out during the International North Water Polynya Study (`http://www.fsg.ulaval.ca/giroq/now`) being part of the International Arctic Polynya Programme (IAPP, `http://www.aosb.org/iapp/iapp.html`).

During winter and springtime the polynya has a strong heat loss by net radiation and atmospheric sensible and latent heat fluxes, which is compensated by the heat release of the freezing process. During summer the polynya gains energy by shortwave radiation. With the sea surface being still near freezing point, a stable boundary layer (SBL) develops over the polynya, if warm air is advected. In this case, the sensible heat flux represents an additional energy input regardless of cloud conditions.

The topography of Nares Strait and Smith Sound is not only important for the NOW formation, but can lead also to channeling of the flow in the ABL. The increased wind speed has then a feedback with the sea-ice/ocean interface,

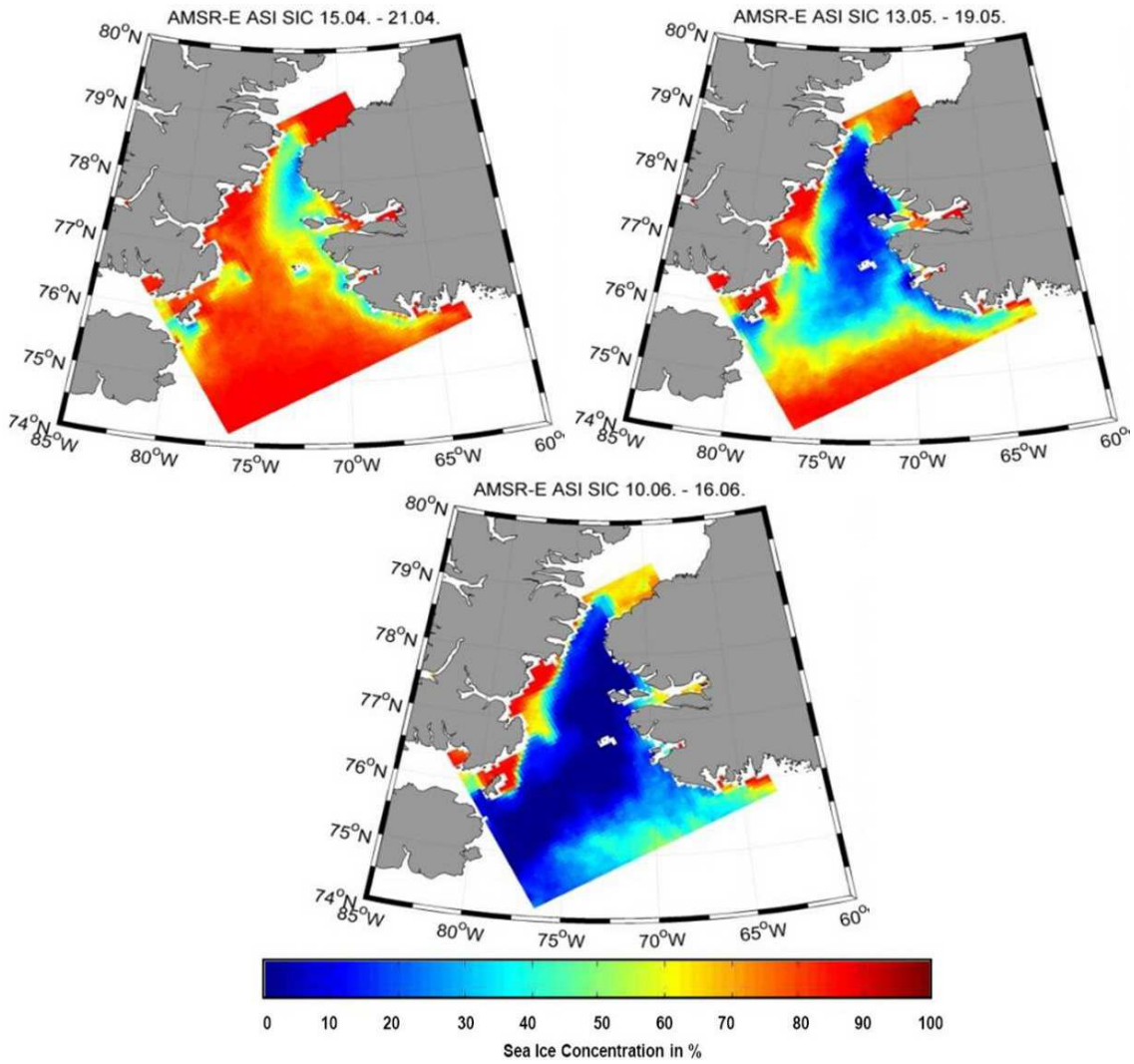

Figure 1.5: Mean weekly AMSR-E sea-ice concentrations (in %) in the NOW region for mid of April (upper left panel), May (upper right panel) and June (lower panel) (averaged over 2003 – 2010; *Preußer et al.*, 2011.)

leading to increased ice advection and surface exchange processes. A pronounced wind maximum due to channelling is found by *Samelson et al.* (2006) and *Samelson and Barbour* (2008) indicating that pressure gradients resulting from the topography of the Nares Strait cause a LLJ (Figure 1.6).

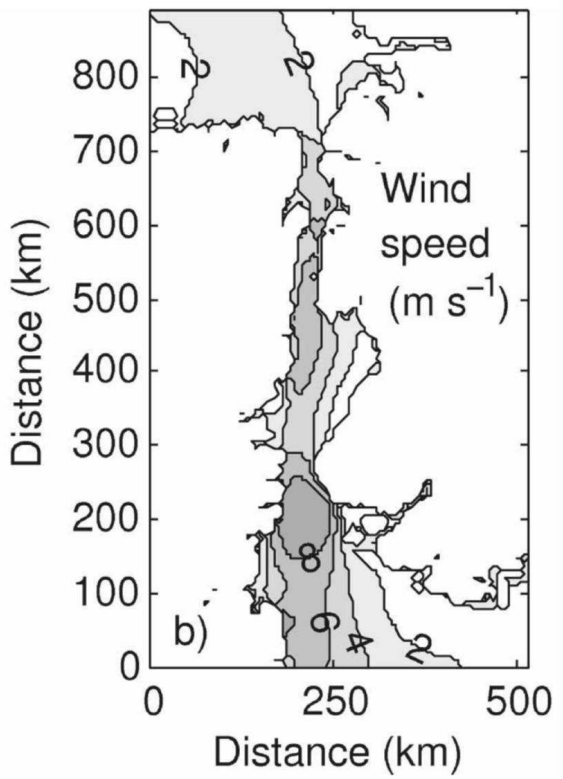

Figure 1.6: Mean magnitude of hourly vector mean 10 m-wind for January 2005 from Polar MM5 (*Bromwich et al.*, 2001) simulations (*Samelson and Barbour*, 2008).

1.3 Participants

IKAPOS was an experiment of the Department of Environmental Meteorology of the University of Trier in cooperation with the Alfred Wegener Institute (AWI) Bremerhaven. The research aircraft POLAR 5 was operated by AWI. The aircraft instrumentation was operated by AWI and by FIELAX Gesellschaft für wissenschaftliche Datenverarbeitung mbH, Bremerhaven.

The IKAPOS field experiment participants were the pilots Keith Krueger and Erik Bengtsson, the flight engineer Michael McCrae (all Kenn Borek Air Ltd., Canada), the instrument operators Johannes Käßbohrer (FIELAX) and Christoph Petersen (AWI), and the researchers Günther Heinemann (mission leader) and Thomas Ernsdorf (both University of Trier).

1.4 Acknowledgments

Thanks go to Gerit Birnbaum, Martin Gehrmann, Andreas Herber, Manuel Sellmann and Daniel Steinhage (all AWI) for help and support during the preparation phase. Heinz Finkenzeller (AWI) is acknowledged for organizing the experiment logistics.

The permission of research flights over the North Water, the Humboldt Glacier and the Kochkyst was given by the Ministry of Housing, Infrastructure

and Transport in Greenland.

For support during the experiment, thanks go to:
- the Danish Meteorological Institute (DMI) for comprehensive weather information and satellite data, and
- the personnel at Qaanaaq airport for help and support.

Until June 2011, a considerable amount of data has been supplied by different groups and organizations, which we would like to acknowledge:
- the DMI for data of synoptic weather stations,
- the NOAA's (National Oceanic and Atmospheric Administration) National-Weather Service for surface weather station data of Thule airbase,
- Konrad 'Koni' Steffen (Cooperative Institute for Research in Environmental Science (CIRES), Boulder) for data from the NEEM (North Greenland Eemian Ice Drilling) weather station of the GC-Net (Greenland Climate Network),
- the National Geophysical Data Center of NOAA for global high-resolution DEMs (Digital Elevation Models, `http://www.ngdc.noaa.gov/mgg/`),
- the NASA (U.S. National Aeronautics and Space Administration) for MODIS (Moderate Resolution Imaging Spectroradiometer) data,
- the ESA (European Space Agency) for ASAR data,
- the DWD (Deutscher Wetterdienst, Offenbach) for analyses of the GME (Globalmodell des Deutschen Wetterdienstes),
- the Physical Sciences Division of the NOAA for NCEP/DOE (National Centers for Environmental Prediction/Department of Energy) reanalyses, and
- the European Centre for Medium-Range Weather Forecasts (ECMWF) for ERA-Interim reanalyses.

IKAPOS is supported by the Deutsche Forschungsgemeinschaft (DFG) under grant HE2740/9. The aircraft programme was funded by the Alfred Wegener Institute (AWI).

Chapter 2

Experimental setup

2.1 Experimental area

The experimental area is located in northwestern Greenland (Figure 2.1, 2.2). The steep coast is characterized by glaciers of the inland ice sheet. One of them is Humboldt Glacier, with a front width of 110 km the widest tidewater glacier in the Northern Hemisphere. The Humboldt Glacier calves into the Nares Strait, which separates northwest Greenland and Ellesmere Island (Canada). Through the Nares Strait sea-ice export rates from the Arctic Ocean are significant (see e.g. *Dunbar*, 1973; *Barber et al.*, 2001a; *Kwok*, 2005; *Samelson et al.*, 2006; *Kwok et al.*, 2010). In the south Smith Sound (40 km to 50 km wide) links Nares Strait with Baffin Bay, the NOW region. In contrast to the NOW, sea-ice exists throughout most of the year at Melville Bay. The adjacent land area of Lauge Kochkyst is almost completely ice-covered. Steenstrup Glacier is the widest glacier of this ice front.

Qaanaaq airport (IATA airport code: NAQ, ICAO airport code: BGQQ, 77.48°N, 69.38°W, 16 m ASL) was the basis for the research flights. It lies at the coast of Murchison Sound (connected with northernmost Baffin Bay) on a peninsula, 4 km northwest of Qaanaaq town (also called Thule, Figure 2.3, 2.4). A plateau glacier with a maximum thickness of 1,000 km is located at a distance of about 3 km inland covering the peninsula for the most part (Figure 2.4). It drains in streams through the tundra at the coast. The inland ice sheet is separated from the plateau glacier and begins about 25 km north of Qaanaaq.

Qaanaaq was chosen as the base of IKAPOS, because it provides relatively good logistic conditions. Qaanaaq is the main town of northern Greenland (approximately 650 inhabitants, see *Statistics Greenland*, 2010) with an extensive infrastructural network. Qaanaaq airport is the only civil airport north of Upernavik (Figure 2.1); approximately 110 km south the United States Air Force base 'Thule Airbase' is positioned. From Qaanaaq the planned measurement areas over the NOW and at the coast of the Kochkyst and of the Humboldt Glacier (Figure 2.2) are within reach by using the aircraft POLAR 5 (see Chapter 2.3).

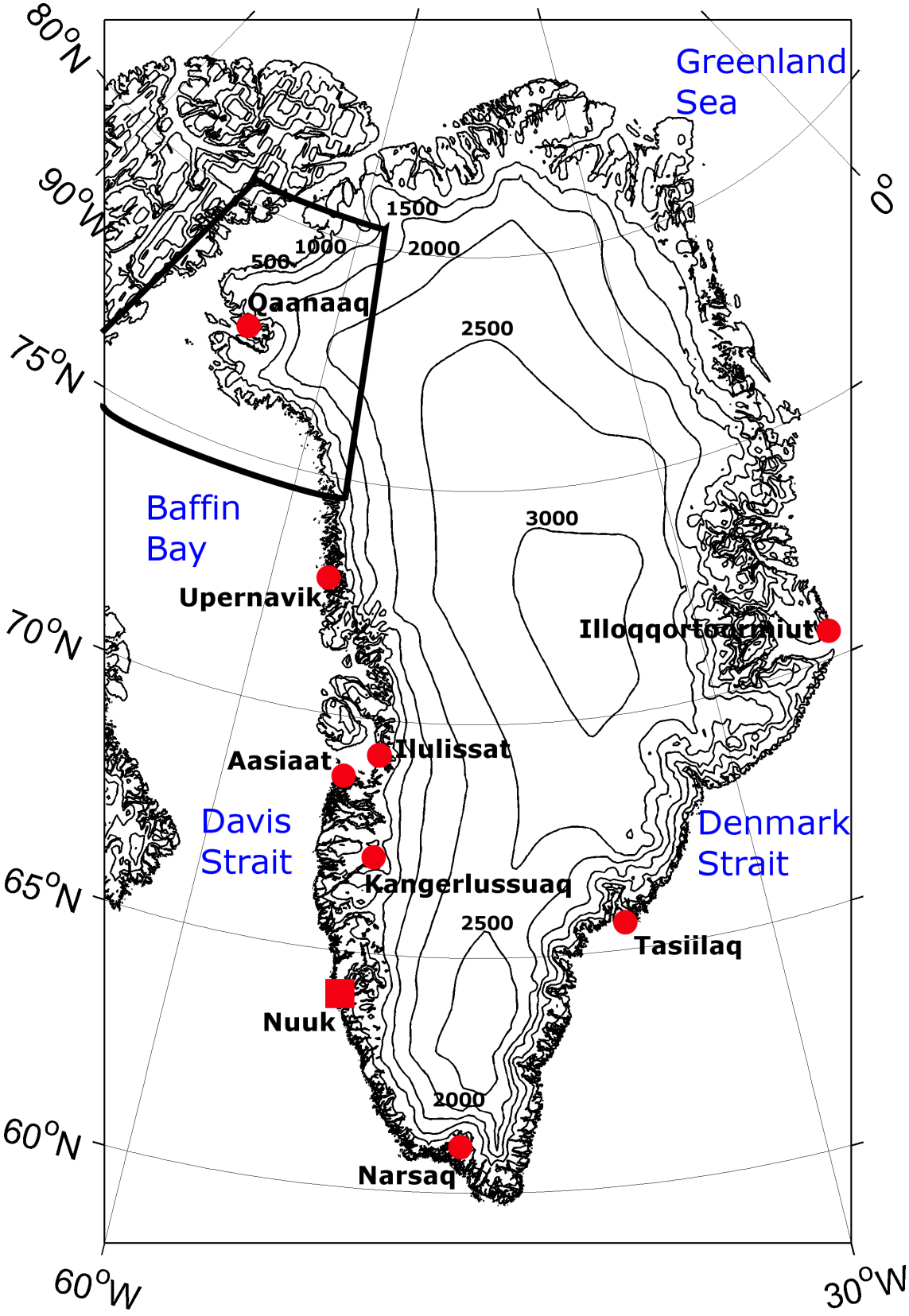

Figure 2.1: Map of Greenland with topography (ETOPO5 dataset; *NGDC*, 1988). The elevation contour interval is 500 m. The experimental area (see Figure 2.2) is indicated by a tetragon.

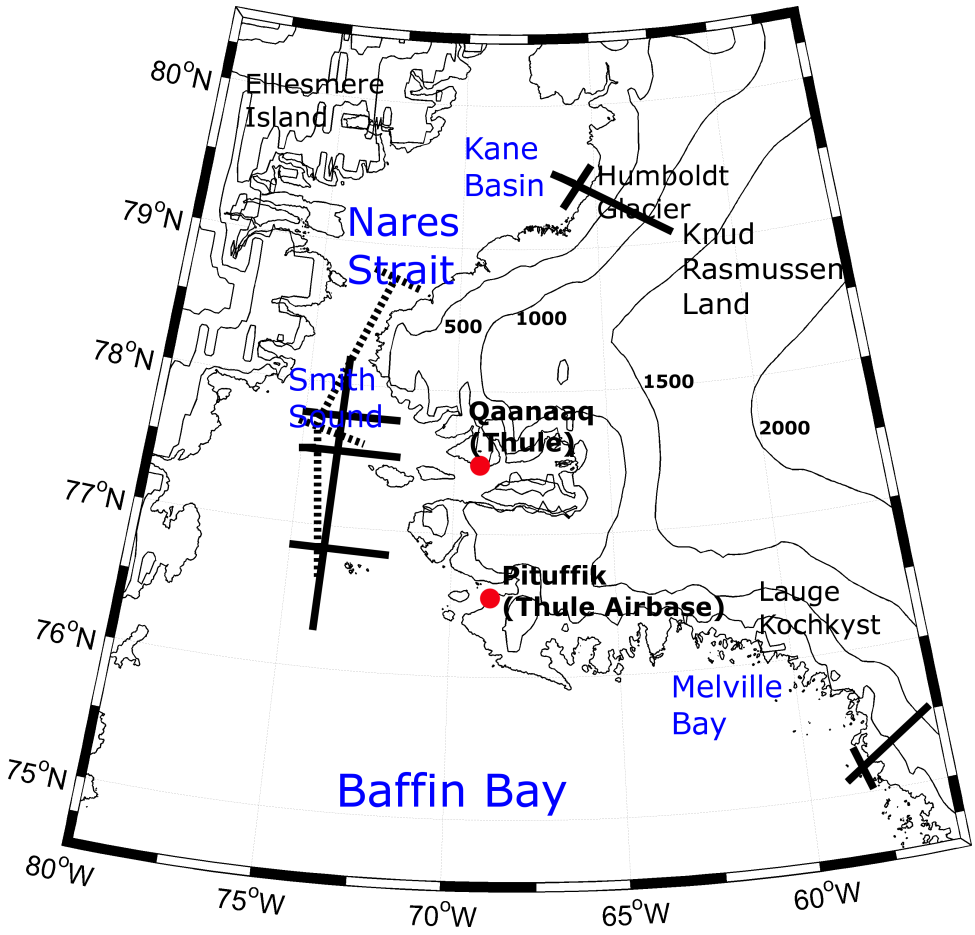

Figure 2.2: Experimental areas. Schematic plots of the flight patterns are presented by thick lines in the experimental area.

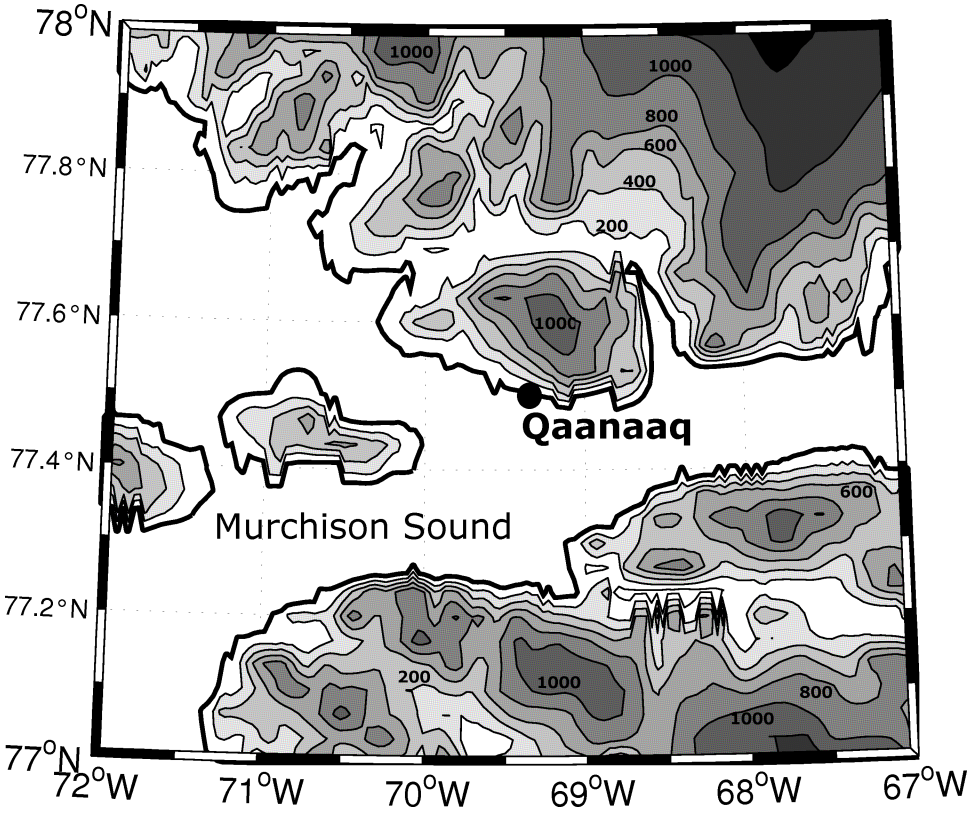

Figure 2.3: Topography of the Qaanaaq region (ETOPO2v2 dataset; *NGDC*, 2006). The elevation contour interval is 200 m.

Figure 2.4: Qaanaaq town. Photo taken on port side of the POLAR 5 aircraft, 12 June 2010.

2.2 Field phase chronology

Preparation phase

March 2007:	First IKAPOS science plan
November 2007:	Funding of the IKAPOS project by DFG (Deutsche Forschungsgemeinschaft)
December 2007:	Positive evaluation of the aircraft campaign by AWI aircraft commission, campaign in Greenland scheduled for May 2009
30 April 2008:	Meeting at AWI in Bremerhaven
August 2008:	Shift of the campaign to May 2010
October 2009:	Shift of the campaign to June 2010
29, 30 October 2009:	Meeting at AWI in Bremerhaven
November 2009:	Sea survival training
December 2009:	Final IKAPOS science plan
March 2010:	Application at Nunavut Research Institute (NRI) for flights over Canadian territory
April 2010:	Application at Government of Greenland
May 2010:	Flight permission by Government of Greenland
26 May 2010:	Meeting at AWI in Bremerhaven
May – June 2010:	Integration of the aircraft instrumentation
June 2010:	Information by Nunavut Research Institute (NRI) that no flight permission will be possible
03 June 2010:	Ground test

Experiment phase

07, 08 June 2010:	Ferry flights of POLAR 5 from AWI in Bremerhaven via Keflavik to Kangerlussuaq
09 June 2010:	Arrival of POLAR 5 at Qaanaaq
10 June 2010:	Nose boom conversion from transit mode to survey mode, no take-off possible due to surface fog
12 June 2010:	Calibration flight CAL
14 June 2010:	Flight mission KA1, most of the flight RAX (radiation) sensor processing failed
15 June 2010:	Flight mission NOW1
17 June 2010:	Flight mission KA2, RAX sensor processing failed
18 June 2010:	Flight mission NOW2, RAX sensor processing failed
19, 20 June 2010:	Repair of the radiation sensor processor
22 June 2010:	Flight mission NOW3, no data recording of the CR-2 dew point mirror
23 June 2010:	Flight mission NOW4, Weekly science report
27 June 2010:	Departure of POLAR 5 at Qaanaaq
28, 29 June 2010:	Ferry flights of POLAR 5 from Kangerlussuaq via Keflavik to AWI in Bremerhaven

Wrap-up phase

16 July 2010:	Preliminary data processing at University of Trier
21 October 2010:	De-briefing of IKAPOS at AWI in Bremerhaven
30 October 2010:	Inter-comparison measurements with the research aircraft ATR 42-320 (SAFIRE) in Toulouse
25 December 2010:	Processing of calibrated data

2.3 Aircraft and instrumentation

Aircraft measurements has been performed in the atmospheric boundary layer (ABL) using the research aircraft POLAR 5 (Figure 2.5). Since October 2007 the rebuilt DC-3 (Douglas Company) 1942, converted by Basler Turbo Conversions (therefore, also known as Basler BT-67), is in operation for research in polar regions. It can be equipped with a combined ski-wheel system and it has a deicing system. During IKAPOS skies were not required.

POLAR 5 has a length of 20.66 m, a wing span of 29 m, a maximum scientific cargo of 2,500 kg, a maximum range (without cargo) of 1,900 km and a typical cruising speed of 100 m s^{-1} (during transit flights). To ensure a spatial resolution as high as possible measurements were performed at typical speed of around 65 – 70 m s^{-1}.

Besides navigational and basic meteorological instrumentation (Figure 2.5) the aircraft was equipped with downward and upward looking sensors for solar and terrestrial radiation, a surface radiation thermometer and two high-precision laser altimeters to determine the surface roughness from flight heights below 2,500 m AGL (above ground level) (Table 2.1). Surface conditions were recorded as well with a downward looking video and a photo camera (Canon EOS-1D MARK III, 0.1 Hz) linked with a GPS receiver (GPSMap 60). In addition an upward adjusted video camera was installed.

POLAR 5 was instrumented with a turbulence measurement system collecting data on a nose boom (Figure 2.5, 2.6). High-resolution measurements at a sampling rate of 100 Hz allow for the calculation of turbulent heat, moisture and momentum fluxes (Table 2.2).

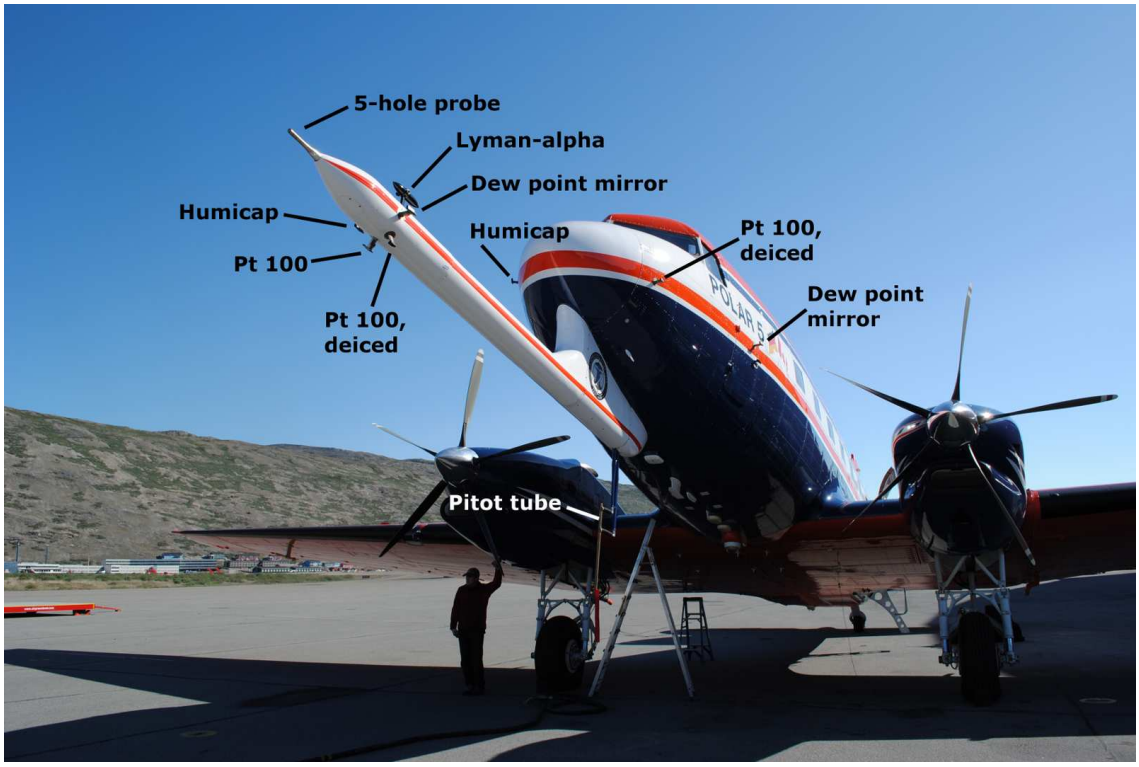

Figure 2.5: Research aircraft POLAR 5 at Kangerlussuaq. Wind, temperature and humidity sensors are marked.

Table 2.1: POLAR 5 basic meteorological instrumentation.

Quantity	Sampling	Sensor, manufacturer
Position	1 Hz	2 GPS, Trimble RTS
Position/orientation	50 Hz	INS, Honeywell Laseref V
Height	100 Hz	Radar altimeter, Honeywell
	20 Hz	Laser altimeter PS100(E), IBEO
	200 Hz	Laser altimeter LD90-3, RIEGL
Air pressure/air speed	20 Hz	Pitot tube and static pressure sensor, Rosemount
Surface temperature	20 Hz	KT-15.85D, Heitronics
Downward and upward radiation fluxes	20 Hz	2 Pyranometer PSP, Eppley 2 Pyrgeometer PIR, Eppley
Air temperature	20 Hz	Pt100 open wire deiced, Rosemount
Air humidity	1 Hz	Dew point mirror CR-2, Buck Research Instruments
	20 Hz	Humicap HMT333, Vaisala

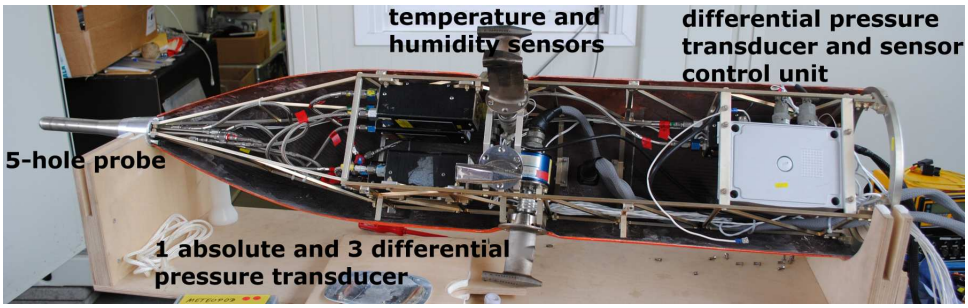

Figure 2.6: Inner view of the turbulence measurement system of the nose boom.

Table 2.2: Turbulence measurement system instrumentation.

Quantity	Sampling	Sensor, manufacturer
3D wind	100 Hz	5-hole probe, Rosemount
Air temperature	100 Hz	Pt100 open wire deiced, Rosemount
	100 Hz	Pt100 open wire, Rosemount
Air humidity	100 Hz	Lyman-α , Buck Research
	100 Hz	Humicap HMT333, Vaisala
	100 Hz	Dew point mirror 1011B, General Eastern

2.4 Surface-based measurements

In the coastal area of northwestern Greenland data are available from four synoptic weather stations. They are located at the airport of Qaanaaq (77.48°N, 69.38°W, 16 m ASL), at Thule airbase (76.53°N, 68.75°W, 77 m ASL), on the island Kitsissut in the northern Baffin Bay (76.63°N, 73°W, 11 m ASL) and on the island Kitsissorsuit south of Melville Bay (74.03°N, 57.82°W, 40 m ASL; Figure 2.7). Following quantities are measured every hour (Qaanaaq airport, Thule airbase) respectively every 3 hours (Kitsissut, Kitsissorsuit) at each station: Wind direction and wind speed (both 10 minutes mean), air pressure, air temperature and humidity. Besides, the METARs (Meteorological Aerodrome Reports) of Qaanaaq airport and Thule airbase give information about the dew point temperature, the cloud type, ceiling and coverage, the visibility and about fog existence.

On the ice sheet of northwestern Greenland four GC-Net (Greenland Climate-Network) Automatic Weather Stations (AWS) provided observations at following locations: on Petermann Glacier (80.68°N, 60.29°W, 37 m ASL), on Humboldt Glacier (78.53°N, 56.83°W, 1995 m ASL), above Lauge Kochkyst (GITS, 77.14°N, 61.04°W, 1869 m ASL) and at the NEEM (North Greenland Eemian Ice Drilling) camp (77.50°N, 50.87°W, 2454 m ASL; Figure 2.7). Each AWS is equipped with instruments to sample air temperature, wind speed and direction, air humidity, air pressure, precipitation rate and surface net radiation (solar and terrestrial). Hourly average data are transmitted via satellite. Data are made available by Konrad Steffen (CIRES).

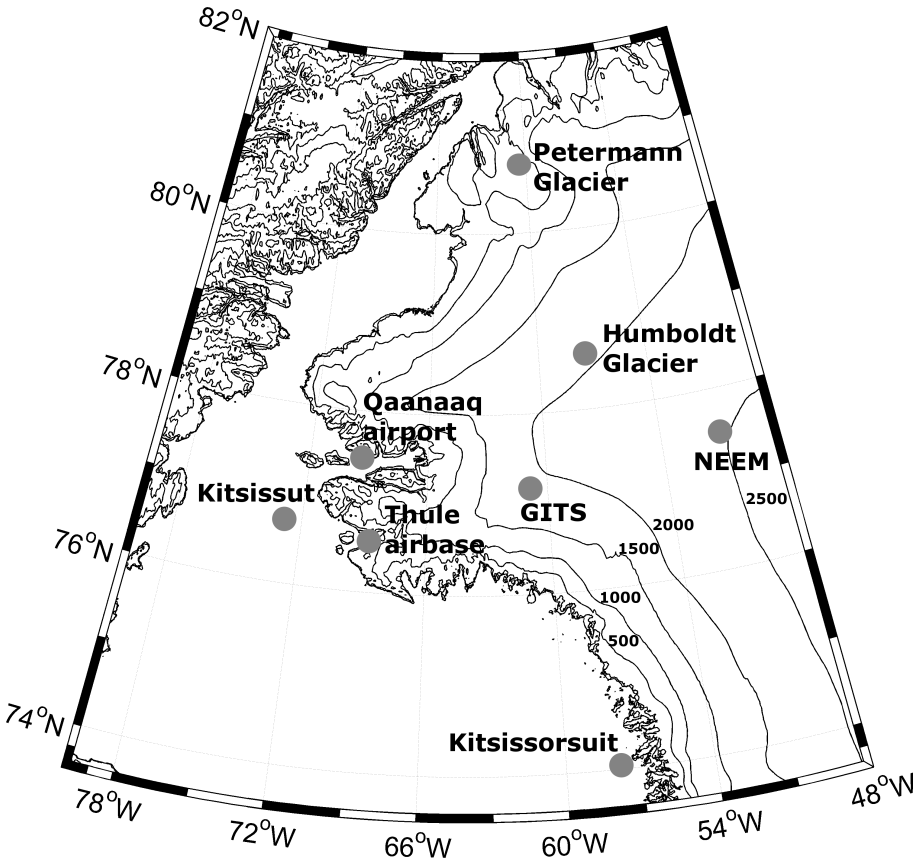

Figure 2.7: Surface based weather stations in northwestern Greenland. The elevation contour interval is 500 m (based on ETOPO2v2 dataset; *NGDC*, 2006).

2.5 Satellite data

NASA (U.S. National Aeronautics and Space Administration) provides near-real-time MODIS (Moderate Resolution Imaging Spectroradiometer) data from the sun-synchronous Earth Observing Systems (EOS) Terra and Aqua (see Table 2.3). Based on these data true color satellite images (up to 250 m resolution) were obtained by NASA's MODIS Rapid Response System (`http://rapidfire.sci.gsfc.nasa.gov/`). In addition, MODIS true color images for the coastal regions of Greenland were provided by the Center for Ocean and Ice (COI) in Denmark (`http://ocean.dmi.dk/arctic/modis.php`). During IKAPOS digital MODIS data were stored at the Department of Environmental Meteorology (University of Trier, Germany) and processed to provide brightness and sea-ice surface temperature for the experimental area with a resolution of 1 km.

Data from the Advanced Microwave Scanning Radiometer (AMSR) on board EOS Aqua were calculated to daily sea-ice concentration (6.25 km resolution) via the ARTIST (Arctic Radiation and Turbulence Interaction Study) algorithm of *Spreen et al.* (2008) by the Center for Marine and Atmospheric Science (Hamburg, Germany). During IKAPOS, the Department of Environmental Meteorology in Trier converted these data to sea-ice concentration maps for the experimental area. NSIDC (U.S. National Snow and Ice Data Center) supplied SSM/I (Special Sensor Microwave Imager) daily sea-ice concentration maps with spatial resolution of 25 km. Weekly sea-ice charts based on a combination of passive and active infrared and microwave satellite data for eastern Canada and western Greenland (Nares Strait and Baffin Bay) were also provided by the Canadian Ice Service (CIS) and by the COI in Denmark.

The European Space Agency (ESA) operates the Advanced Synthetic Aperture Radar (ASAR) on board the ENVISAT (Environmental Satellite). ASAR data were available as near-real-time quicklook images (150 m resolution) by ESA. In order to study sea-ice extent, types and motion ASAR data were acquired after the end of the field phase (see Table 2.4).

Table 2.3: List of available Terra and Aqua MODIS Level 1B data (1 km) covering the experimental areas. Cases within the research flights are bold.

Date	Satellite	UTC in hh:mm	Filename
14 June	Terra	01:55	A2010165.0155.005.2010165100156
		15:15	A2010165.1515.005.2010165231043
		18:30	A2010165.1830.005.2010166021346
	Aqua	07:30	A2010165.0730.005.2010165180630
		10:45	**A2010165.1045.005.2010166161625**
		14:00	A2010165.1400.005.2010166162030
15 June	Terra	01:00	A2010166.0100.005.2010166072409
		17:35	**A2010166.1735.005.2010167002439**
	Aqua	06:35	A2010166.0635.005.2010166183403
		09:50	A2010166.0950.005.2010166191216
		13:05	**A2010166.1305.005.2010167170157**
17 June	Terra	**15:45**	**A2010168.1545.005.2010168212435**
		17:25	**A2010168.1725.005.2010168234625**
		19:00	A2010168.1900.005.2010169022640
		22:15	A2010168.2215.005.2010169061532
	Aqua	08:00	A2010168.0800.005.2010168183944
		14:30	**A2010168.1430.005.2010169145159**
18 June	Terra	01:30	A2010169.0130.005.2010169072731
		18:05	**A2010169.1805.005.2010170014650**
		21:20	A2010169.2120.005.2010170031857
	Aqua	07:05	A2010169.0705.005.2010169152914
		10:20	**A2010169.1020.005.2010170152525**
		16:50	**A2010169.1650.005.2010170155053**
22 June	Terra	01:05	A2010173.0105.005.2010173072201
	Aqua	06:40	A2010173.0640.005.2010173201841
		09:55	A2010173.0955.005.2010174152359
		16:25	**A2010173.1625.005.2010174153118**
23 June	Terra	01:50	A2010174.0150.005.2010174080222
		18:25	**A2010174.1825.005.2010175015706**
		21:40	A2010174.2140.005.2010175033930
	Aqua	09:00	A2010174.0900.005.2010174173128
		12:15	A2010174.1215.005.2010175161646
		15:30	**A2010174.1530.005.2010175161512**

Table 2.4: List of available ENVISAT ASAR Alternating Polarisation Medium-resolution (APM) Level 1B data (150 m) covering the experimental areas. Cases within the research flights are bold.

Date	UTC in hh:mm	Filename
14 June	16:44–16:49	ASA_WSM_1PNPDE20100614_164352_000003062090_00198_43338_8778
15 June	00:56–01:06	ASA_WSM_1PNPDE20100615_005613_000005872090_00203_43343_8853
	16:12–16:16	ASA_WSM_1PNPDE20100615_161217_000002262090_00212_43352_9041
17 June	**15:11–15:14**	**ASA_WSM_1PNPDE20100617_151056_000001592090_00240_43380_9543**
18 June	01:02–01:10	ASA_WSM_1PNPDE20100618_010158_000005022090_00246_43386_9625
	16:19–16:22	**ASA_WSM_1PNPDE20100618_161917_000001842090_00255_43395_9794**
22 June	**15:54–15:56**	**ASA_WSM_1PNPDE20100622_155333_000001222090_00312_43452_0987**
23 June	**17:02–17:03**	**ASA_WSM_1PNPDE20100623_170149_000000982090_00327_43467_1207**

Chapter 3

Flight mission overview

3.1 Flight Strategy

The basic flight pattern to investigate the katabatic wind structure at Humboldt Glacier and at Kochkyst consists of a cross-section normal to the glacier front above sea-ice/ocean and glacier (up to a height of around 1,200 m AGL) and a cross-section parallel to the glacier front above sea-ice (Figure 3.1). This flight pattern allows for studying the SBL of the katabatic wind layer over the ice sheet and the modification of the flow passing over the sea-ice/ocean. Thus, the dynamical aspects of the flow transition can be explored.

The katabatic flight pattern itself consists of two main elements (see e.g. *Heinemann*, 1998):

- A series of vertical profiles (temps) between the minimum flight level (around 40 m AGL) and 300 to 500 m AGL (Figures 3.2, 3.3). These vertical profiles are intended to acquire the 3D structure of the planetary boundary layer (PBL) in a short period of time.
- Constant level runs (legs) at various heights above ground, typically 40, 65 and 100 or 200 m AGL (Figures 3.2, 3.3). These runs allow the determination of turbulent fluxes.

To encounter the most stable PBL stratification the pattern needs to be flown during early morning hours if the surface is not melting (see Section 1.2). A wind forcing by synoptic pressure gradients was of particular interest for the summertime conditions during IKAPOS.

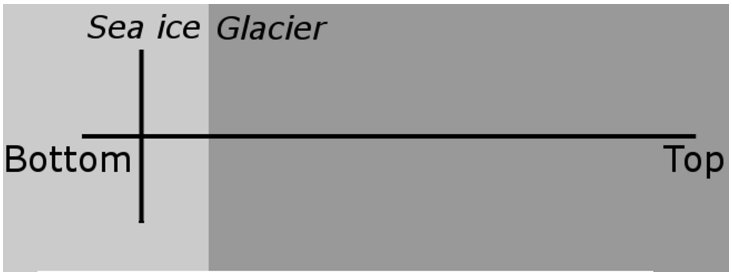

Figure 3.1: KA flight strategy. Top view.

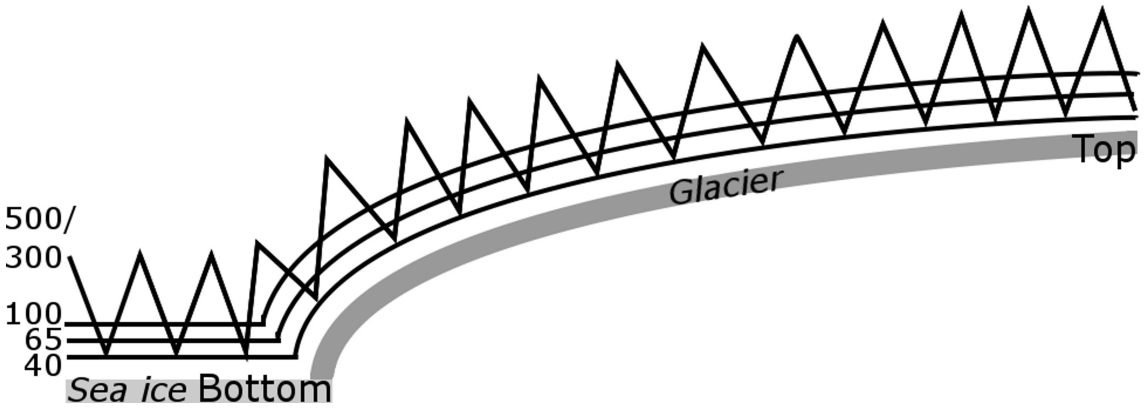

Figure 3.2: KA flight strategy of the central flight section. Lateral view.

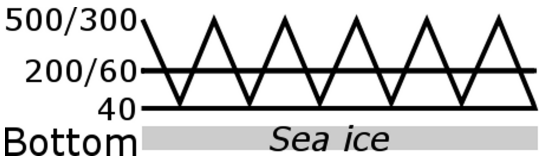

Figure 3.3: KA flight strategy of the flight section parallel to the glacier front. Lateral view.

The basic flight pattern to investigate the air/sea interaction over the NOW consists of a transect (central section) of 170 to 200 km in north-south direction and two cross-profiles of 65 to 70 km (Figure 3.4). This flight pattern allows for the study the ABL modification associated with the formation of the internal boundary layer over the NOW as well as the exchange processes at the surface.

The NOW pattern itself consists of two main elements:

- For the central section a series of high vertical profiles between the minimum flight level (around 40 m AGL) and 800 m AGL (Figure 3.5) and for the cross-profiles temps up to 350 m AGL (Figure 3.6).
- For the central section a constant level run at minimum height (40 m AGL, Figure 3.5) and for the cross-profiles legs at 40 and 65 m AGL (Figure 3.6).

Based on weather forecasts (mainly by model predictions of the DMI, Environment Canada and the Norwegian Meteorological Institute) and sea-ice conditions the flight location/programme was chosen. The final decision, if a flight mission if a flight could be performed, was made immediately before the take-off, depending on the local weather conditions (fog or low clouds).

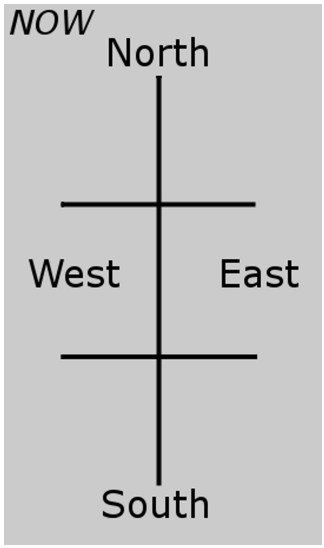

Figure 3.4: NOW flight strategy. Top view.

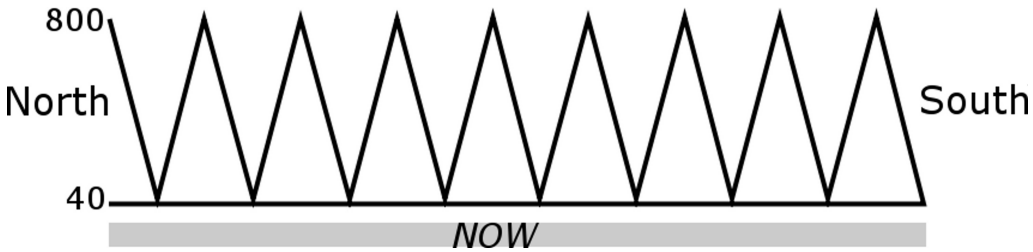

Figure 3.5: NOW flight strategy of the central flight section. Lateral view.

Figure 3.6: NOW flight strategy of the cross-profiles. Lateral view.

3.2 Overview of the flight missions

A total of six flight missions could be performed during the experiment (Table 3.1). For different synoptic situations four flights over the NOW (15, 18, 22, 23 June) and one flight each over the Humboldt Glacier (14 June) and the Steenstrup Glacier (17 June) took place. A calibration flight was performed on 12 June.

The NOW flights were performed from morning to afternoon and lasted 4 to 5 hours without transfer flights. In general, northerly flow from Nares Strait through Smith Sound, in contrast to the polynya warm winds prevailed during these flights. Research flights NOW1 to NOW3 took place within Smith Sound and northern Baffin Bay. In order to study the atmosphere/sea-ice/ocean exchange processes for the same area at different days the flight patterns of NOW2 and NOW3 were very similar. In addition to northern Baffin Bay and Smith Sound, channeling effects of southern Kane Basin were investigated during NOW4.

The flight over the Humboldt Glacier (14 June) was performed during cloud-free and weak synoptic winds in the early morning in order to capture the most pronounced SBL. The flight on 17 June took place over the Steenstrup Glacier during the afternoon. Conditions of large synoptic pressure gradients and a melting glacier surface appeared.

A detailed overview of the atmospheric characteristics during the flights is given by Table 3.2. Channeling and mountain effects occured at each NOW flight.

On 11 and 21 June and from 24 June to the end of the campaign no take-offs were possible due to surface fog at Qaanaaq airport. The repair of the radiation sensor processor took two days so that on 19 and 20 June no flights could be performed.

Table 3.1: Overview of the flight missions (I): Flight times (implicate transfer times to the areas of investigation) and flight schemes.

Time		Flight scheme	
Day of 2010	UTC, duration in hh:mm	Topic, location	Programme
12 June	13:50–17:05 03:15	CAL Smith Sound, Inglefield Land	Calibration maneuver
14 June	07:45–12:25 04:40	KA1 Humboldt Glacier	AB, Q1aQ1b
15 June	12:45–18:25 05:40	NOW1 Smith Sound, northern Baffin Bay	AB, Q1aQ1b, Q2aQ2b
17 June	13:35–17:55 04:20	KA2 Steenstrup Glacier	AB, Q1aQ1b
18 June	13:55–18:50 04:55	NOW2 Smith Sound, northern Baffin Bay	AB1, Q1aQ1b, Q3aQ3b
22 June	12:15–17:20 05:05	NOW3 Smith Sound, northern Baffin Bay	AB1, Q1aQ1b, Q3aQ3b
23 June	13:15–18:35 05:20	NOW4 Northern Baffin Bay, Smith Sound, southern Kane Basin	CM1B1, Q4aQ4b, Q5aQ5b

Table 3.2: Overview of the flight missions (II): Way points with ABL characteristics. h denotes the height of the SBL, $T(h)$ denotes the temperature at this height and T_0 denotes the temperature at the surface (radiation temperatures for KA2 and NOW2 are not available). ΔT is the difference ($T(h)$–T_0). The wind speed at the lowest flight level and the maximum wind speed are denoted by ff_{LFL} and ff_{max}, respectively. The upper air flow (Ua flow) is determined from high aircraft temps (about 800 m AGL) during the flight programme.

Flight	Point	Characterisics							
		h in m	$T(h)$ in °C	T_0 in °C	ΔT in K	ff_{LFL} in m s^{-1}	$h_{ff,max}$ in m	ff_{max} in m s^{-1}	Ua flow in m s^{-1} (dir in °)
KA1	A	230	1.9	-0.7	2.6	3	-	-	4 (80)
	B	90	-4.3	-7.7	3.4	8	40	8	
	Q1a	150	2.4	-0.7	3.1	2	-	-	
	Q1b	150	2.7	-0.9	3.6	2	-	-	
NOW1	A	80	4.4	-0.2	4.6	16	70	20	7 (30)
	B	170	4.0	1.9	2.1	11	170	15	11 (350)
	Q1a	110	3.9	0.1	3.8	11	100	19	-
	Q1b	-	-	3.6	-	5	-	-	-
	Q2a	160	3.5	1.3	2.2	13	160	18	-
	Q2b	-	-	1.1	-	9	-	-	-
KA2	A	80	4.5	-	-	5	20	5	6 (340)
	B	-	-	-	-	13	110	14	
	Q1a	150	3.6	-	-	4	60	6	
	Q1b	120	4.4	-	-	5	40	6	
NOW2	A	140	1.7	-	-	15	110	18	10 (50)
	B1	300	1.2	-	-	6	300	10	8 (120)
	Q1a	170	-0.4	-	-	14	160	18	-
	Q1b	-	-	-	-	4	-	-	-
	Q3a	180	0.6	-	-	10	170	14	-
	Q3b	50	1.6	-	-	5	-	-	-
NOW3	A	130	2.0	-0.6	2.6	15	120	22	17 (20)
	B1	190	1.8	0.9	0.9	13	190	20	15 (340)
	Q1a	130	2.1	-0.4	2.5	15	130	22	-
	Q1b	-	-	2.0	-	5	-	-	-
	Q3a	130	2.9	-0.9	3.8	15	130	21	-
	Q3b	80	3.6	3.2	0.4	3	-	-	-
NOW4	C	370	2.1	-0.3	2.4	4	-	-	8 (40)
	M1	170	3.8	-0.1	3.9	13	140	21	8 (20)
	B1	190	3.8	-0.2	4.0	6	70	8	1 (350)
	Q4a	250	1.7	0.1	1.6	2	-	-	-
	Q4b	280	1.6	1.1	0.5	2	-	-	-
	Q5a	150	4.0	0.3	3.7	12	120	19	-
	Q5b	50	5.6	1.2	4.4	5	30	5	-

3.3 Flight CAL: 12 June 2010

The purpose of the flight CAL was the in-field calibration of the aircraft instrumentation. Among the calibrated quantities are the misalignments of the radiation sensors and the coefficients for the five-hole probe.

The following list summarizes the flight programme during CAL:

1. Climb to 10,000 ft (3,000 m).
2. Squared box, on each side:
   (a) Five minutes straight flight at constant level.
   (b) Five oscillations +/- 10° pitch angle.
   (c) Five oscillations +/- 10° roll angle.
   (d) Five oscillations +/- 10° yaw angle.
   (e) 90° right turn to the next side.
3. Full circle left at 20° roll angle.
4. Full circle right at 20° roll angle.
5. Cross pattern:
   Five minutes go-and-return flight in along-wind direction.
   Five minutes go-and-return flight in cross-wind direction.

CAL was performed over Smith Sound and the adjacent land of Greenland. The positions of the flight pattern are shown in Table 3.3 and Figure 3.7. The flight schedule and 3D flight path are presented in Table 3.4 and Figure 3.8.

Table 3.3: Geographic coordinates of the way points for CAL.

Flight pattern	Way point coordinates	
	Latitude in °N	Longitude in °W
Squared box	77.841	73.009
	78.121	74.898
	78.511	73.539
	78.238	71.578
Cross	77.994	73.916
	78.362	72.605
	78.313	74.215
	78.035	72.313

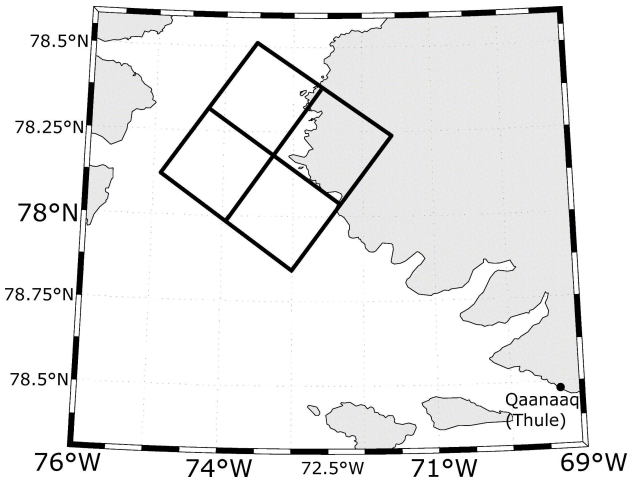

Figure 3.7: Schematic plot of the flight pattern during CAL.

Table 3.4: Schedule for CAL.

Flight pattern	Event number	Begin, UTC in hh:mm:ss	End, UTC in hh:mm:ss	Calibration maneuver
Squared box	01	14:12:06		Begin leg
	02	14:18:00	14:18:53	5 pitch angles +/-10°
	03	14:19:05	14:20:03	5 roll angles +/-10°
	04	14:20:14	14:20:58	5 yaw angles +/-10°
	05		14:25:19	End leg
	06	14:26:04		Begin leg
	07	14:29:52	14:30:34	5 pitch angles +/-10°
	08	14:30:42	14:31:22	5 roll angles +/-10°
	09	14:31:35	14:32:32	5 yaw angles +/-10°
	10		14:38:52	End leg
	11	14:39:29		Begin leg
	12	14:43:43	14:44:35	5 pitch angles +/-10°
	13	14:44:52	14:45:42	5 roll angles +/-10°
	14	14:45:56	14:46:42	5 yaw angles +/-10°
	15		14:52:41	End leg
	16	14:53:15		Begin leg
	17	14:57:53	14:58:52	5 pitch angles +/-10°
	18	14:58:55	14:59:49	5 roll angles +/-10°
	19	15:00:07	15:01:02	5 yaw angles +/-10°
	20		15:07:30	End leg
Full circles	21	15:08:46	15:10:48	Left circle at 20°
	22	15:10:51	15:12:58	Right circle at 20°
Cross pattern	23	15:22:36	15:35:24	Leg
	24	15:38:20	15:50:29	Return leg
	25	16:00:44	16:13:41	Leg
	26	16:15:33	16:28:20	Return leg

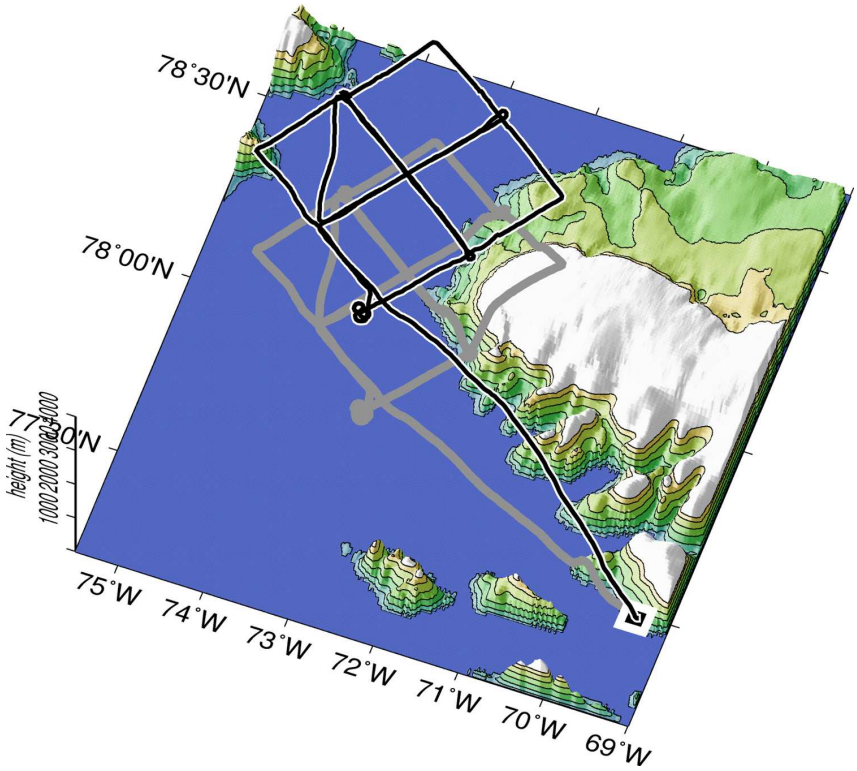

Figure 3.8: CAL flight path: perspective view from southeast. The gray line depicts the projection of the 3D trajectory onto the ground. The horizontal axes give geographic latitude and longitude, respectively, the vertical axis gives the height (above sea level). Contour lines are indicated every 100 m (up to 600 m ASL). Qaanaaq airport is indicated by a square.

The synoptic weather situation during CAL was characterized by a trough over west Greenland and southerly winds over north Greenland (Figure 3.9). In general, the GME analysis shows weak pressure gradients associated with 10 m-wind speeds lower than 2.5 m s^{-1} at the measurement area. GME 2-m temperatures are around 0 °C.

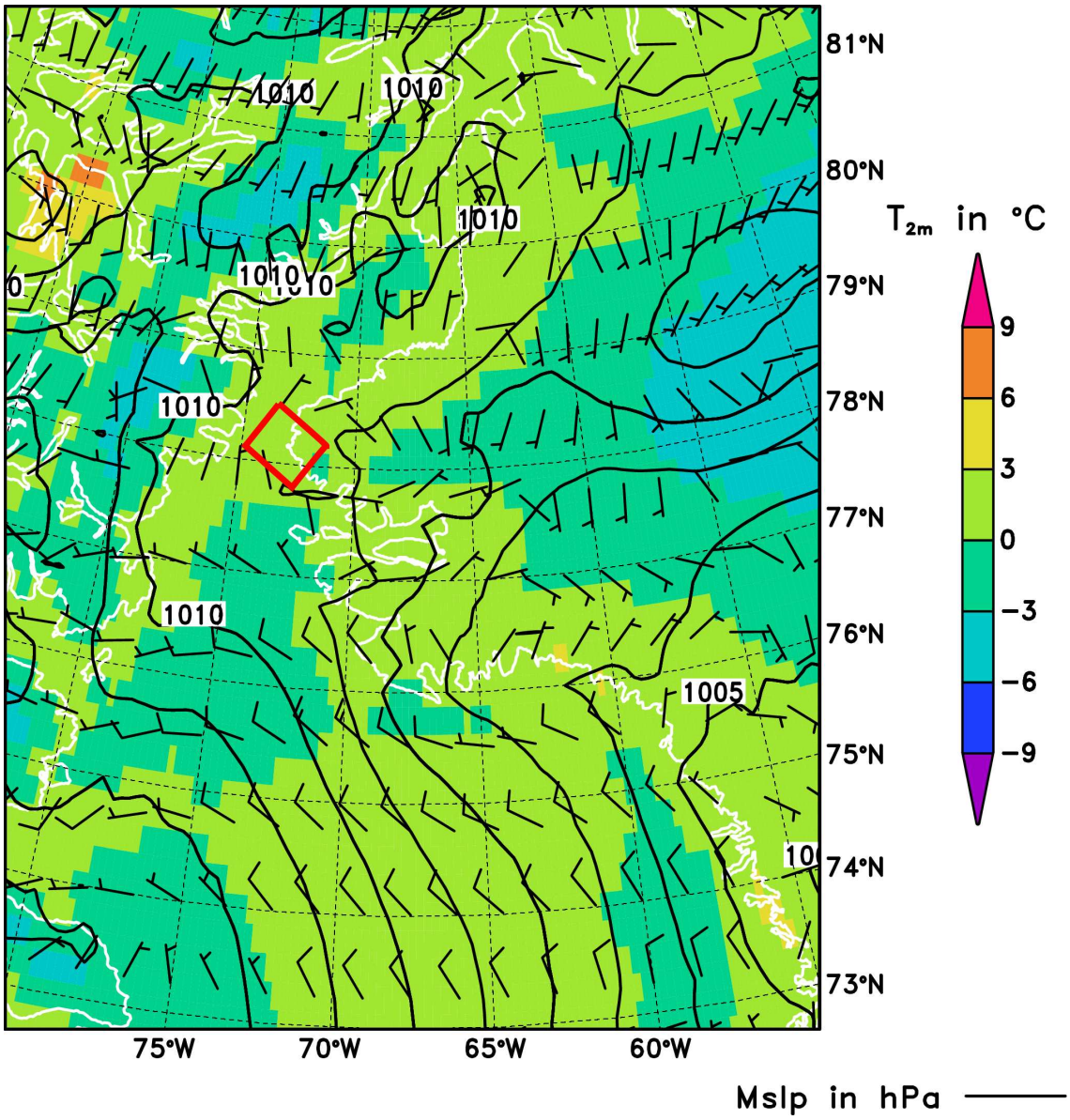

Figure 3.9: GME analysis 12 June 2010, 1800 UTC. Mean sea level pressure (isolines every 1 hPa), 10 m-wind (vectors, half barb: 5 kn ≈ 2.6 ms^{-1}, full barb: 10 kn ≈ 5.2 m s^{-1}) and 2 m-air temperature (shaded) are displayed. The measurement area is indicated by a red tetragon.

3.4 Flight KA1: 14 June 2010

The measurement pattern of flight KA1 started at point B (for positions see Table 3.5, Figure 3.10) above the Humboldt Glacier. From there a series of shallow aircraft temps between 33 m and 235 AGL were performed on the central line down the glacier to point A (for flight schedule and 3D flight path see Table 3.7, Figure 3.11). Then three constant level runs were flown on A–B at average heights of 68 m, 40 m and 98 m AGL. The length of one leg is about 96 km (Table 3.6). Next, high aircraft temps were flown up to 524 m AGL on the same line to point A. After that a transfer flight section took place to point Q1a. From there temps from 524 m to 37 m AGL were flown on the cross-profile Q1 (32 km) in front of the glacier followed by two legs at 36 m and 190 m AGL on average, respectively.

Unfortunately, the radiation data of the first part of the flight were lost due to problems with the data acquisition system. The recording of the radiation data started during leg A–B in a height of 98 m AGL at 0953 UTC.

Table 3.5: Mean geographic coordinates of the way points for KA1.

Way point	Coordinates	
	Latitude in °N	Longitude in °W
A	79.551	66.441
B	79.149	62.277
Q1a	79.584	65.340
Q1b	79.344	66.180

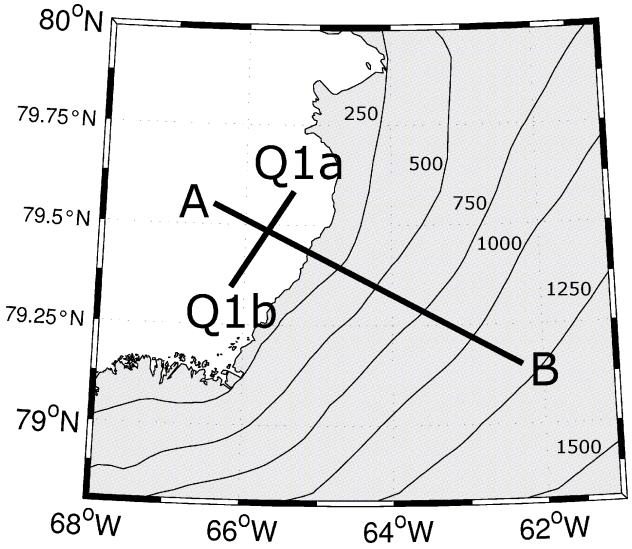

Figure 3.10: Topography (isolines every 250 m) and schematic plot of the flight pattern for KA1.

Table 3.6: Distances of the legs for KA1.

Leg	Distance in km
A–B	96
Q1	32

Table 3.7: Schedule for KA1. Mean heights (legs) and minimum and maximum heights (temps) are indicated. If neither a leg nor a temp are marked a transfer flight section took place.

	Begin		End				
Event number	UTC in hh:mm:ss	Position	UTC in hh:mm:ss	Position	Leg	Temp	Radar height in m
01	08:31:44	B	08:50:57	A		x	33–235
02	08:54:59	A	09:20:25	B	x		68
03	09:23:26	B	09:48:04	A	x		40
04	09:50:30	A	10:18:02	B	x		98
05	10:34:02	B	10:56:45	A		x	37–524
06	10:56:46	A	11:07:55	Q1a			
07	11:07:56	Q1a	11:16:40	Q1b		x	36–480
08	11:19:36	Q1b	11:28:36	Q1a	x		36
09	11:30:55	Q1a	11:40:26	Q1b	x		190

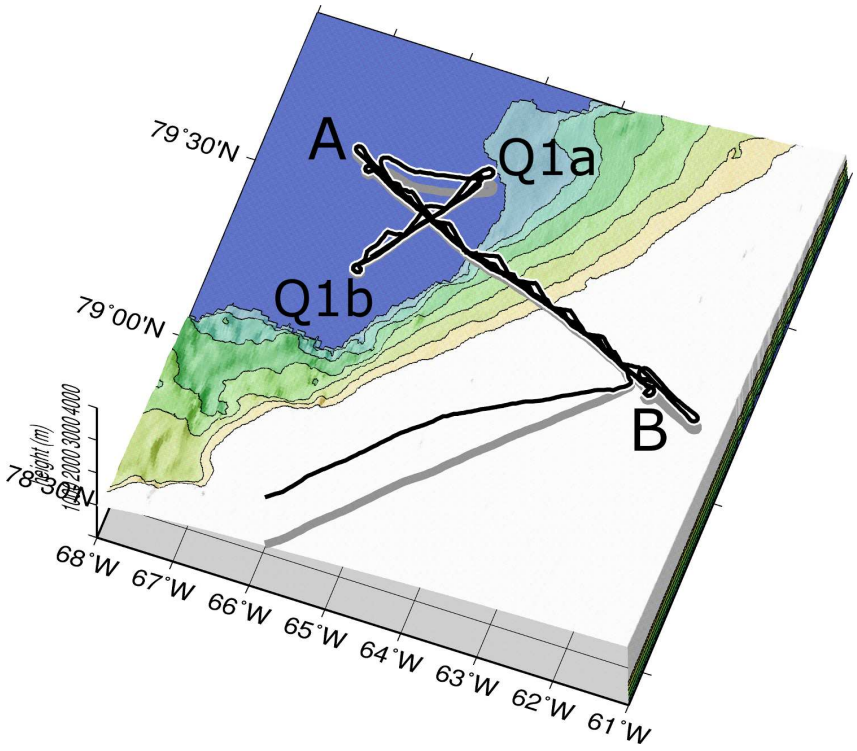

Figure 3.11: As Figure 3.8, but for the KA1 flight path. Way points are indicated.

The general sea-ice conditions in the experimental area were as follows. Sea-ice concentration of central and southern Nares Strait was mostly lower than 50 % (for sea-ice maps/conditions see Figures 3.12 – 3.15). Just alongside the coast of Canada there was a narrow band of high sea-ice concentration. Fast-ice existed at the bays and fjords along Canada and Greenland. At Smith Sound the ice bridge described in e.g. *Barber et al.* (2001a), *Yao and Tang* (2003) and *Kwok et al.* (2010) was broken up at the side of Greenland so that pack ice from the north could drift southward.

South of Smith Sound the NOW extended over more than 300 km southwards (Figure 3.12). The NOW has mostly ice concentrations less than 40 % (except at the coast of Canada). In the south the NOW was bordered by the sea-ice of western Baffin Bay. The coastal area of West Greenland was mostly ice-free as a consequence of the warm West Greenland Current (see e.g. *Bâcle*, 2000; *Melling et al.*, 2001; *Barber et al.*, 2001b). The coast of Melville Bay was characterized by fast-ice.

The Kane Basin in front of Humboldt Glacier was covered with fast-ice as well, so that the entire flight programme of KA1 was performed over glacier or sea-ice.

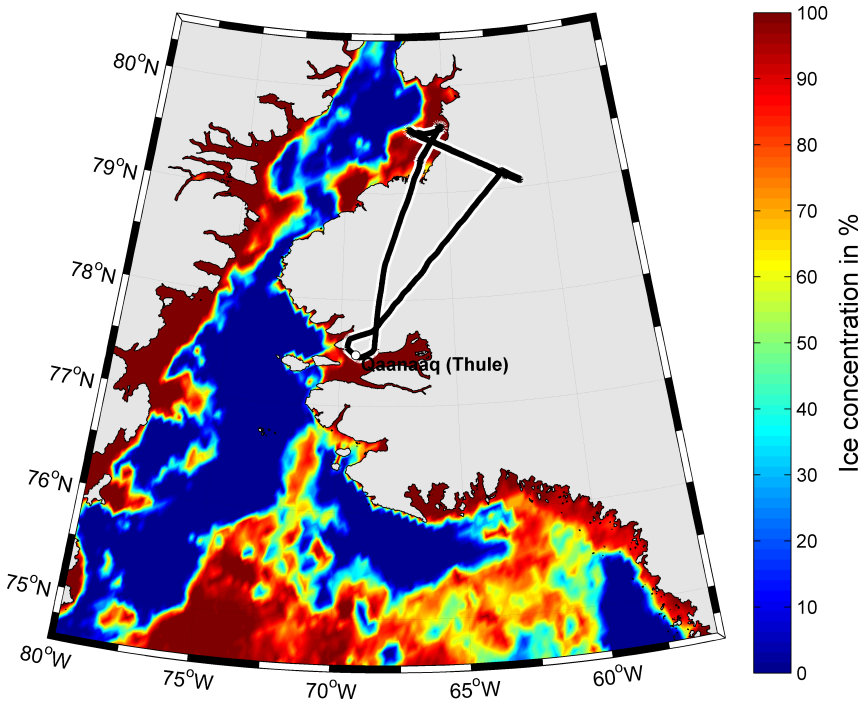

Figure 3.12: KA1 flight path superimposed on the AMSR-E mean sea-ice concentration for 14 June 2010.

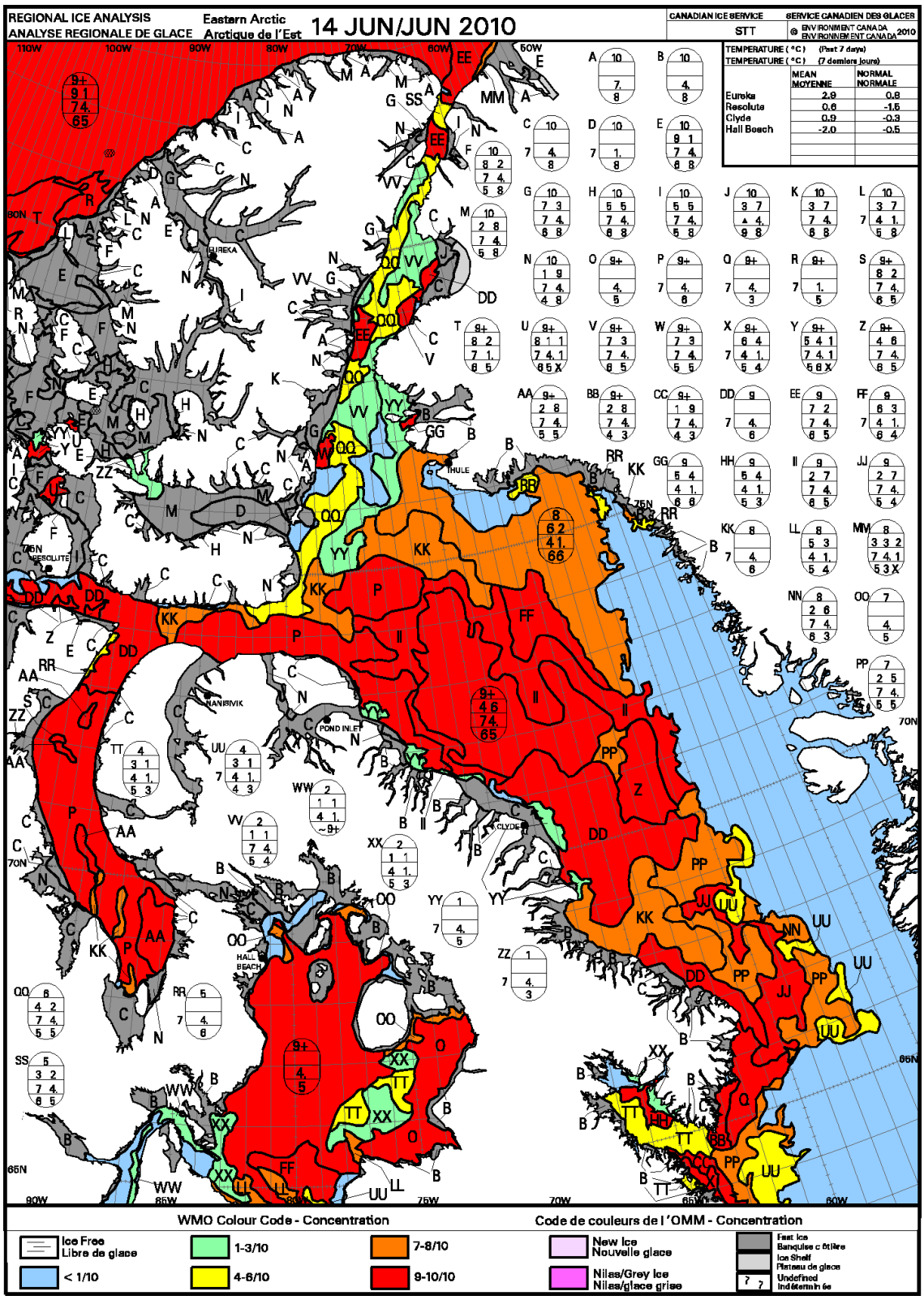

Figure 3.13: Sea-ice chart from Environmental Canada valid for the week of 14 June 2010.

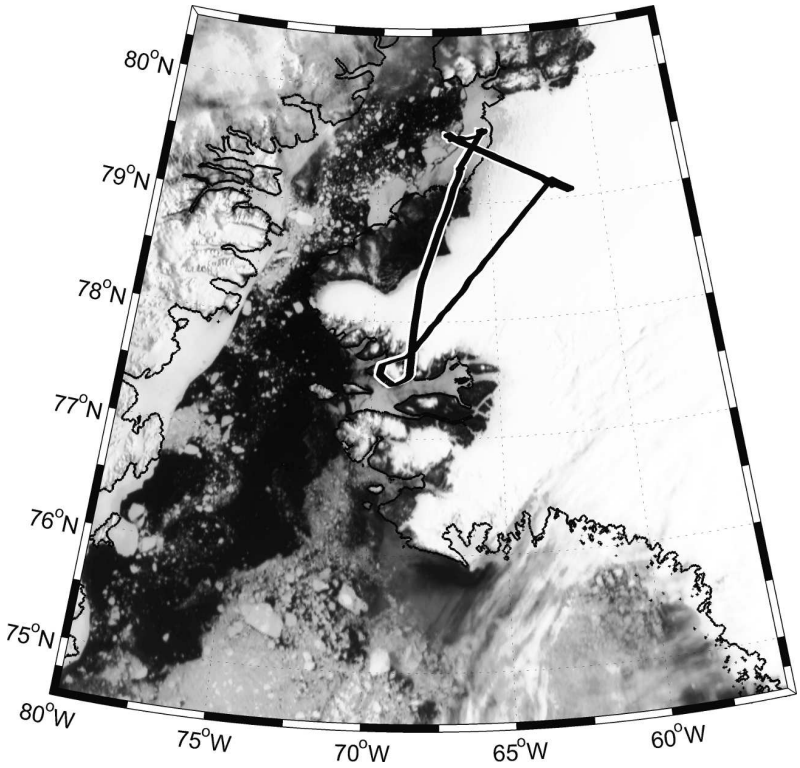

Figure 3.14: KA1 flight path superimposed on the MODIS channel 1 (620 – 670 nm) image for 14 June 2010, 1045 UTC.

Figure 3.15: Humboldt Glacier as seen from the Kane Basin on 14 June 2010, 1114 UTC.

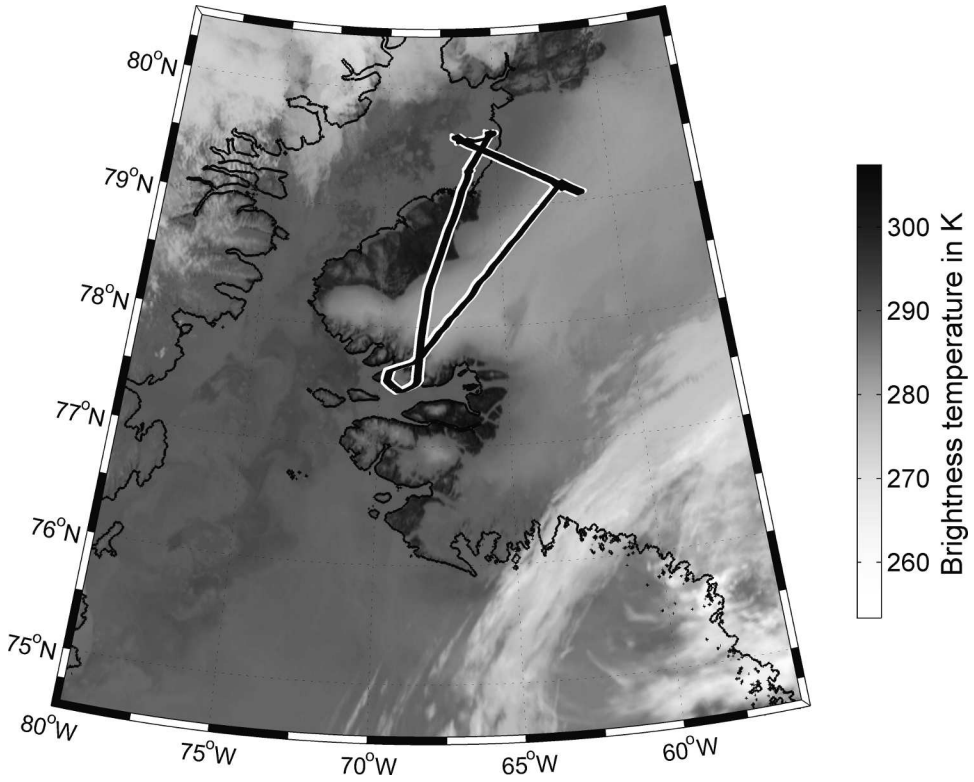

Figure 3.16: KA1 flight path superimposed on the MODIS channel 31 infrared brightness temperature image for 14 June 2010, 1045 UTC.

On 14 June 2010 the synoptic weather situation was characterized by a low pressure system over central Greenland. Over northern Baffin Bay a weak cyclone was forming (Figure 3.17). The experimental area was cloud-free (Figures 3.14, 3.16). In general, weak pressure gradients were present (Figure 3.17). Over Humboldt Glacier the GME analysis shows weak winds ($\leq$ 2.5 m s^{-1}). Here, the 2 m-temperature was somewhat higher than 0 °C. Up the slope the analysed wind direction turned clockwise from east to south-west. The temperature decreased below 0 °C.

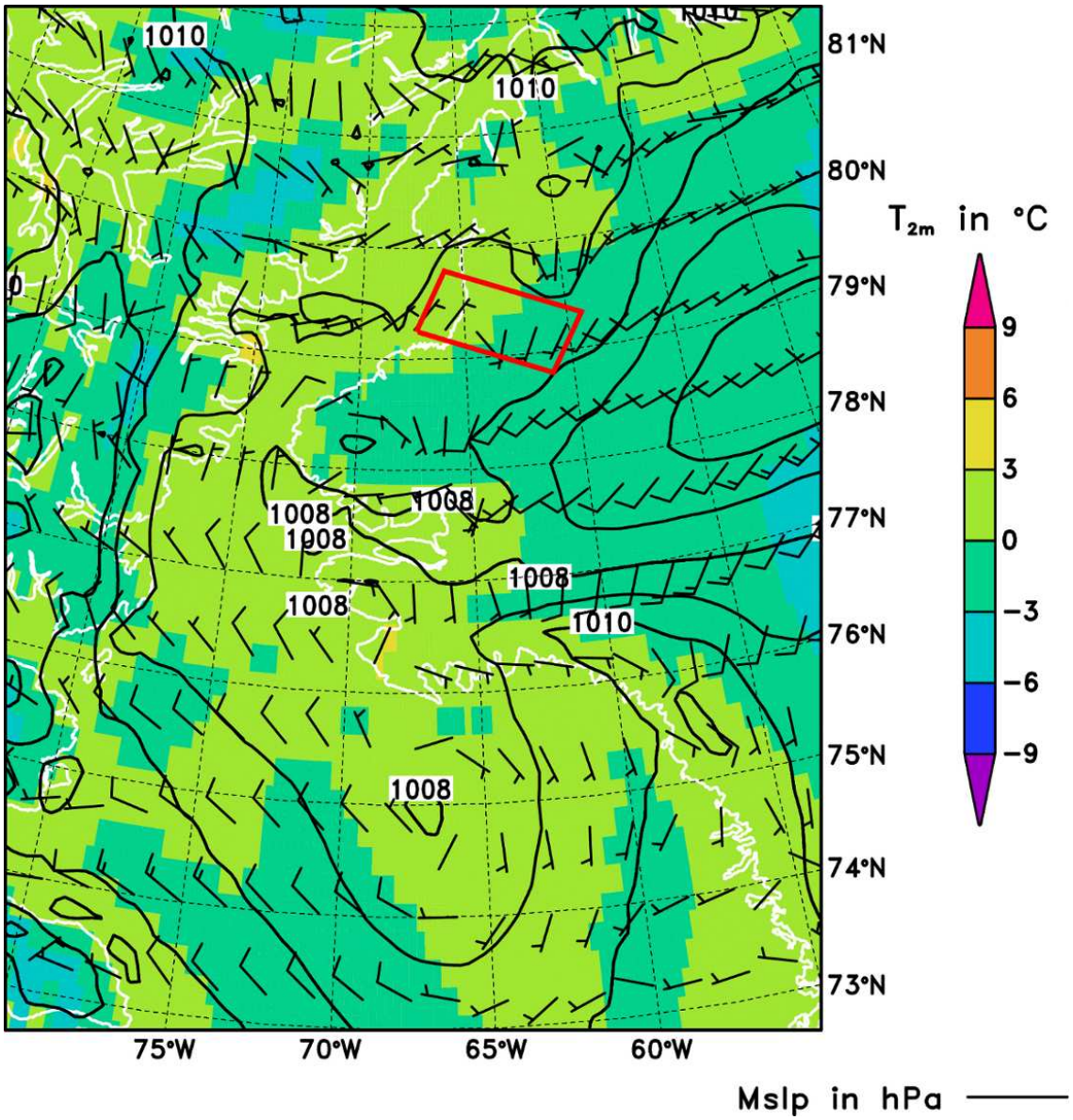

Figure 3.17: As Figure 3.9, but for the GME analysis for 14 June 2010, 1200 UTC.

3.5 Flight KA2: 17 June 2010

The flight programme of KA2 started at point A in front of the Steenstrup Glacier (for position see Table 3.8, Figure 3.18). From there a series of aircraft temps between 20 m and 340 m AGL up the glacier to point B were performed (for flight schedule and 3D flight path see Table 3.10, Figure 3.19). Then three constant level runs were flown on B–A at 40 m, back on A–B at 95 m and terminal on B–A at 66 m AGL on average. The length of one leg is about 75 km (Table 3.9).

Next, a low level leg (36 m AGL on average) was flown to Q1a, the starting point of a cross-profile Q1. Q1 is located in front of the glacier and has a length of 39 km. The cross-profile Q1 consisted of one aircraft temp part (22 m to 201 m AGL) followed by two constant level runs at mean heights of 36 m and 63 m.

Unfortunately, during KA2 all measured radiation data were lost due to problems with the radiation data acquisition processor.

Table 3.8: Mean geographic coordinates of the way points for KA2.

Way point	Coordinates	
	Latitude in °N	Longitude in °W
A	75.104	58.995
B	75.450	56.703
Q1a	75.053	58.419
Q1b	75.301	58.686

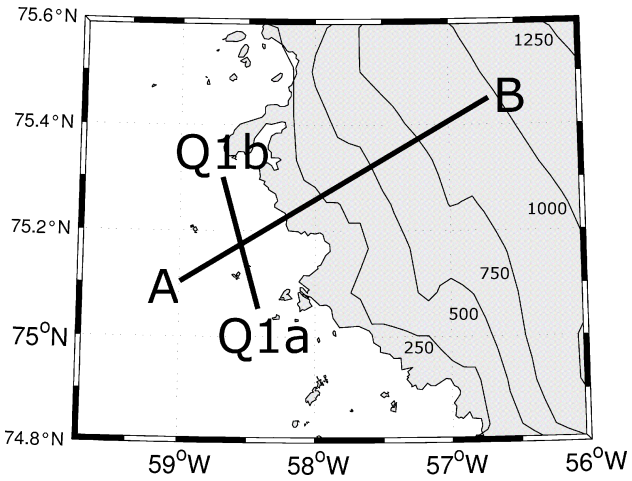

Figure 3.18: Topography (isolines every 250 m) and schematic plot of the flight pattern for KA2.

Table 3.9: Distances of the legs for KA2.

Leg	Distance in km
A–B	75
Q1	29

Table 3.10: As Table 3.7, but for the schedule for KA2.

	Begin		End				
Event number	UTC in hh:mm:ss	Position	UTC in hh:mm:ss	Position	Leg	Temp	Radar height in m
01	14:48:26	A	15:05:31	B		x	20–340
02	15:08:29	B	15:26:14	A	x		40
03	15:28:05	A	15:48:17	B	x		95
04	15:52:03	B	16:12:24	A	x		66
05	16:13:50	A	16:18:32	Q1a	x		36
06	16:20:47	Q1a	16:28:20	Q1b	x		22–201
07	16:30:23	Q1b	16:37:40	Q1a	x		36
08	16:41:08	Q1a	16:49:21	Q1b	x		63

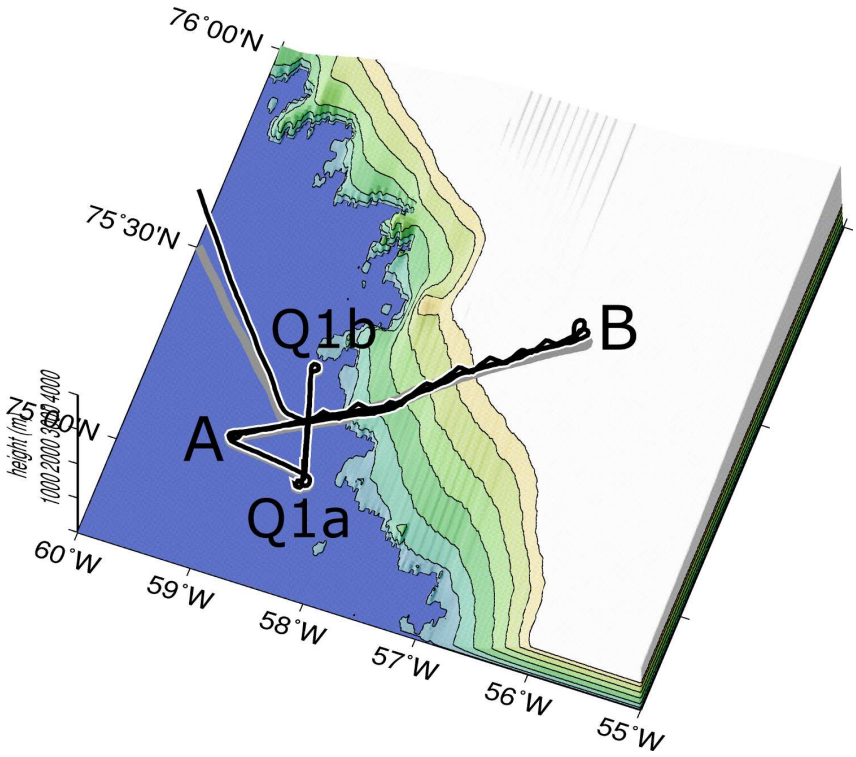

Figure 3.19: As Figure 3.8, but for the KA2 flight path. Way points are indicated.

In comparison to 14 June 2010 the sea-ice concentration at Melville Bay was distinctly lower on 17 June 2010 (compare Figures 3.12, 3.14 with 3.20, 3.21). A–B was performed over open water, sea-ice and the Steenstrup Glacier (Figures 3.20 – 3.24). Q1 took place over sea-ice.

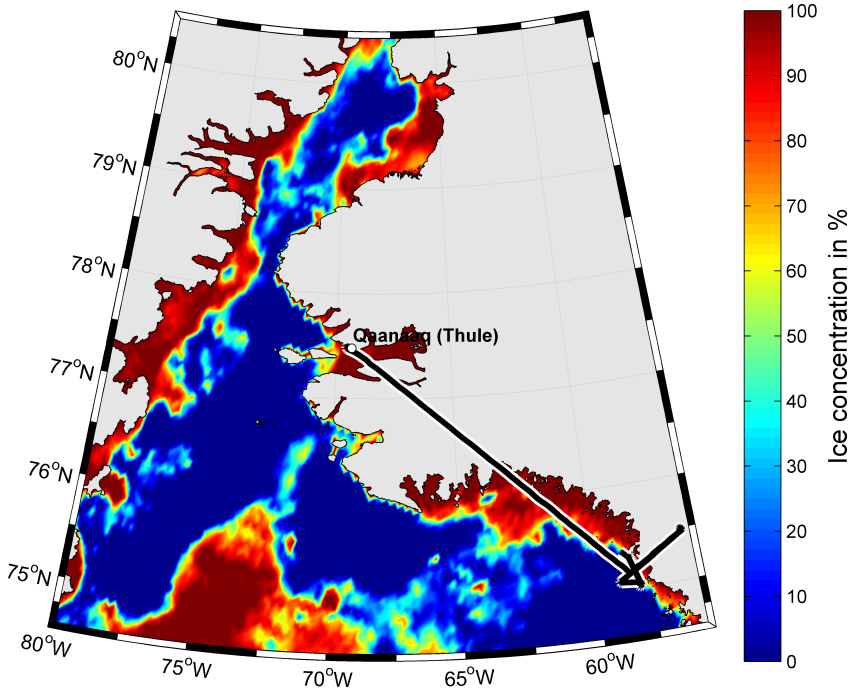

Figure 3.20: KA2 flight path superimposed on the AMSR-E mean sea-ice concentration for 17 June 2010.

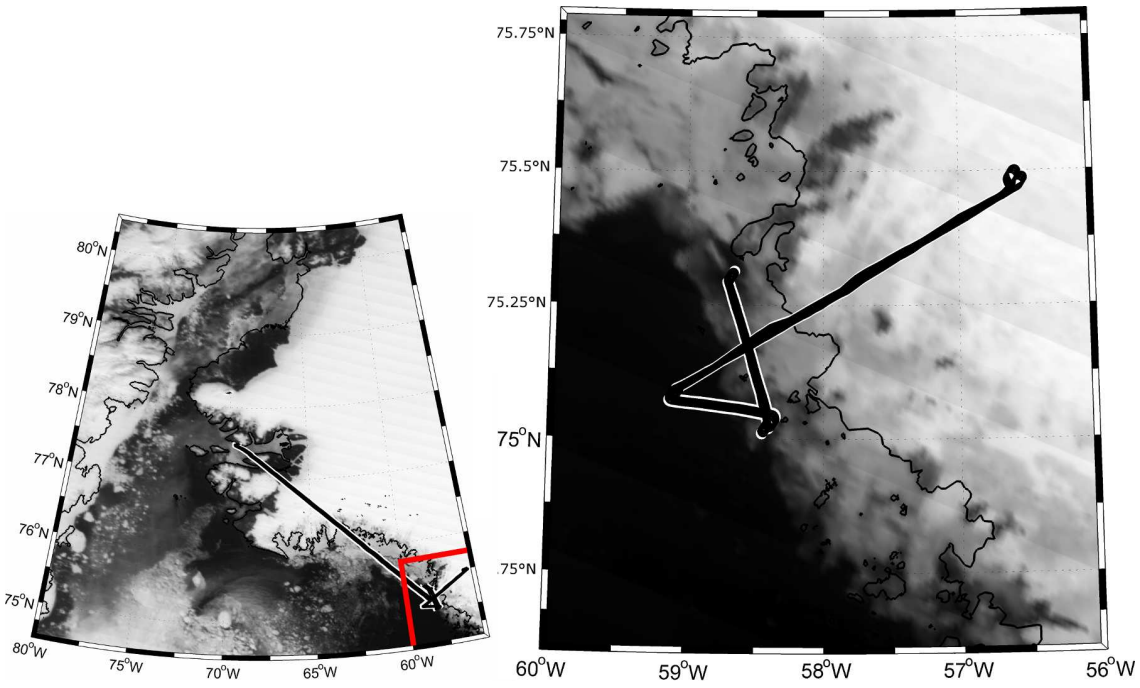

Figure 3.21: KA2 flight path superimposed on the MODIS channel 1 (620 – 670 nm) image for 17 June 2010, 1545 UTC. Left panel: The experimental area is marked in the lower right corner. Right panel: Experimental area. Transfer flight sections are eliminated.

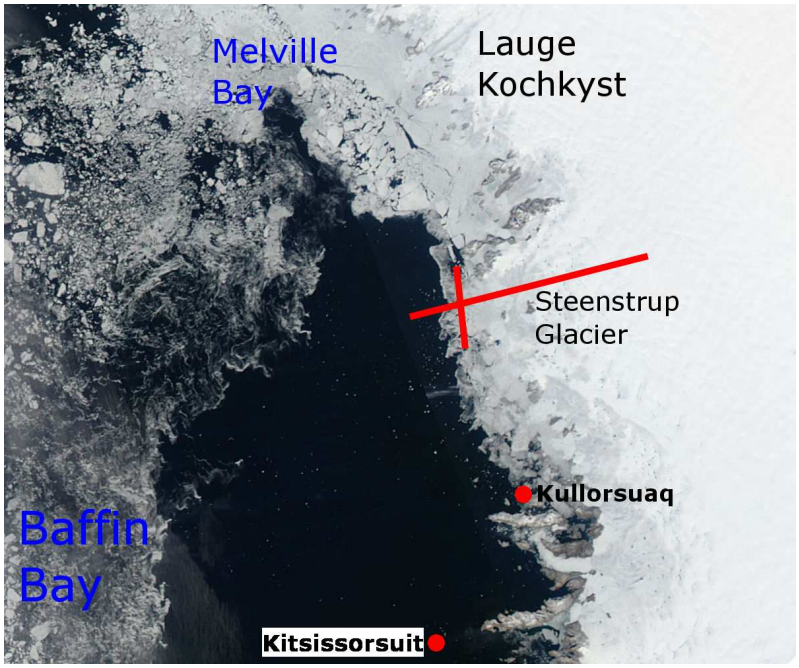

Figure 3.22: MODIS channel 1, 4, 3 true color image for 17 June 2010, 1545 UTC (modified from DMI) indicating the experimental area of KA2. The schematic flight pattern is shown as red lines.

Figure 3.23: Photo of the transition zone sea-ice/open water taken at a height of about 85 m AGL on port side of the POLAR 5 aircraft, 17 June 2010, 1625 UTC.

Figure 3.24: Photo of the ablation zone of the Steenstrup Glacier taken at a height of about 65 m AGL, 17 June 2010, 1600 UTC.

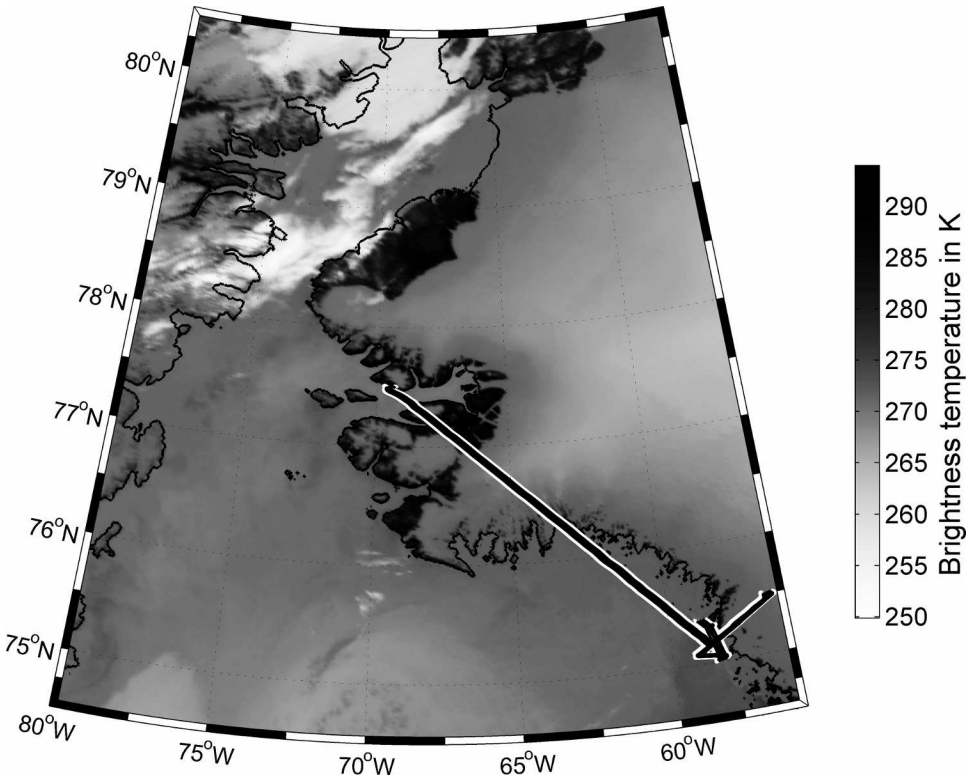

Figure 3.25: KA2 flight path superimposed on the MODIS channel 31 infrared brightness temperature image for 17 June 2010, 1545 UTC.

On 17 June 2010 the synoptic weather situation was characterized by a trough extending along the west coast of Greenland. It was associated with northerly winds at northern Baffin Bay and offshore winds from Lauge Kochkyst (Figure 3.26). The GME analysis shows 10 m-wind speeds of around 2.5 to 5 m s^{-1} down the Steenstrup Glacier (Figure 3.26). During KA2 no clouds were present (Figures 3.21 – 3.23, 3.25). While the visibility was excellent in the area of investigation, surface fog moved from the ice-free sea in northeast direction to Qaanaaq airport during flight KA2. In the afternoon the 2 m-temperature increased at Lauge Kochkyst to values above 3 °C, while the temperature stayed close to 0 °C above the glaciers (Figure 3.26).

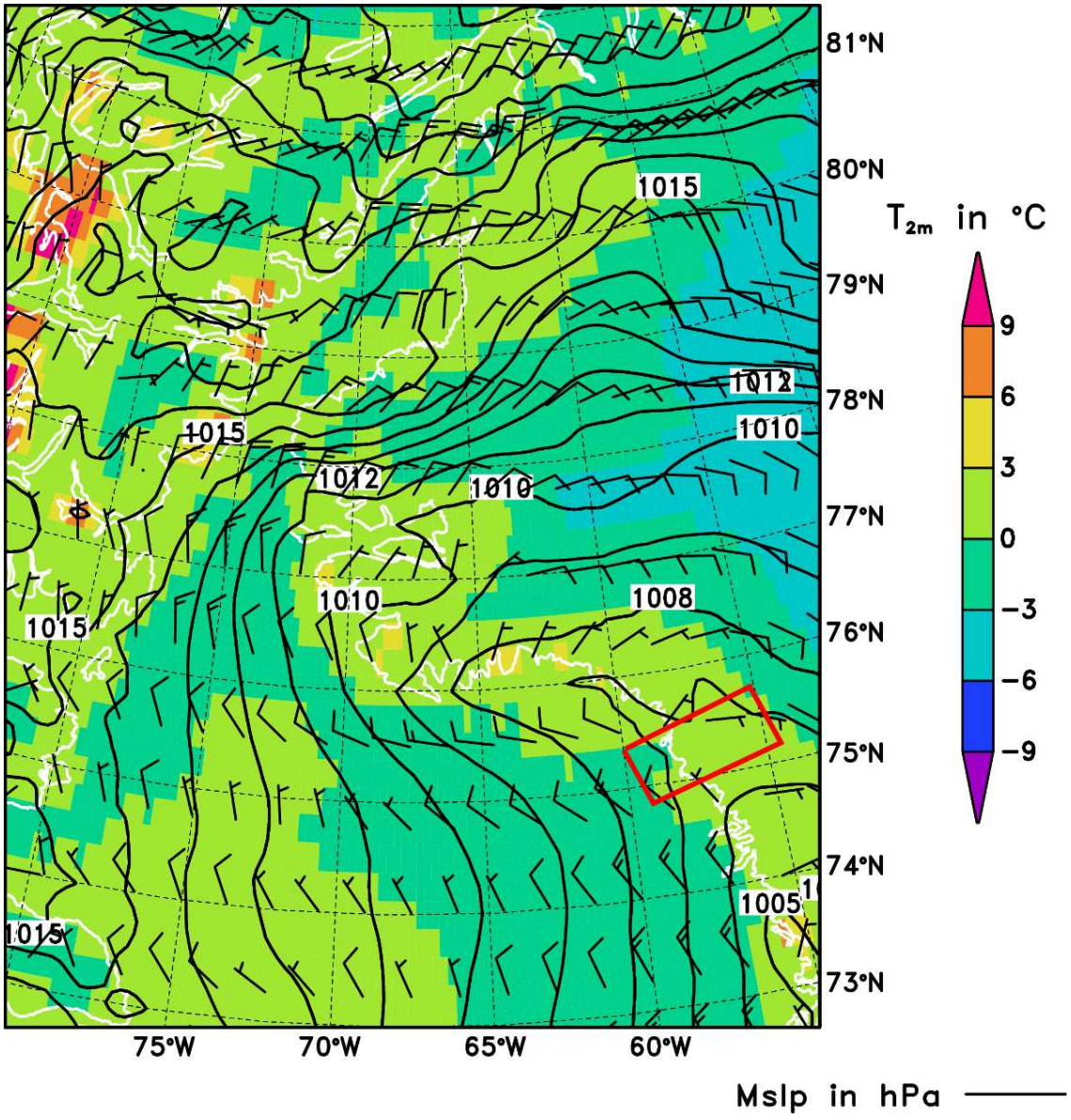

Figure 3.26: As Figure 3.9, but for the GME analysis for 17 June 2010, 1800 UTC.

3.6 Flight NOW1: 15 June 2010

The first NOW flight mission started at point A located at Smith Sound (for position see Table 3.11, Figure 3.27). From there a series of high aircraft temps (up to 800 m AGL) were performed southward to point B at northern Baffin Bay (for flight schedule and 3D flight path see Table 3.13, Figure 3.28). Then a constant level run (37 m AGL on average) with a length of 203 km (Table 3.12) was flown back.

Next, a transfer flight section took place to point Q1a. From there temps across the central line AB to point Q1b were flown in a range of 34 m to 332 m AGL followed by two constant low level runs on Q1 at mean heights of 38 m and 66 m AGL. This flight programme (one temp series, two legs at different heights) was repeated on a parallel cross-profile Q2 106 km south of Q1. According to a different PBL height the altitudes were slightly different than for Q1, and the length of Q2 was 4 km longer (a total of 70 km). Q1 and Q2 were restricted by the fact that there was no flight permission for Canadian territory.

Table 3.11: Mean geographic coordinates of the way points for NOW1.

Way point	Coordinates	
	Latitude in °N	Longitude in °W
A	78.189	73.477
B	76.362	74.001
Q1a	77.751	74.758
Q1b	77.749	71.951
Q2a	76.792	74.725
Q2b	76.798	71.960

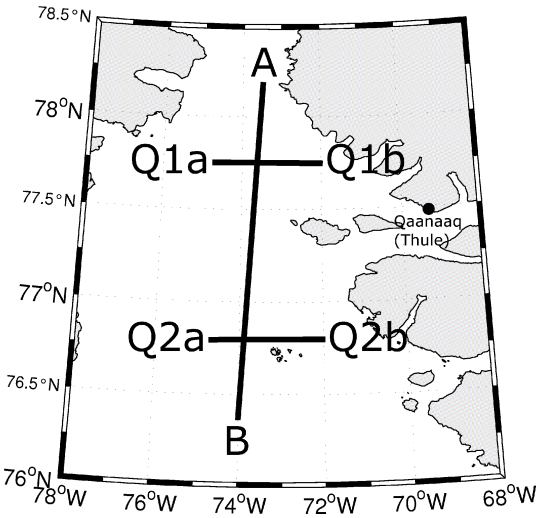

Figure 3.27: Schematic plot of the flight pattern during NOW1.

Table 3.12: Distances of the legs for NOW1.

Leg	Distance in km
A–B	203
Q1	66
Q2	70

Table 3.13: As Table 3.7, but for the schedule for NOW1.

	Begin		End				
Event number	UTC in hh:mm:ss	Position	UTC in hh:mm:ss	Position	Leg	Temp	Radar height in m
01	13:13:49	A	13:58:48	B		x	31–801
02	14:01:50	B	15:06:09	A	x		37
03	15:06:10	A	15:20:46	Q1a			
04	15:20:47	Q1a	15:39:02	Q1b		x	34–332
05	15:41:17	Q1b	15:58:55	Q1a	x		38
06	16:00:31	Q1a	16:21:27	Q1b	x		66
07	16:21:28	Q1b	16:56:18	Q2a			618
08	16:56:19	Q2a	17:15:46	Q2b		x	33–359
09	17:19:32	Q2b	17:39:10	Q2a	x		37
10	17:41:06	Q2a	18:00:32	Q2b	x		65

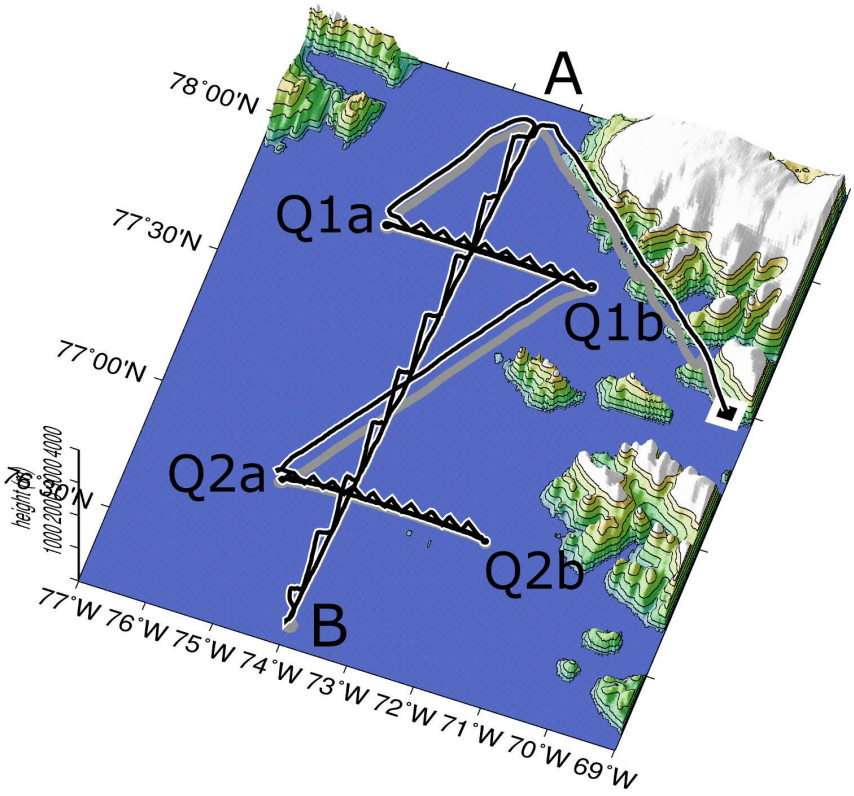

Figure 3.28: As Figure 3.8, but for the NOW1 flight path. Way points are indicated.

Most time of flight NOW1 was performed over open water area (for sea-ice maps/conditions see Figures 3.29 – 3.31). However, the NOW was covered by some ice floes.

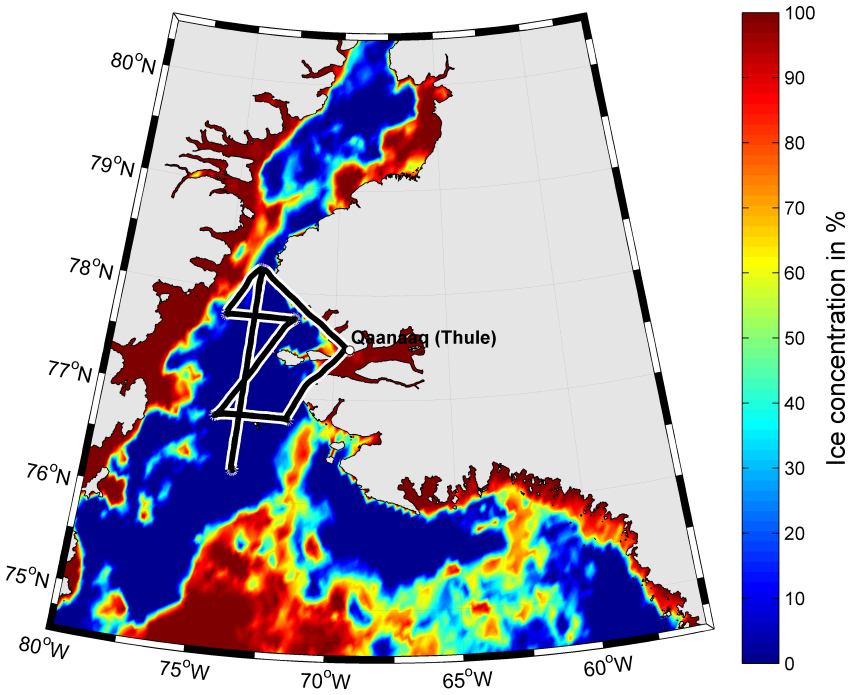

Figure 3.29: NOW1 flight path superimposed on the AMSR-E mean sea-ice concentration for 15 June 2010.

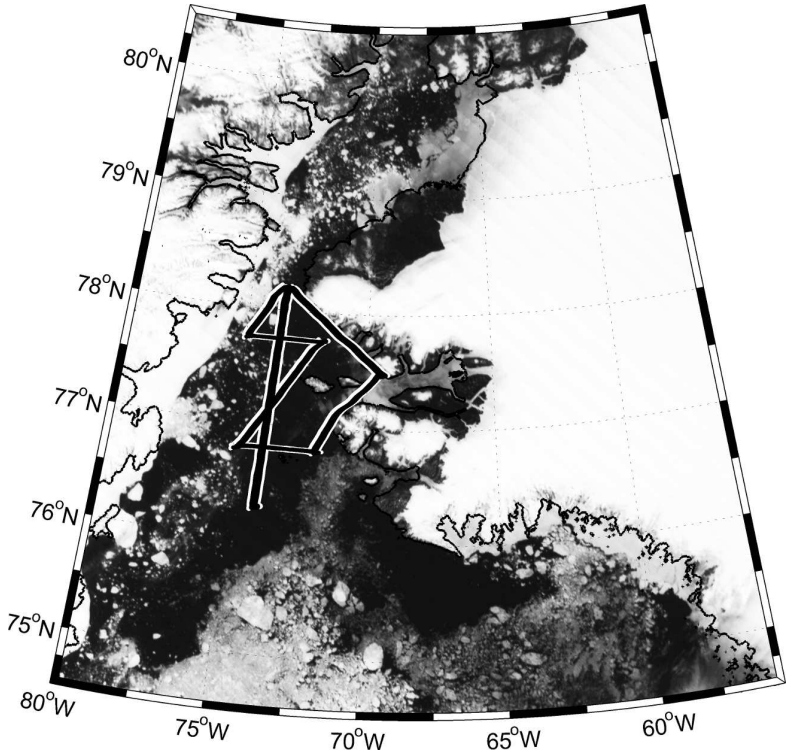

Figure 3.30: NOW1 flight path superimposed on the MODIS channel 1 (620 – 670 nm) image for 15 June 2010, 1735 UTC.

Figure 3.31: Photo of the NOW taken at a height of about 35 m AGL on bow side of the POLAR 5 aircraft, 15 June 2010, 1438 UTC.

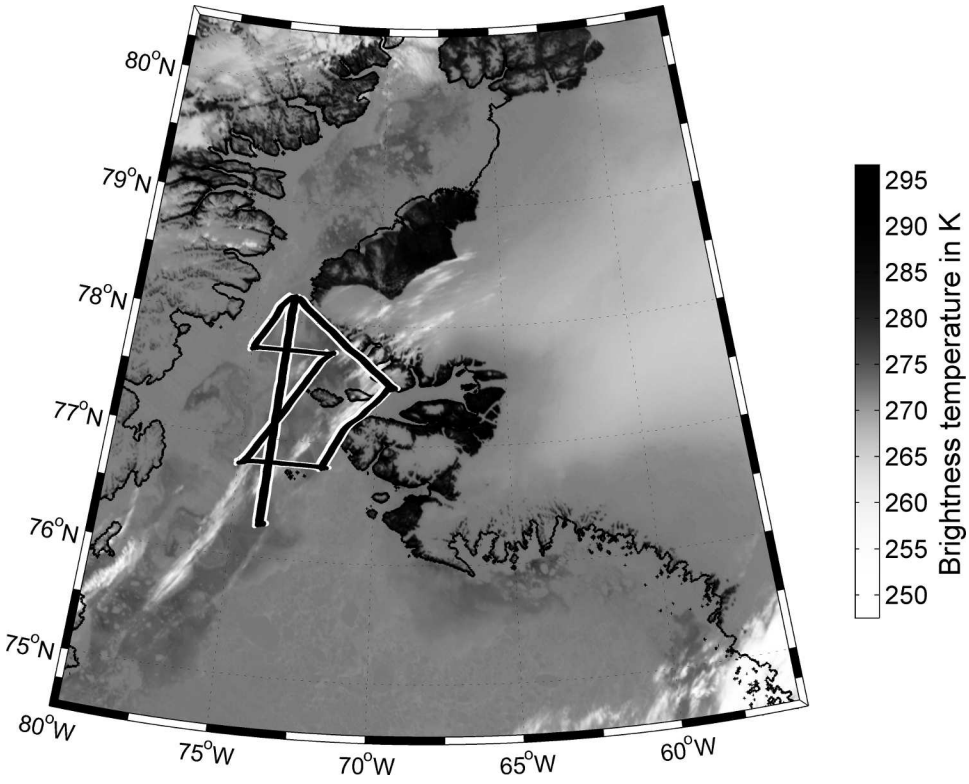

Figure 3.32: NOW1 flight path superimposed on the MODIS channel 31 infrared brightness temperature image for 15 June 2010, 1735 UTC.

The synoptic situation during NOW1 was dominated by an intense cyclone over western Greenland (center over Melville Bay, Figure 3.33). The GME analysis shows strong pressure gradients with 10 m-wind speeds up to 12 m s^{-1} above the NOW. In general, northerly winds were observed during the flight. Almost no clouds were present (Figures 3.30 – 3.32). GME 2-m temperatures are close to the freezing point of water (Figure 3.33).

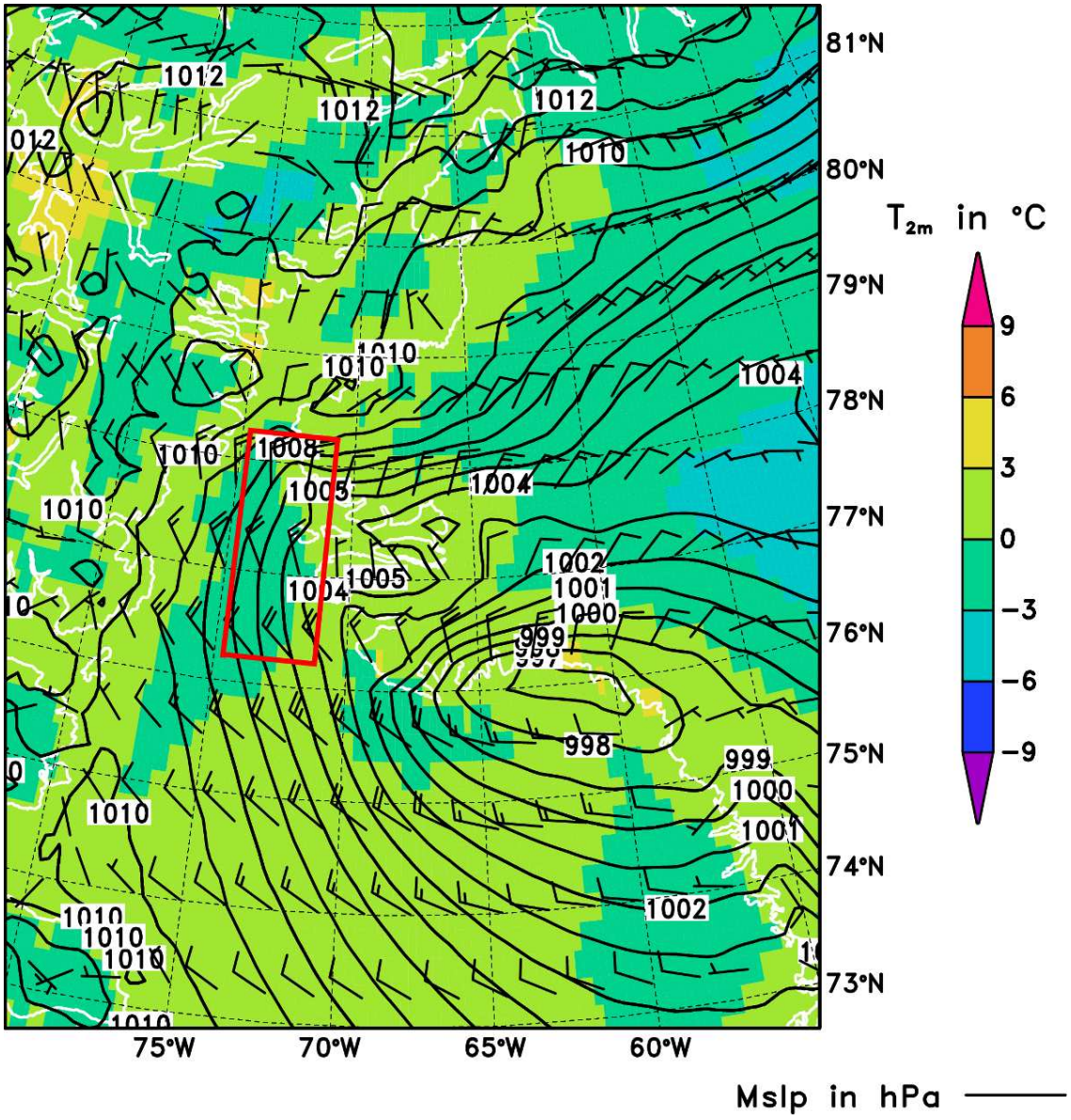

Figure 3.33: As Figure 3.9, but for the GME analysis for 15 June 2010, 1200 UTC.

3.7 Flight NOW2: 18 June 2010

The flight programme of NOW2 started at the same location as of NOW1 (point A at Smith Sound, for position see Table 3.14, Figure 3.34) with a series of high aircraft temps between 31 m and 785 m AGL southward to point B1 (for flight schedule and 3D flight path see Table 3.16, Figure 3.35). Leg A–B1 is shorter than A–B flown on 15 June (167 km compared to 203 km, compare Table 3.15 with 3.12). After temps to point B1 a constant low level run (40 m AGL on average) was flown back to point A.

Next, aircraft temps were performed to point Q1a in a range of 33 m to 337 m AGL. Then cross-profile Q1 was flown with temps followed by two constant level runs on Q1 at 39 m and 65 m AGL on average, respectively. On a parallel cross-profile Q3 27 km southward of Q1 this flight pattern (one temp series and two legs) was repeated with slightly different altitudes.

As on 17 June 2010 the radiation data processor failed.

Table 3.14: Mean geographic coordinates of the way points for NOW2.

Way point	Coordinates	
	Latitude in °N	Longitude in °W
A	78.199	73.499
B1	76.700	74.002
Q1a	77.747	74.748
Q1b	77.747	71.995
Q3a	77.501	74.773
Q3b	77.504	72.016

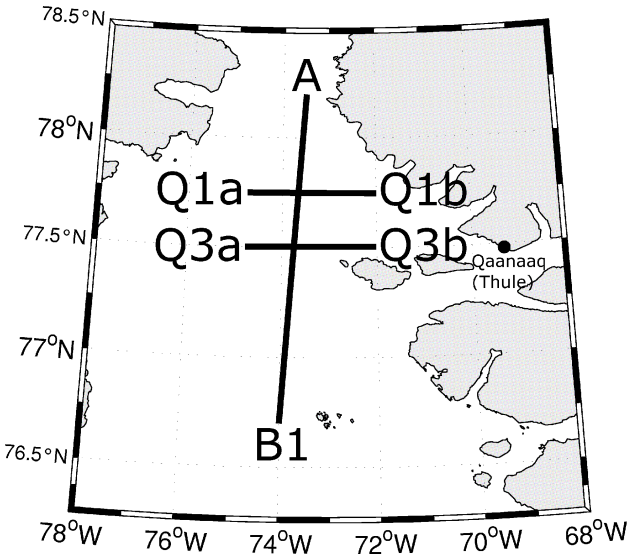

Figure 3.34: Schematic plot of the flight pattern during NOW2.

Table 3.15: Distances of the legs for NOW2.

Leg	Distance in km
A–B1	167
Q1	65
Q3	66

Table 3.16: As Table 3.7, but for the schedule for NOW2.

	Begin		End				
Event number	UTC in hh:mm:ss	Position	UTC in hh:mm:ss	Position	Leg	Temp	Radar height in m
01	14:20:27	A	15:02:56	B1		x	31–785
02	15:06:02	B1	16:01:22	A	x		38
03	16:02:38	A	16:14:36	Q1a		x	33–337
04	16:16:24	Q1a	16:32:53	Q1b		x	30–333
05	16:35:20	Q1b	16:54:38	Q1a	x		39
06	16:57:17	Q1a	17:15:48	Q1b	x		65
07	17:15:49	Q1b	17:23:40	Q3b			
08	17:23:41	Q3b	17:41:04	Q3a	x		41
09	17:44:24	Q3a	18:01:19	Q3b		x	31–333
10	18:03:53	Q3b	18:22:24	Q3a	x		68

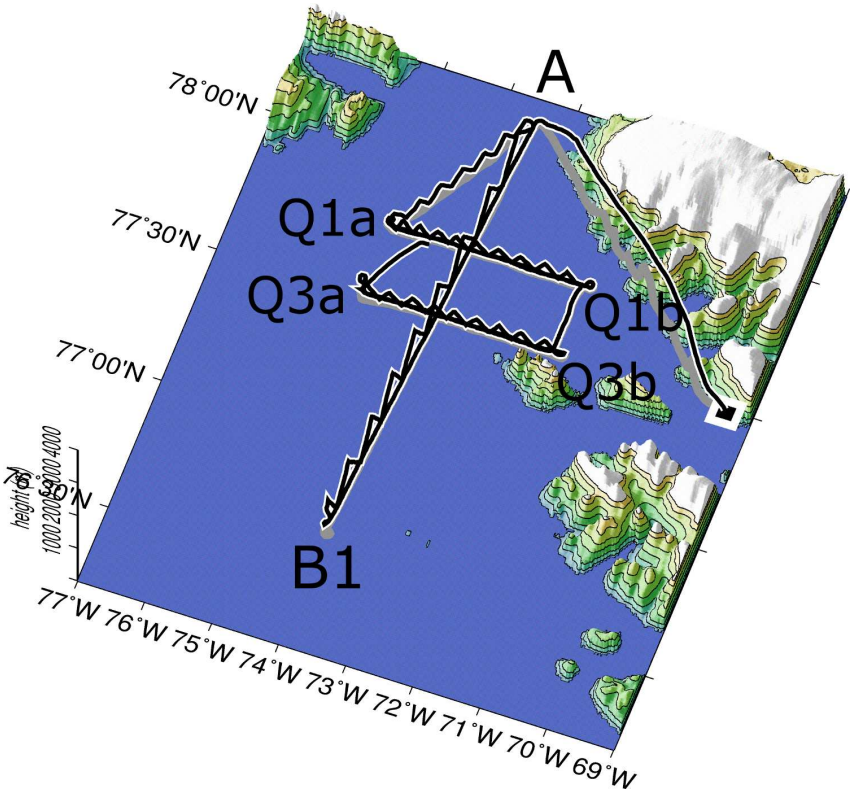

Figure 3.35: As Figure 3.8, but for the NOW2 flight path. Way points are indicated.

Most of the NOW2 flight mission took place over open water area (for sea-ice maps/conditions see Figures 3.36 – 3.37). The western part of northerly Baffin Bay was still characterized by high sea-ice coverage. The aircraft section A–Q1a was performed along the ice margin and over sea-ice. Like point Q1a the southern point Q3a is located at the ice edge. In particular the area south of point Q3a was covered by ice floes.

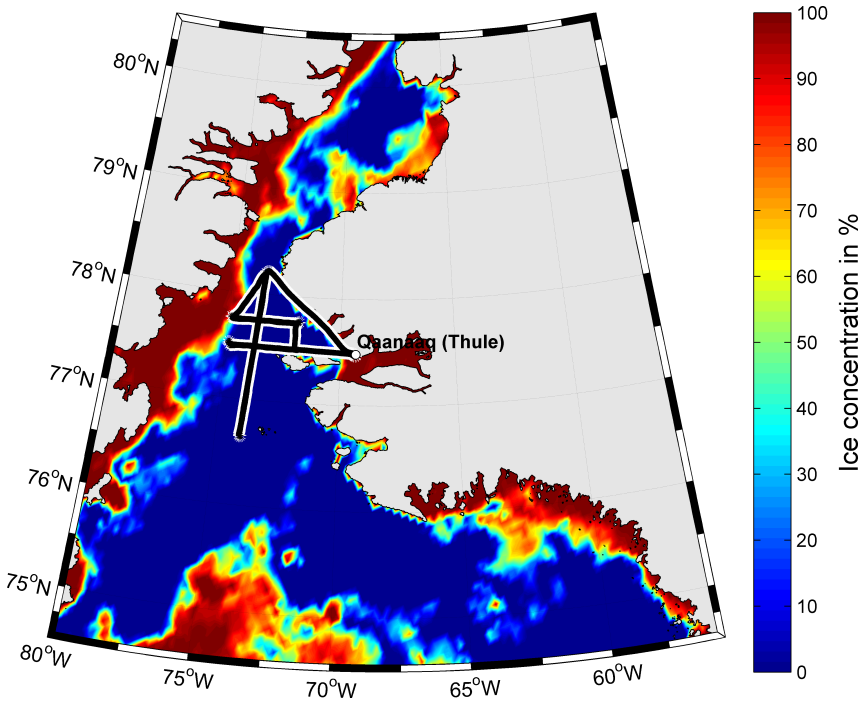

Figure 3.36: NOW2 flight path superimposed on the AMSR-E mean sea-ice concentration for 18 June 2010.

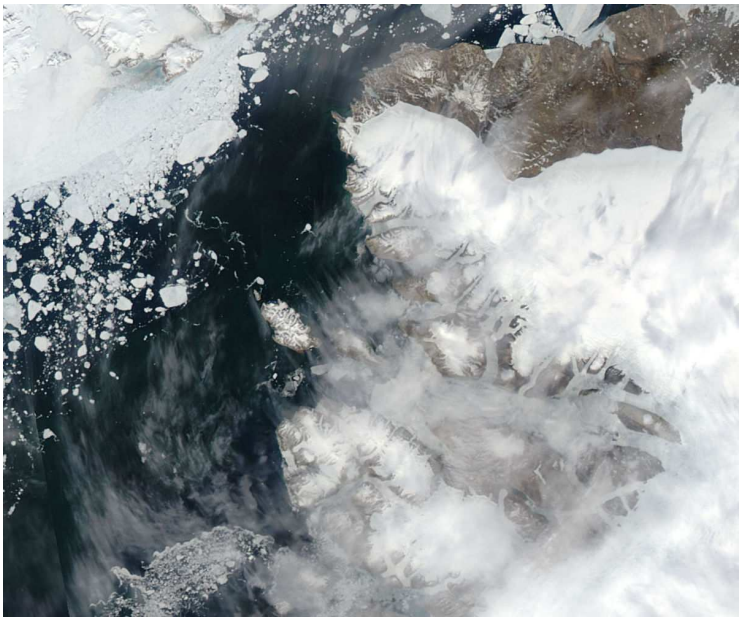

Figure 3.37: MODIS channel 1, 4, 3 true color image of Smith Sound for 18 June 2010, 1515 UTC (obtained from DMI).

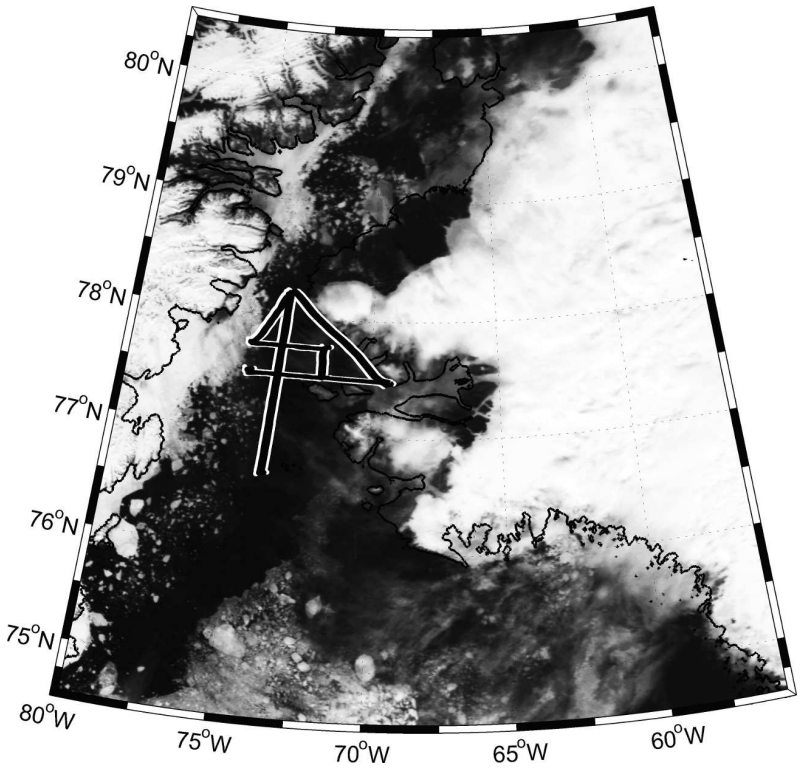

Figure 3.38: NOW2 flight path superimposed on the MODIS channel 1 (620 – 670 nm) image for 18 June 2010, 1650 UTC.

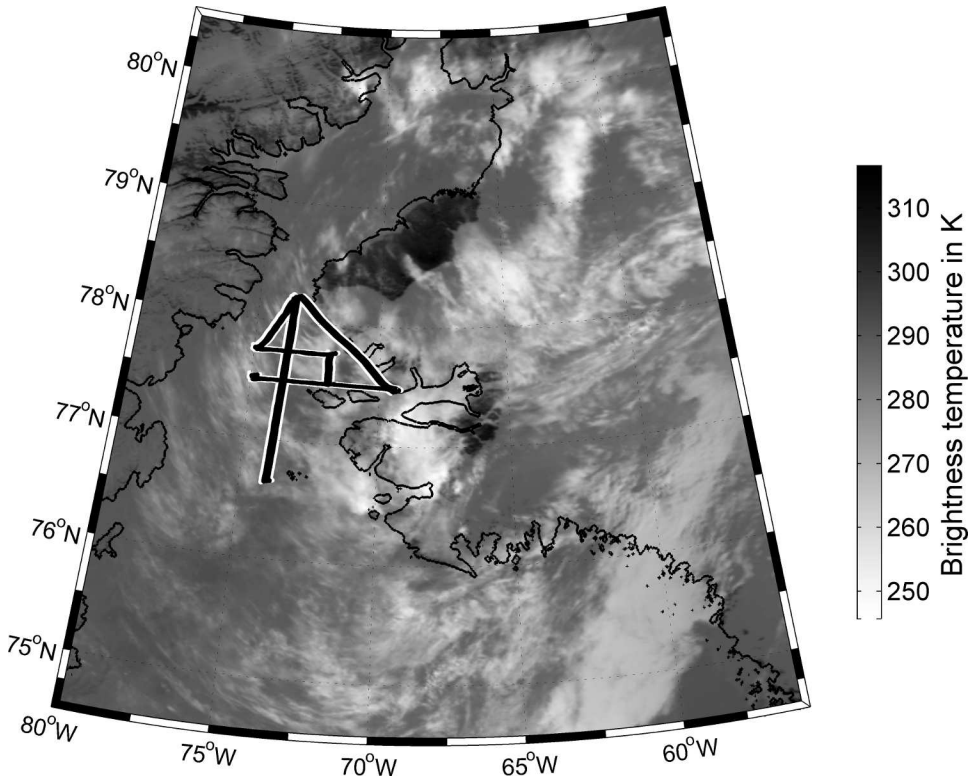

Figure 3.39: NOW2 flight path superimposed on the MODIS channel 31 infrared brightness temperature image for 18 June 2010, 1650 UTC.

The synoptic situation during NOW2 was characterized by a mesoscale low over Baffin Bay (Figure 3.40) accompanied with cirrus clouds (Figures 3.38 – 3.39, 3.41 and 3.42). Relatively warm air was advected to the south (Figure 3.40). As consequence of channeling effects at Smith Sound – the topography is steep on both sides of the Nares Strait – even the GME analysis shows 10 m-wind speed maxima of 18 m s^{-1}. Thus, sea-ice export was increased considerably by the channeling effect. In the Baffin Bay the wind speed decreased to approximately 5 m s^{-1} (Figure 3.40). Over the NOW the analysed 2 m-temperature is around 0 °C.

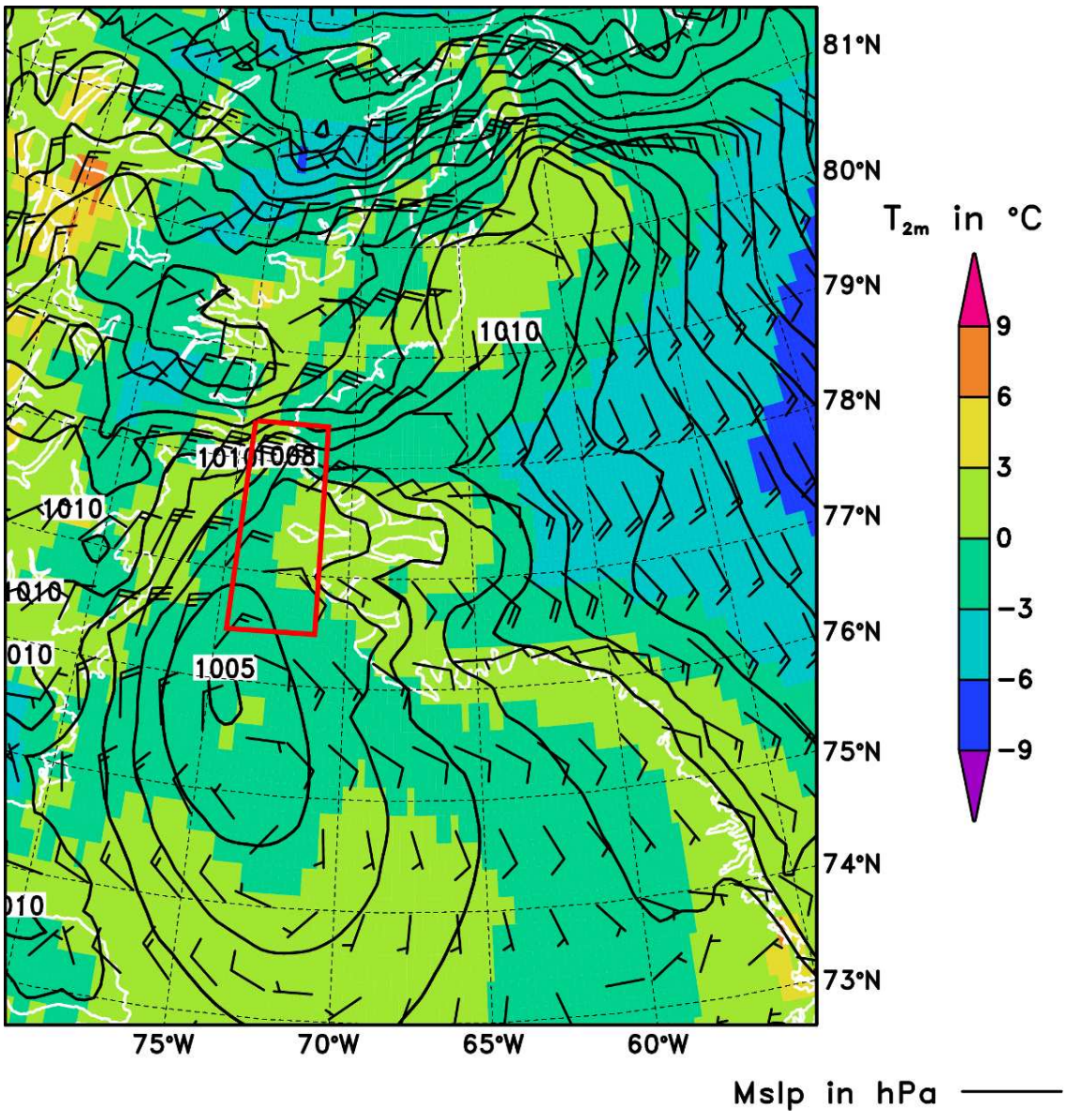

Figure 3.40: As Figure 3.9, but for the GME analysis for 18 June 2010, 1200 UTC.

Figure 3.41: Cloud conditions during NOW2. Photo taken at a height of about 95 m AGL on port side of the POLAR 5 aircraft, 18 June 2010, 1425 UTC.

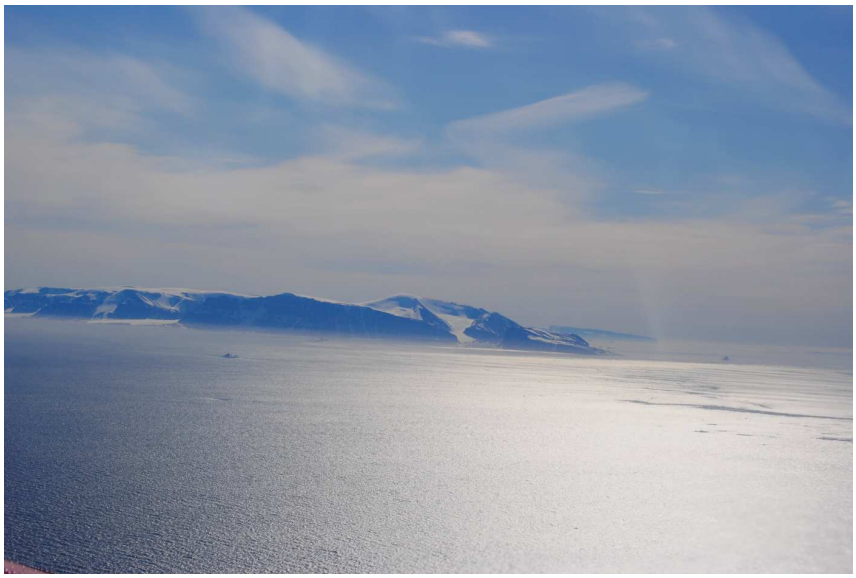

Figure 3.42: Cloud conditions during NOW2. Photo taken at a height of about 615 m AGL on port side of the POLAR 5 aircraft, 18 June 2010, 1425 UTC.

3.8 Flight NOW3: 22 June 2010

A flight programme similar to 18 June was flown with only some slight differences of the mean way point coordinates and altitudes (compare Tables 3.14 – 3.16 with 3.17 – 3.19, Figures 3.34, 3.35 with 3.43, 3.44).

After the repair of the radiation data acquisition processor, the recording of radiation data worked again. Though, data of the CR-2 dew point mirror of the basic instrumentation (Table 2.1) could not be processed.

Table 3.17: Mean geographic coordinates of the way points for NOW3.

Way point	Coordinates	
	Latitude in °N	Longitude in °W
A	78.197	73.509
B1	76.699	73.986
Q1a	77.751	74.768
Q1b	77.750	71.951
Q3a	77.500	74.779
Q3b	77.501	72.001

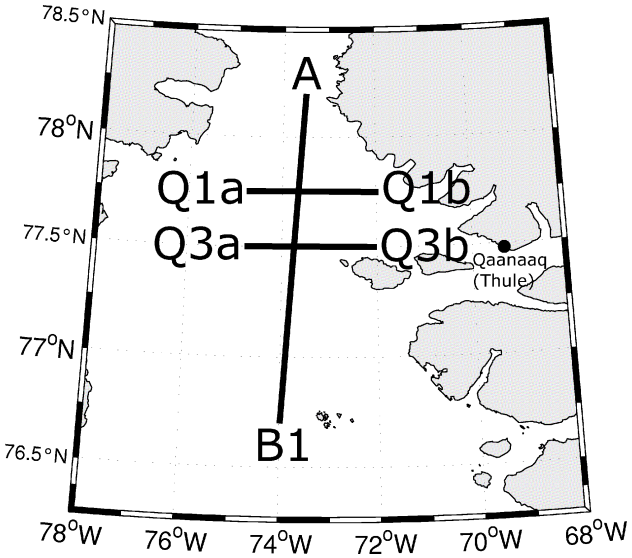

Figure 3.43: Schematic plot of the flight pattern during NOW3.

Table 3.18: Distances of the legs for NOW3.

Leg	Distance in km
A–B1	167
Q1	66
Q3	67

Table 3.19: As Table 3.7, but for the schedule for NOW3.

	Begin		End				
Event number	UTC in hh:mm:ss	Position	UTC in hh:mm:ss	Position	Leg	Temp	Radar height in m
01	12:42:37	A	13:21:04	B1		x	29–810
02	13:22:54	B1	14:21:06	A	x		40
03	14:21:59	A	14:34:04	Q1a		x	30–341
04	14:36:02	Q1a	14:55:24	Q1b		x	27–348
05	14:57:22	Q1b	15:16:50	Q1a	x		40
06	15:18:45	Q1a	15:37:50	Q1b	x		63
07	15:37:51	Q1b	15:45:55	Q3b	x		
08	15:45:56	Q3b	16:04:29	Q3a	x		38
10	16:07:00	Q3a	16:26:00	Q3b		x	26–343
11	16:28:13	Q3b	16:47:56	Q3a	x		63

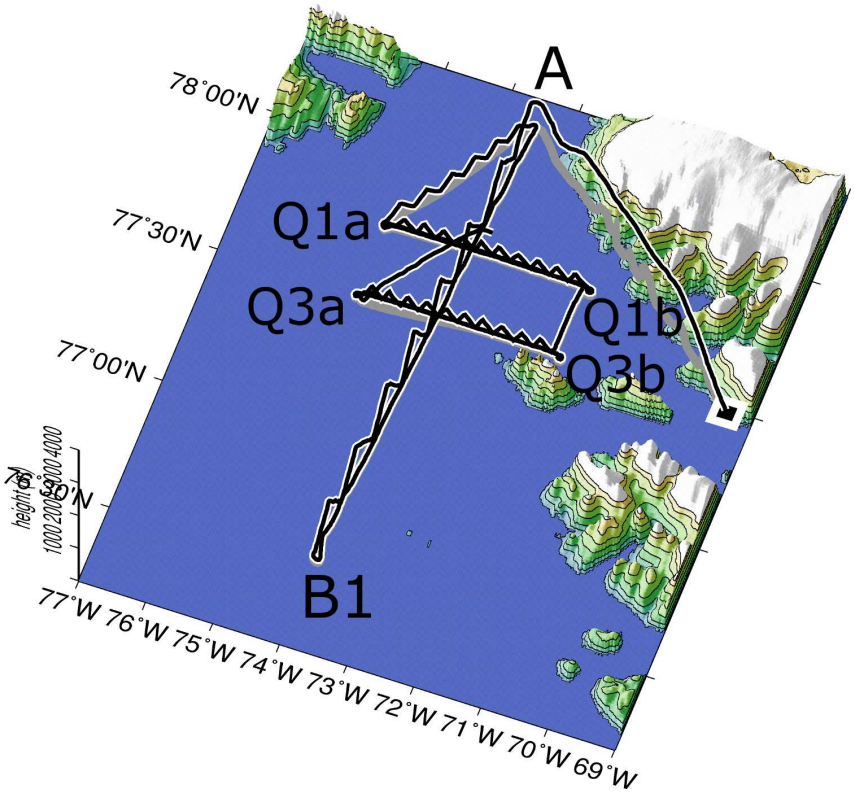

Figure 3.44: As Figure 3.8, but for the NOW3 flight path. Way points are indicated.

In contrast to the previous flight (NOW2) the width of the ice band along the coast of Ellesmere Island has changed at some places, and was more consolidated (compare Figures 3.36, 3.38 with 3.45, 3.47). Points Q1a and Q3a were still at the ice edge.

Overall, on 22 June 2010 the open water area was larger south of Smith Sound than on 14 June 2010 (compare Figures 3.45 – 3.47 with 3.12 – 3.14), while sea-ice concentration was higher at Nares Strait . Ice was blocked by an arch built up at Smith Sound, a quite common phenomena (see e.g. *Barber et al.*, 2001a; *Yao and Tang*, 2003; *Kwok et al.*, 2010). Except a small opening at the coast of Greenland the arch was closed completely.

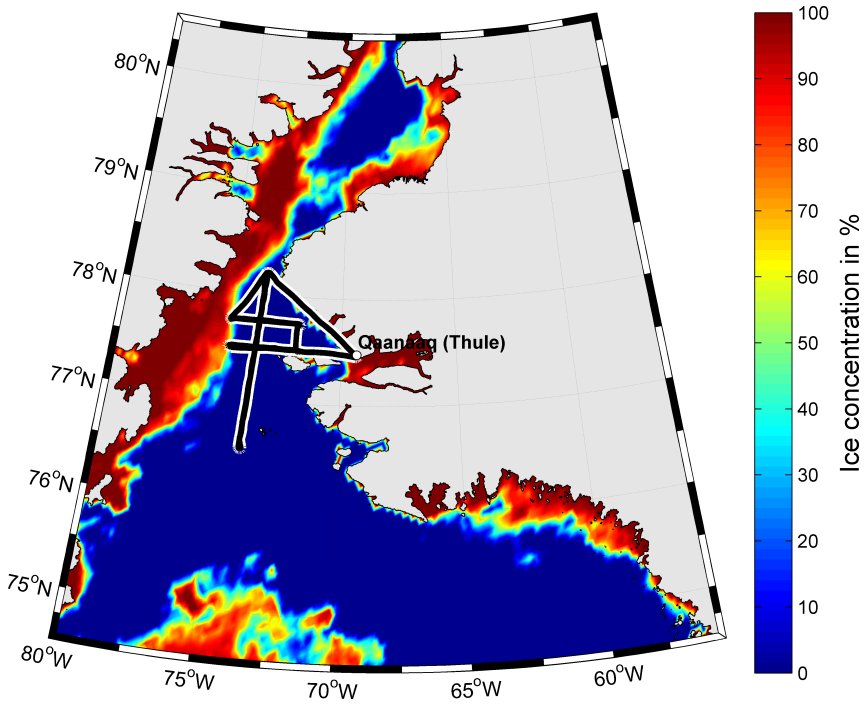

Figure 3.45: NOW3 flight path superimposed on the AMSR-E mean sea-ice concentration for 22 June 2010.

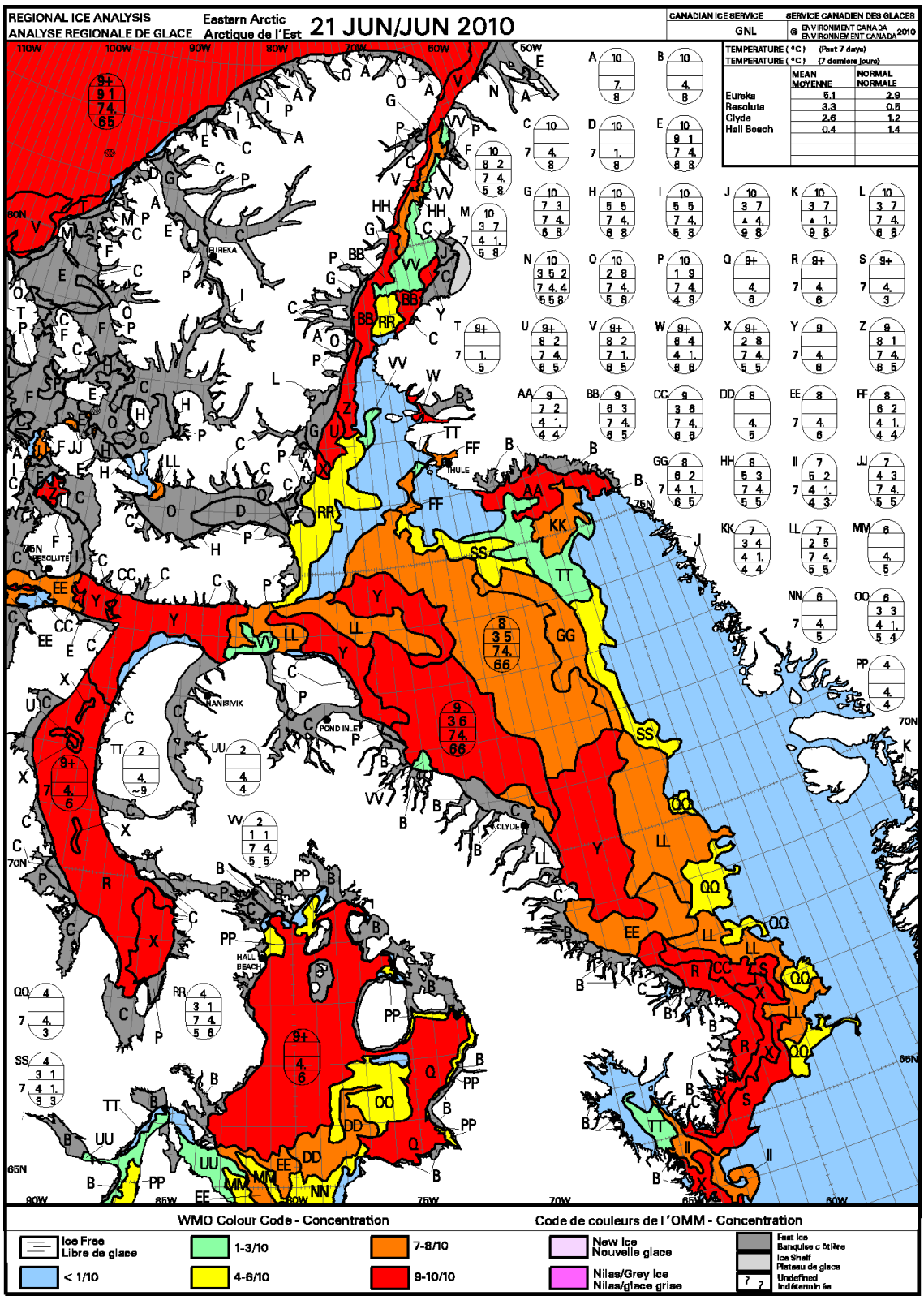

Figure 3.46: Sea-ice chart from Environmental Canada valid for the week of 21 June 2010.

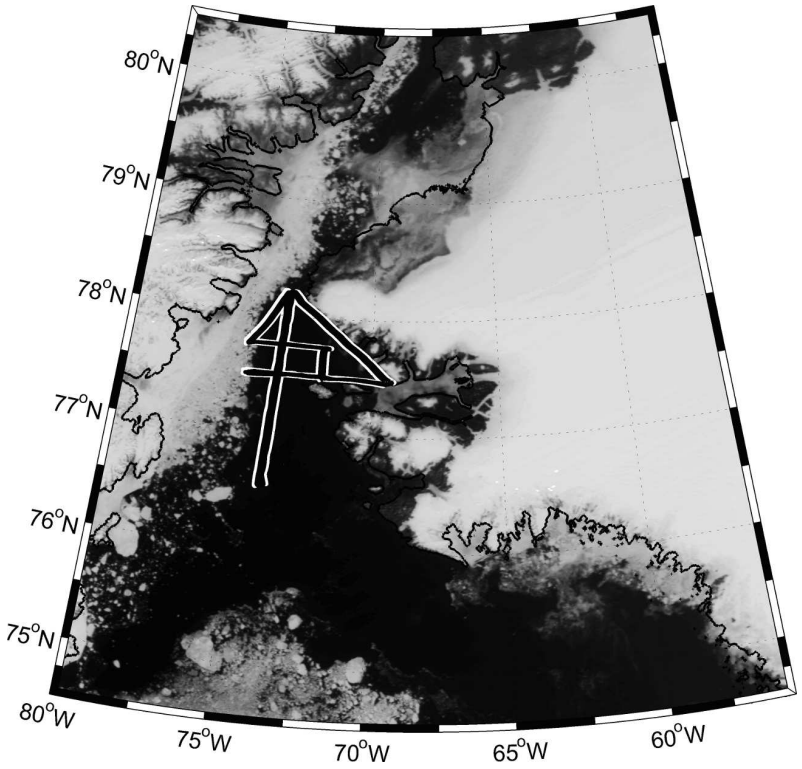

Figure 3.47: NOW3 flight path superimposed on the MODIS channel 1 (620 – 670 nm) image for 22 June 2010, 1625 UTC.

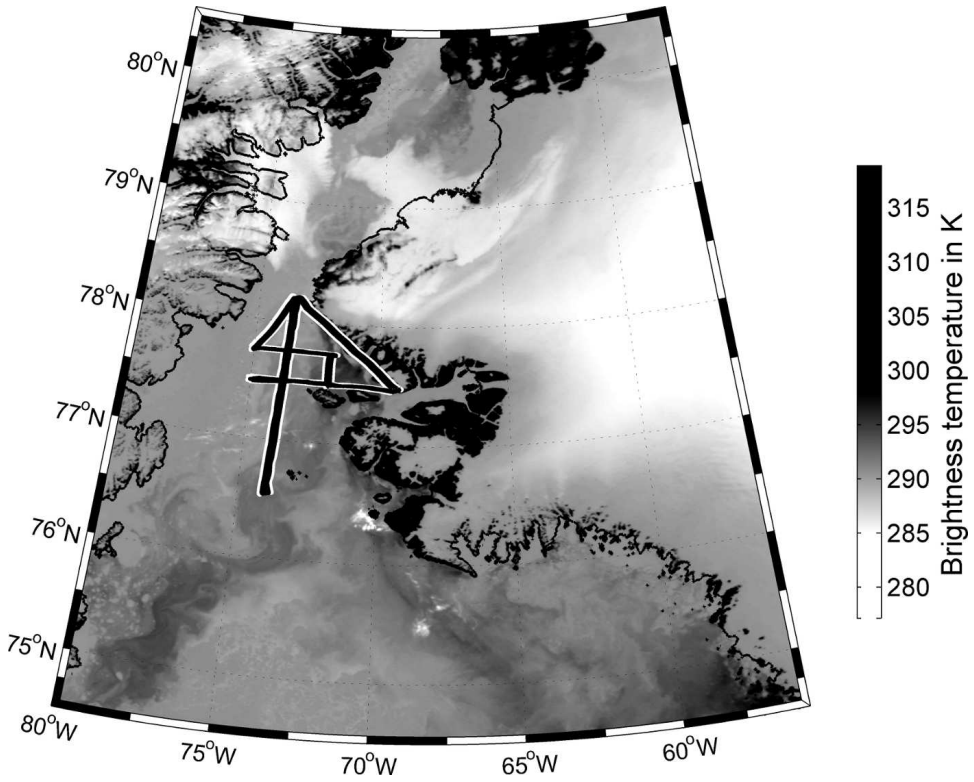

Figure 3.48: NOW3 flight path superimposed on the MODIS channel 31 infrared brightness temperature image for 22 June 2010, 1625 UTC.

During NOW3 a low pressure system over Lauge Kochkyst was associated with northerly winds through Nares Strait and over most parts of the NOW (Figure 3.49). The GME analysis shows 10 m-wind speeds ranging from around 5 to 10 m s^{-1}. Strong winds are analysed in northern Baffin Bay close to Smith Sound. A wind speed gradient is visible by different wave heights in Figures 3.50 and 3.51. Over central NOW the analysed 2 m-temperature was close to 0 °C, while in the coastal areas temperatures were generally between 0 and 5 °C (Figure 3.49). During the flight no clouds were present (Figures 3.47, 3.48). The infrared satellite image (Figure 3.48) indicates higher surface temperatures at point B1 than at point A.

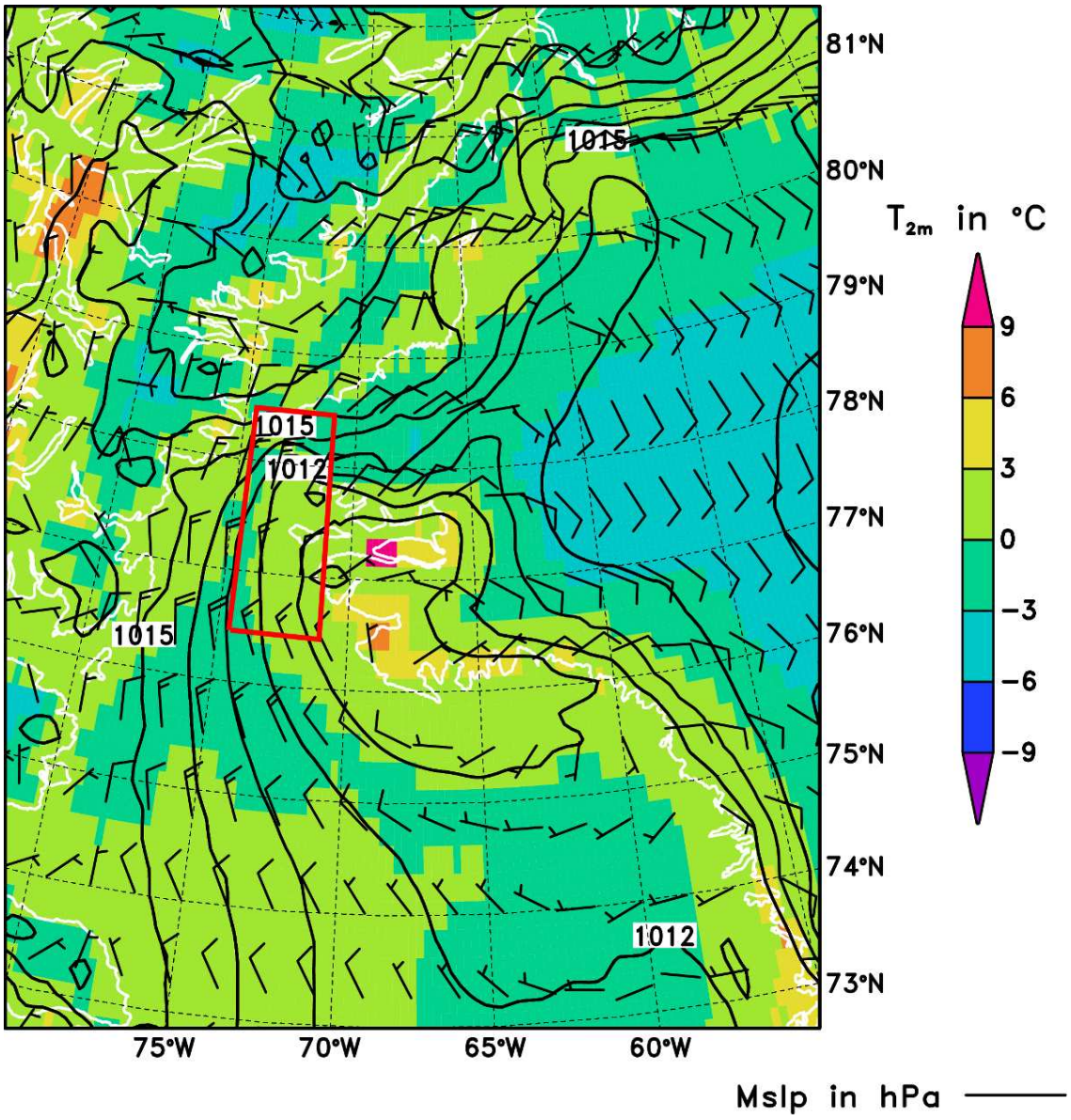

Figure 3.49: As Figure 3.9, but for the GME analysis for 22 June 2010, 1200 UTC.

Figure 3.50: Sea stage during NOW3 at northern Baffin Bay (77.74 °N, 73.65 °W). Photo taken at a height of about 40 m AGL on bow side of the POLAR 5 aircraft, 22 June 2010, 1404 UTC.

Figure 3.51: Sea stage during NOW3 at north-eastern Baffin Bay (77.74 °N, 72.44 °W). Photo taken at a height of about 40 m AGL on port side of the POLAR 5 aircraft, 22 June 2010, 1535 UTC.

3.9 Flight NOW4: 23 June 2010

The flight programme of NOW3 started at point B1 (northern Baffin Bay, for position see Table 3.20, Figure 3.52) with high aircraft temps from 25 m to 791 m AGL in northern direction to point M1 (for flight schedule and 3D flight path see Table 3.22, Figure 3.53). The series of aircraft temps was continued further northward to point C in southern Kane Basin. The distances of B1–M1 and M1–C are about 106 km and 129 km, respectively (Table 3.21). Then a constant level run at a mean height of 64 m AGL was flown back to point M1, followed by a low level run (39 m on average) to point Q4a located 13 km east of C.

On the cross-profile Q4 (Q4b is near the coast of Greenland) one series of temps (30 m to 308 m AGL) two constant level runs at 37 m and 93 m AGL and two higher temps (452 m and 573 m AGL) were flown. The temps were continued from point Q4a to M1. Then cross-profile Q5 was flown, with one series of temps up to 612 m AGL and two constant level runs at 39 m AGL and 96 m AGL on average, respectively. Q5 is quasi parallel to Q4, both profiles have a similar length of about 38 km.

Table 3.20: Mean geographic coordinates of the way points for NOW4.

Way point	Coordinates	
	Latitude in °N	Longitude in °W
B1	76.802	74.054
M1	77.748	74.501
C	78.790	72.010
Q4a	78.850	72.522
Q4b	78.702	71.000
Q5a	77.748	74.683
Q5b	77.600	73.199

Table 3.21: Distances of the legs for NOW4.

Leg	Distance in km
B1–M1	106
M1–C	129
Q4	37
Q5	39

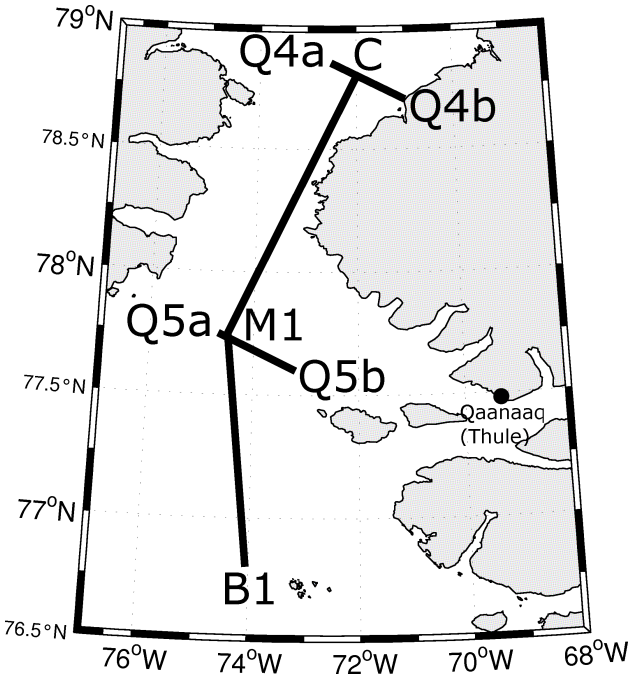

Figure 3.52: Schematic plot of the flight pattern during NOW4.

Table 3.22: As Table 3.7, but for the schedule for NOW4.

	Begin		End				
Event number	UTC in hh:mm:ss	Position	UTC in hh:mm:ss	Position	Leg	Temp	Radar height in m
01	13:44:17	B1	14:09:04	M1		x	25–791
02	14:12:02	M1	14:52:40	C		x	31–805
03	14:57:22	C	15:26:24	M1	x		64
04	15:30:03	M1	16:07:59	Q4a	x		39
05	16:11:11	Q4a	16:18:23	Q4b		x	30–308
06	16:23:33	Q4b	16:34:00	Q4a	x		37
07	16:37:44	Q4a	16:48:59	Q4b	x		93
08	16:51:33	Q4b	16:54:14			x	30–452
	16:54:15		17:01:18	Q4a		x	26–573
09	17:03:06	Q4a	17:30:29	M1		x	32–593
10	17:30:30	M1	17:35:44	Q5a			
11	17:35:45	Q5a	17:46:18	Q5b		x	33–612
12	17:50:15	Q5b	18:00:16	Q5a	x		39
13	18:02:01	Q5a	18:11:59	Q5b	x		96

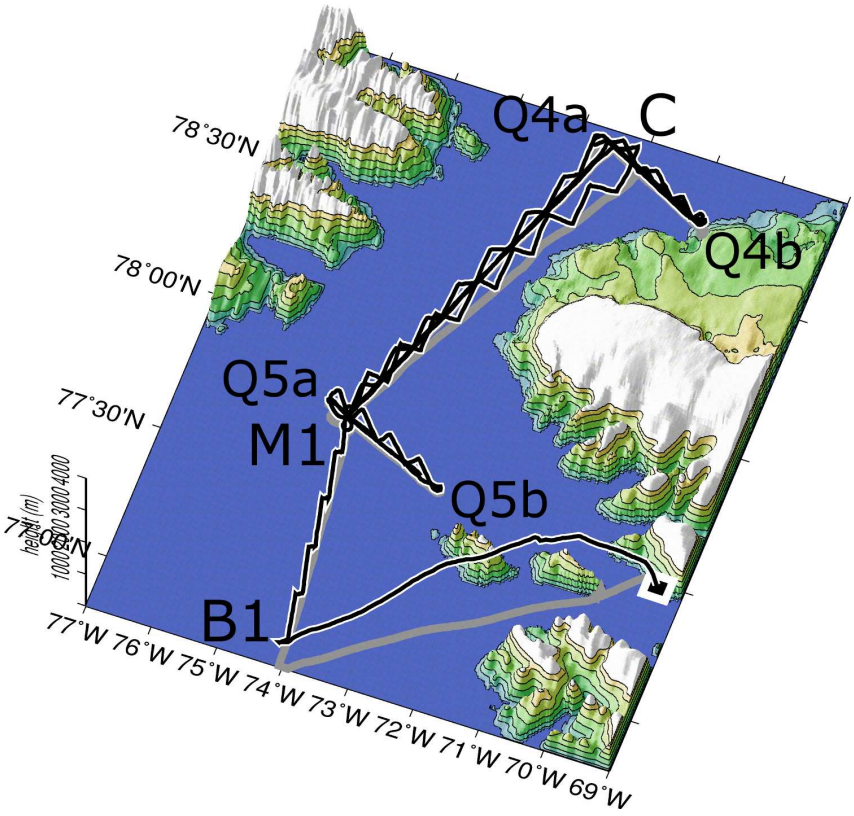

Figure 3.53: As Figure 3.8, but for the NOW4 flight path. Way points are indicated.

In northern part of the NOW4 flight pattern the sea-ice conditions were variable (for sea-ice maps/conditions see Figures 3.54 – 3.58). Smith Sound was almost covered with sea-ice. Sea-ice conditions in the southern Kane Basin are characterized by a large number of sea-ice floes of variable size.

In general, the southern part of NOW4 was flown over open water parallel to the sea-ice front and along the Canadian boarder. Some low clouds were detected near Smith Sound (Figure 3.58).

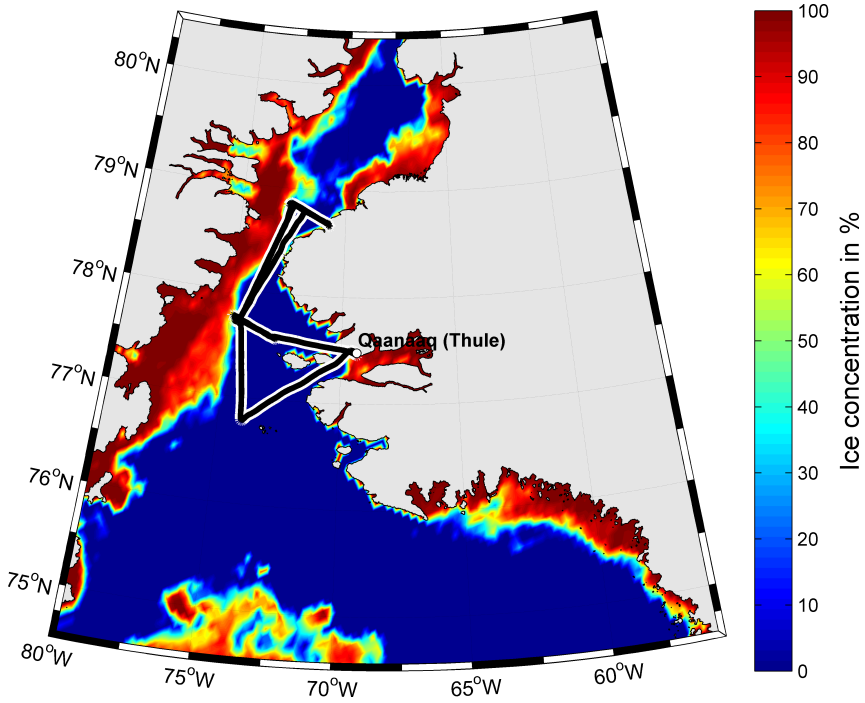

Figure 3.54: NOW4 flight path superimposed on the AMSR-E mean sea-ice concentration for 23 June 2010.

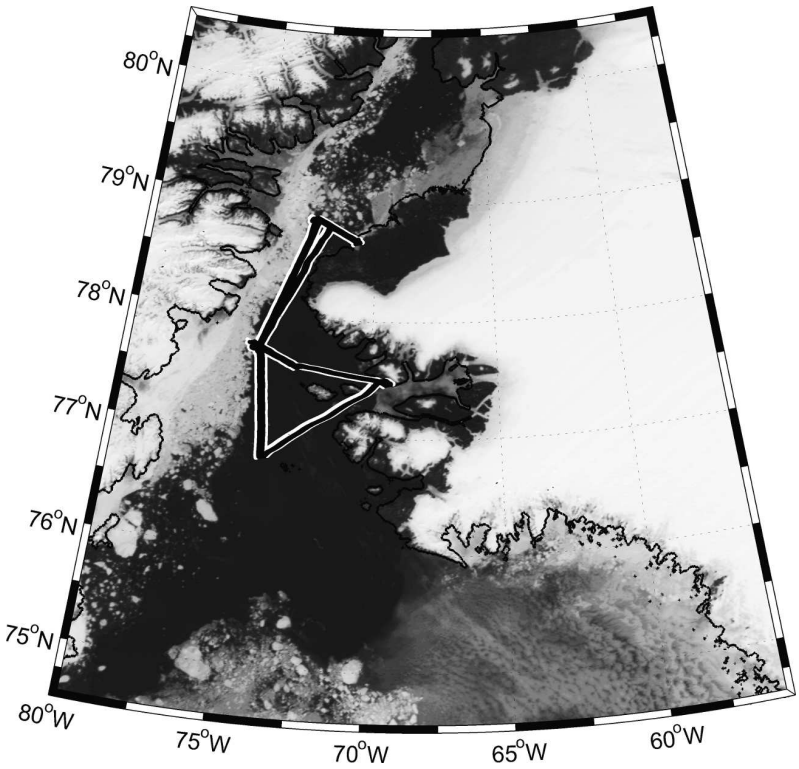

Figure 3.55: NOW4 flight path superimposed on the MODIS channel 1 (620 – 670 nm) image for 23 June 2010, 1530 UTC.

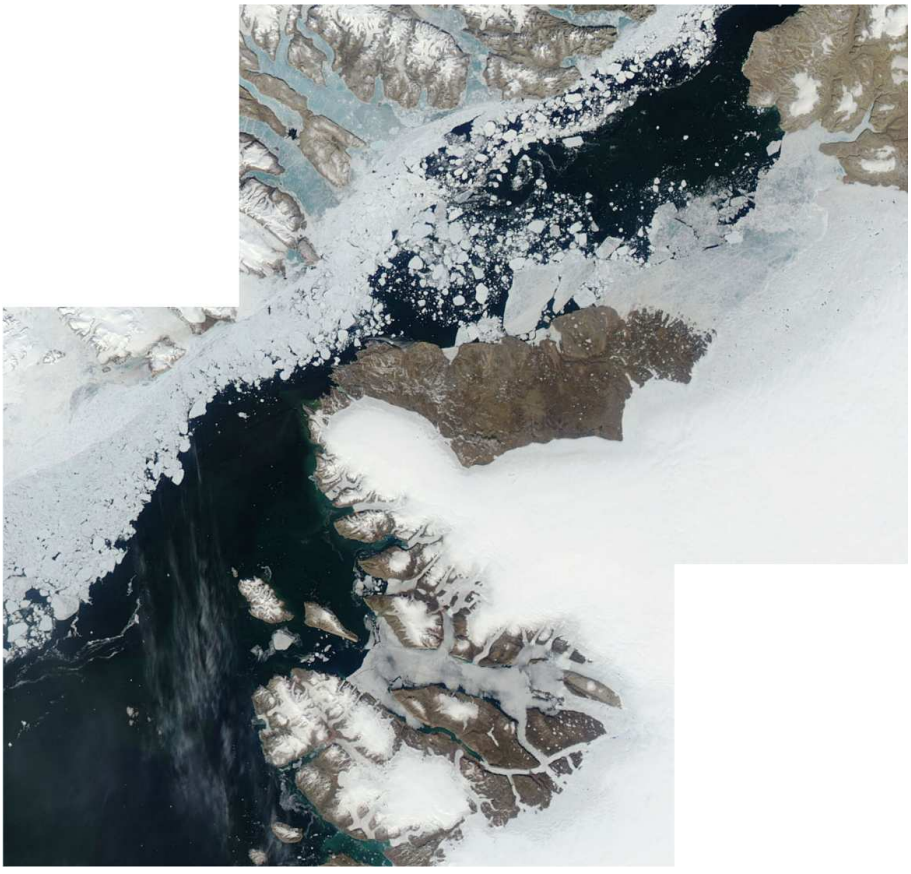

Figure 3.56: MODIS channel 1, 4, 3 true color image of southern Nares Strait for 23 June 2010, 1530 UTC (obtained from DMI).

Figure 3.57: Surface conditions during NOW4 over the central NOW (76.87 °N, 74.07 °W). Photo taken at a height of about 918 m AGL on bow side of the POLAR 5 aircraft, 23 June 2010, 1343 UTC.

Figure 3.58: Surface conditions during NOW4 at Smith Sound (78.45 °N, 73.29 °W). Photo taken at a height of about 75 m AGL on port side of the POLAR 5 aircraft, 23 June 2010, 1508 UTC.

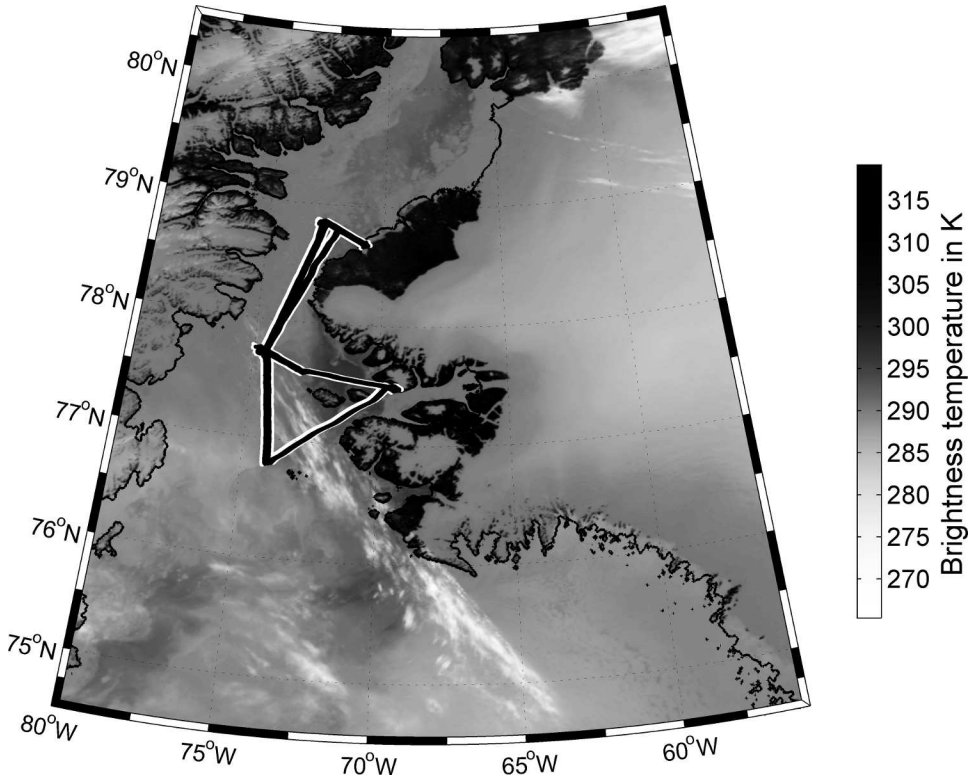

Figure 3.59: NOW4 flight path superimposed on the MODIS channel 31 infrared brightness temperature image for 23 June 2010, 1530 UTC.

The synoptic situation during NOW4 was characterized by a high pressure system over central Greenland and a trough over Baffin Bay (Figure 3.60). In the flight area northerly winds were analysed. In general, the GME 2 m-temperature was slightly higher than 0 °C (Figure 3.60). Temperatures below 0 °C were associated with open water areas. The satellite images (Figures 3.56, 3.59) show some thin clouds south of Smith Sound.

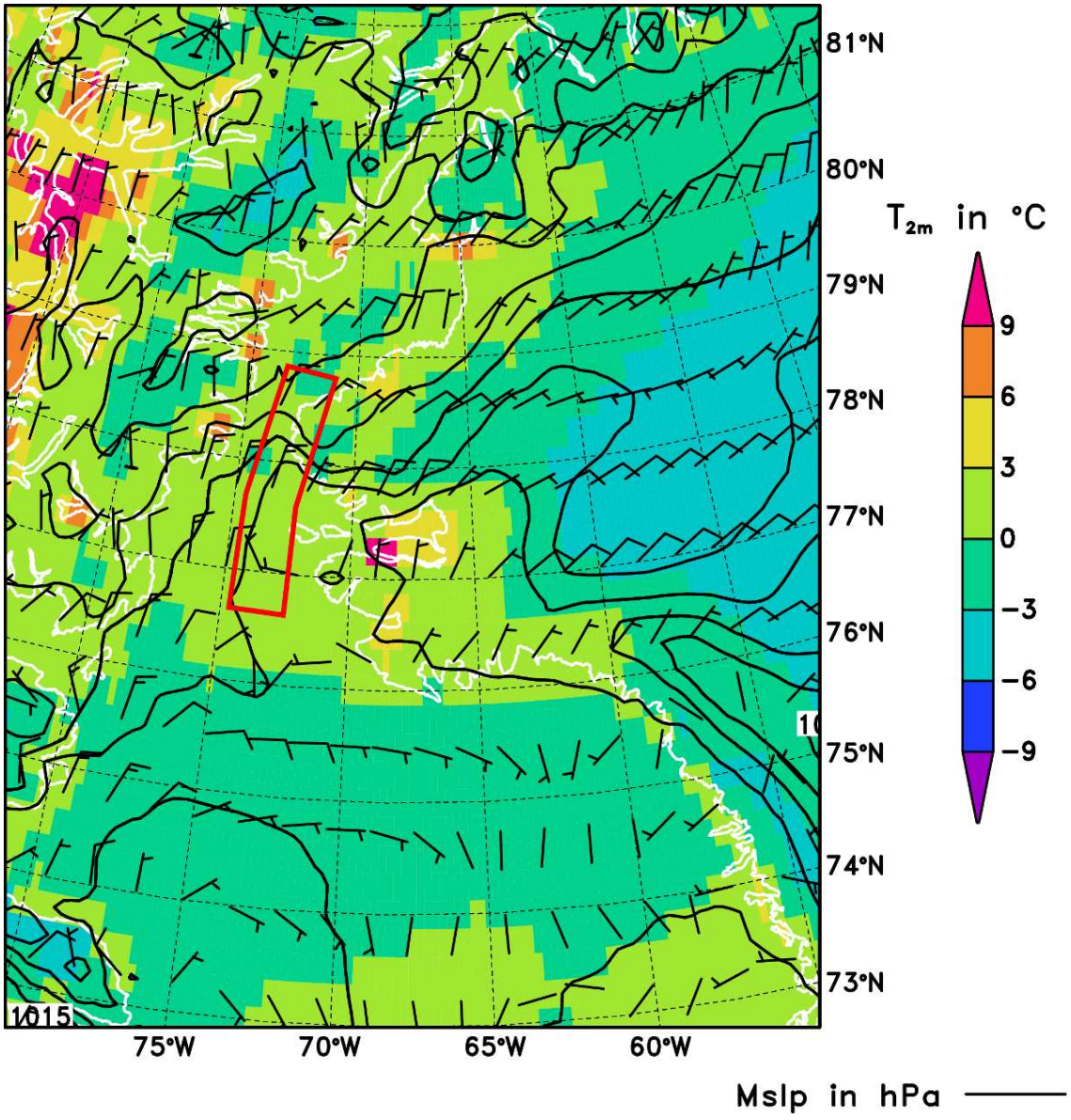

Figure 3.60: As Figure 3.9, but for the GME analysis for 23 June 2010, 1200 UTC.

Chapter 4

POLAR 5 calibration

4.1 General

POLAR 5 carries a large number of sensors. Many of them require calibration in order to derive meteorological quantities (*Lenschow*, 1986). The calibration data needed falls into four groups.

The first group contains conversion factors between sensor signals and physical quantities regarded as fixed values. In this case, either manufacturer-supplied calibration coefficients are used, measurements are supplied digitally as calibrated values or the sensor uses an internal calibration and delivers a "calibrated" electrical signal that can be translated using a simple conversion factor. Such sensors are the radar altimeters, the KT15 radiation thermometer, the dew point mirror, all Pt-100 thermometers, the pressure sensors and the Lyman-α Hygrometer (see Table 2.1).

The second group contains calibration factors that have to be verified in laboratory on a regular schedule. These calibrations are typically repeated in intervals from several months to a few years. Such sensors are humicaps, pyranometers and pyrgeometers.

The third group contains instrument properties that are either undocumented or arise from interactions between sensors and the whole measurement platform. Such coefficients are sensors (plus housing) time constants, aerodynamic recovery factors, pivots between sensor locations and time lags in turbulence data processing.

The fourth group contains coefficients similar to the third group, but specific to each experiment. Such coefficients either (possibly) vary from installation to installation, depend on the actual electrical or mechanical configuration of (optional) sensors, or change with evolving software development of the data acquisition system. In this group, radiation sensor misalignment, local angel-of-attack correction, despiking thresholds, or the representation of missing values are found.

4.2 Input Information

4.2.1 Data tables

As after each experiment, the data actually handed over are inspected for consistency, completeness and anomalies. From IKAPOS, two versions of the data were received: Backup copies of the onboard data acquisition databases and formatted ASCII (American Standard Code For Information Interchange) tables. The ASCII tables either contain voltage, current or resistance values converted (by FILAX) from binary counts using the latest calibration information of the analog-to-digital converters (A/D) from April 2010, data digitally received via the ARINC (Aeronautical Radio Incorporated) bus of the aircraft avionics system, or read digitally from the more complex scientific sensors such as laser altimeters and GPS receivers.

The data of each flight mission are spread over a number of files, each representing a group of sensors. The files are recorded at different data rates, depending on the sensors contained. Unfortunately, the files carry file headers that are similar but different from file to file and some headers contain file metadata and some do not (see Table 4.1). Each line in the data section begins with a time information, which varies in format across the files, too. Missing values are mostly marked by filling the columns with nines, which leads to column-dependent representations of N/A (Not Available) values.

4.2.2 Sensor calibrations

Conversion functions and calibration coefficients regarded as fixed values are taken from manufacturer manuals that were provided by FILAX along with the data tables. Such sensors comprise Pt-100 sensors, pressure transducers, radar altimeter, and the dew point mirror. In a few cases, the used choice of optional output variants was not documented and had to be determined from value ranges or in personal communications.

Calibration information for sensors needing regular calibration was partly supplied along with sensor documentation and partly was collected from each responsible AWI scientists. Among these sensors are the radiation sensors calibrated by PMOD/WRC (Physikalisch-Meteorologisches Observatorium Davos/ World Radiation Center), the humicaps, and the radiation sensor amplifiers. Source and age of the coefficients supplied for the radiation sensor amplifier however remain unclear.

4.2.3 Artefacts

Spikes As known from earlier experiments with POLAR 2, the data acquisition system tends to repeatedly record single values which apparently do not represent measured values, called spikes. Spikes mostly – but not always – contain values clearly outside any reasonable range. In order to identify spikes, a simple method is used that compares the normalized probability density distribution of each recorded channel to a Gaussian error function (*Drüe*, 2001). The threshold is chosen at the value, where the probability density distribution of spike-

Table 4.1: Example for two different file headers (with names anonymized).

```
 1006120101_1_bmet0.dat.gz
# Medusa-P ASCII file generator 1.5 build 091106
# File generated at 10-06-12 18:35:34
#
# Campaign name: IKAPOS
# Startdate:     2010-06-12 13:36:48
# Flight number: 1006120101
# Location:      North-East Greenland
# Aircraft:      Polar-5
# Operator 1:    Xxxxxxxxx Xxxxxxxx
# Operator 2:    Xxxxxxxxx Xxxxxxxx
# Scientist:     Xxxxxx Sxxxxxxx
# Observer:      none
# Comment:       Calibration Flight
# __END_OF_FI_HEADER__
#001:time 002:time_1 003:rFHuGA 004:THuiGA 005:Usci 006:...
⋮
```

```
 1006120101_1_bmet6.dat.gz
# 1:date 2:time 3:ms 4:bmet_palt 5:bmet_bcalt ...
⋮
```

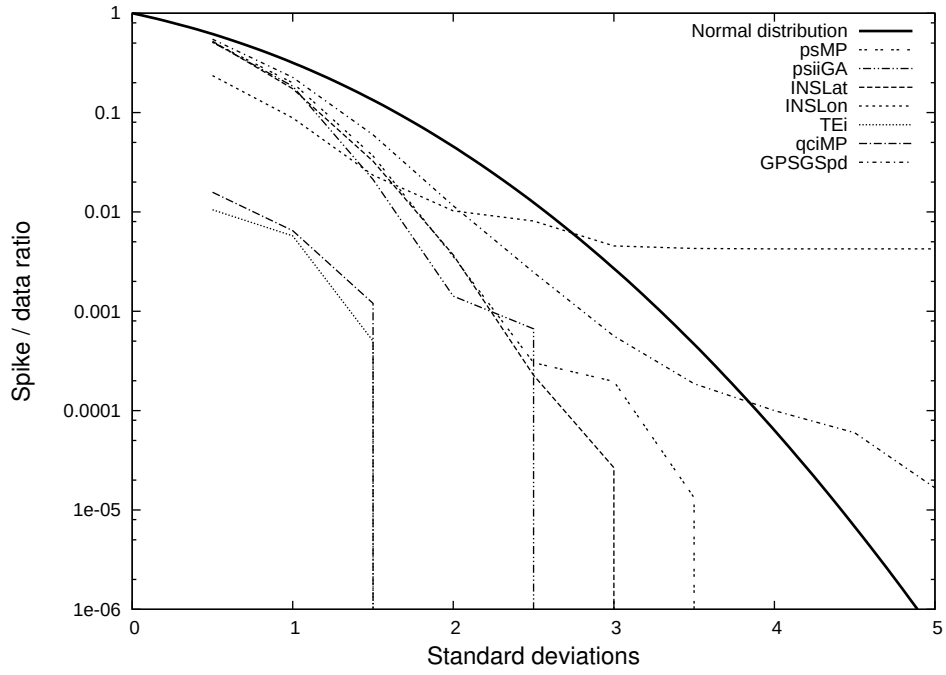

Figure 4.1: Comparison of the normalized probability density function of selected channels and the Gaussian error function. Data show the calibration flight. Note the channels that apparently deviate above 3.5 standard deviations.

contaminated channels starts to decay significantly less than the Gaussian error function.

For IKAPOS, a value of 3.5 standard deviations was determined as a suitable threshold (see Figure 4.1). This is slightly better than for previous experiments with POLAR 2, where values larger than 3 standard deviations above the mean were regarded as spikes.

Resolution issues Closer inspection of the data showed that several channels possibly are not stored with sufficient resolution. Comparison of INS speed and position change yielded that the position indicated by INS seems to stick for several records and then jumps to the next position (Figure 4.2). If this behavior is caused by insufficient position resolution or by the data output interval being slower than the recording rate could not yet be determined.

The resistance of Pt-100 thermometers is stored as `f6.2` (Fortran format), which corresponds to a relatively coarse temperature resolution of about 0.025 K.

4.3 In-flight calibration

Since several calibration coefficients reflect interactions between multiple components for the measurements system operating under flight conditions, they cannot be determined in a laboratory, wind tunnel or even on the ground (see e.g. *Lenschow*, 1986). Among these are time lags, pressure partitioning local angle-of-attack corrections, combined housing sensor time constants, and radia-

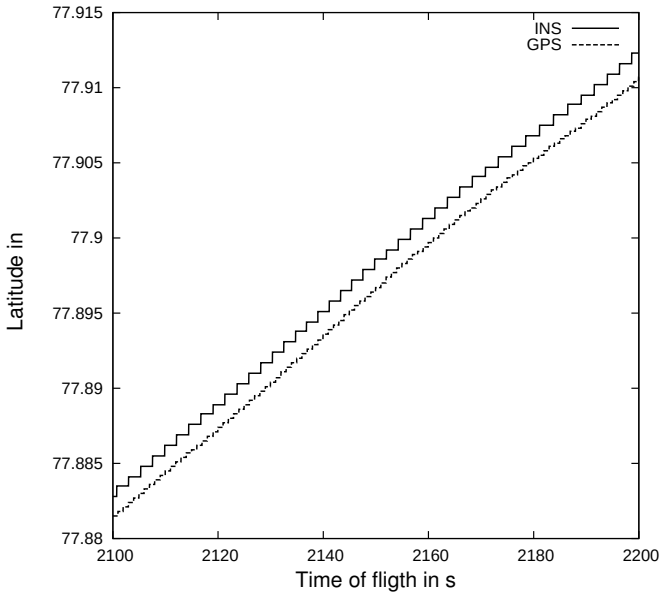

Figure 4.2: Comparison of Latitude recorded by GPS and INS.

tion sensor misalignments (e.g. *Lenschow*, 1986; *Drüe*, 2001; *Vörsmann et al.*, 1989; *Freese*, 1999).

4.3.1 Time lags

Lags between measured data can be caused by different processing speed of the systems supplying information to the data acquisition system:

Analog data are associated with a timestamp upon A/D conversion, which takes a finite period of time. Digital data receive a timestamp when being sent over the ARINC bus (*AEEC*, 2001) or when transmitted digitally to the data acquisition system. Both require the internal software of the sensor to process the measurements and generate a message, which both require a certain processing time, too.

Internal lags of navigation systems may arise from the internal data processing. INS integrates acceleration to yield speed and position, GPS derives position to yield speed. Since both calculations are done at finite time intervals using backward differences, the results may be shifted in time.

Time lags between data groups For the present study, it is assumed that the lag of all quantities grouped in one file is identical. Since they are acquired from the same hardware at the same data rate, it is unlikely that processing speed and hence lags are different. Hence, the differences of the lags between each group of variables had to be determined.

For this purpose, for each pair of groups, a pair of variable was chosen, for which highly correlated values are expected. For example radar height and static pressure. Then, for each of these pairs, a flight leg was chosen, on which both are expected to cover a sufficiently wide range of values. Then for a reasonable range of time differences, mean difference and covariance are calculated (see

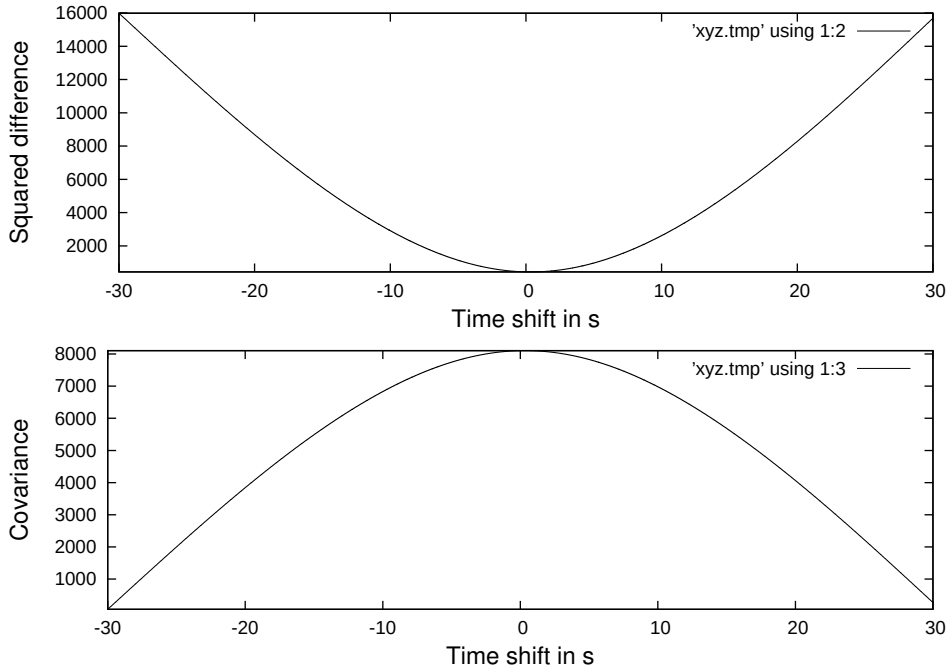

Figure 4.3: Example: time shift of radar height (HradMPm, group navp1) versus pressure height (HICAOmMP, group mpod0). The maximum covariance is found at a shift of –0.23 s.

Figure 4.3 for an example). Depending on the physical relation, the time difference yielding either the minimum difference, minimum, or maximum covariance was chosen (*Drüe*, 2001).

Internal lags of navigation systems To determine possible relative lags of different quantities output by INS and GPS, ground speed was calculated from GPS and INS position as well as from INS accelerations, using instantaneous attitude angles (*Tjernström and Samuelsson*, 1995).

Unfortunately, it turned out that the position resolution is too coarse to derive usable ground speed values. The covariance between such calculated and the

Table 4.2: Lags of all sensor groups relative to INS (vertical) acceleration

Subsystem (filename)	Lag in s	Group contains ...
mpod0	0.1	nose boom turbulence (“MP”)
bmet0	0.15	basic met. sensors (“GA“)
bmet2	1.25	(front) GPS
bmet6	1.30	ADC (air data computer)
rax0	0.1	Radiation sensors
navp0	0.26	INS
navp1	0.33	radar altimeter

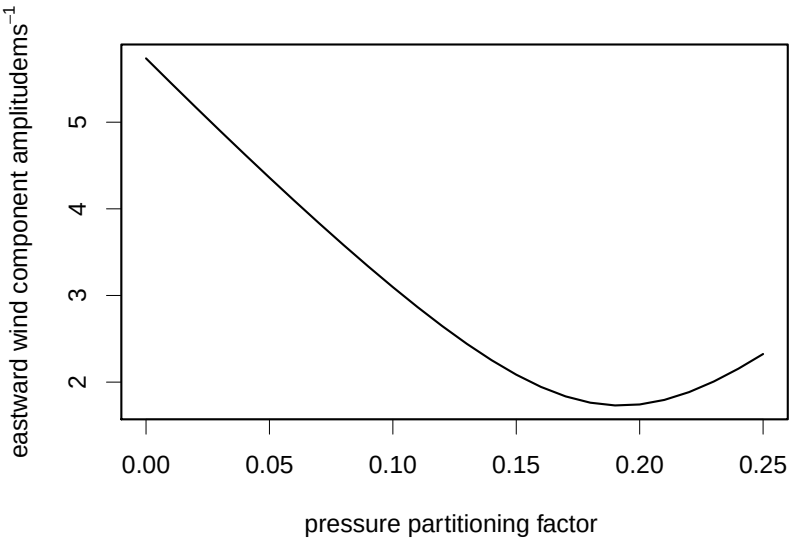

Figure 4.4: Dependence of the amplitude of the eastward wind component during a full circle on the pressure partitioning factor E

recorded ground speed values (on a short time scale) is almost random. In case of the INS, the position "steps" dominate the derived speed even if both time series are low-pass filtered. However, internal lags of the INS could be determined in course of the local angle-of-attack calibration (see Section 4.3.3) and are included in Table 4.2.

4.3.2 True air speed

Theoretically, true air speed (TAS) can be calculated via Bernoulli's equation from the pressure difference between the front hole and the sideward holes of the five-hole probe. But on a real aircraft, the pressure at these side holes is not equal to the static pressure, since air flow is partly decelerated due to the pressure field distortion caused by the aircraft body and engines moving through the air. This is expressed by a static pressure partitioning factor E (*Lenschow*, 1986) which relates measured ("indicated") pressures to the undisturbed values via

$$p_s = p_{si} + q_{ci} \cdot E \tag{4.1}$$

$$q_c = q_{ci} - q_{ci} \cdot E \quad , \tag{4.2}$$

where p_s is static pressure, q_c is dynamic pressure and an "i" appended to the subscript denotes indicated values.

The usual procedure to determine E is to perform a straight flight at constant (pressure) altitude with increasing TAS from close to stall speed to maximum measurement speed. If the wind field is uniform, linear regression or TAS versus ground speed yields E (*Lenschow*, 1986).

Since such a maneuver was not performed during IKAPOS, a different method was used: The data measured during two full circles flown in course of the calibra-

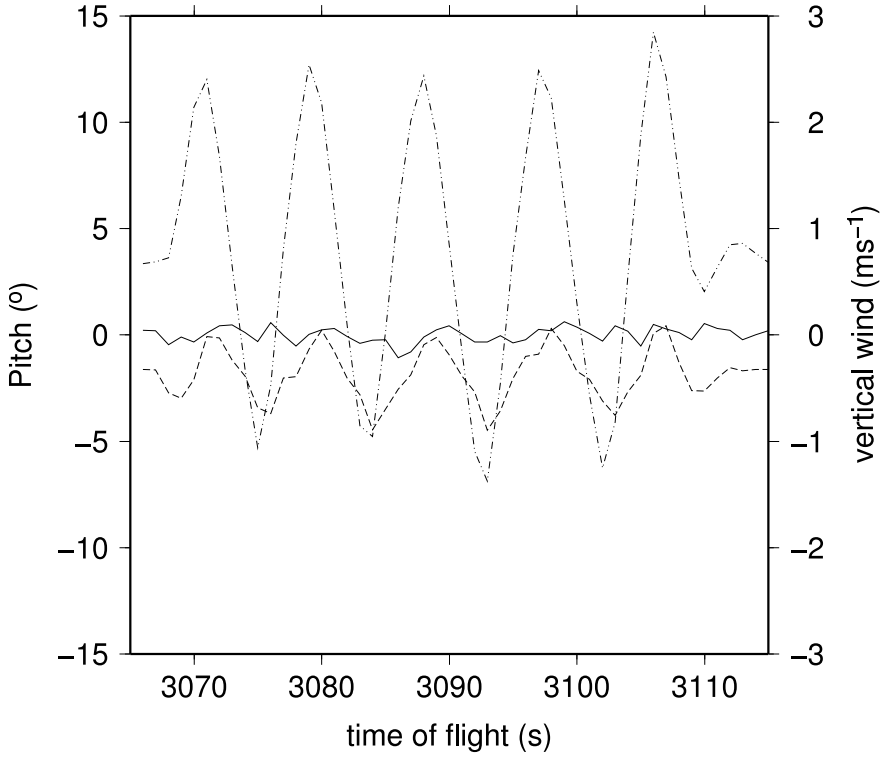

Figure 4.5: Vertical wind (right axis) before (dashed, using manufacturer coefficients) and after calibration (solid). Pitch angle (left axis) is shown as dash-dotted line.

tion flight, the horizontal wind vector was calculated. Then E was varied until the amplitude in both the eastward and northward wind components are minimized (see Figure 4.4). This procedure was performed separately for both circles which yields

$$E = 0.1969 \pm 0.0058 \quad . \tag{4.3}$$

4.3.3 Angle of attack

Similar to the measurement of the static pressure, the pressure field deformation in front of the aircraft causes the angle of attack of the local flow at the tip of the five hole probe to be different from angle of attack of the general airflow around the aircraft (*Lenschow*, 1986). The conversion has to be determined in-flight since the conversion of pressure differences not only depends on the geometry of the five hole probe but also on the flight-dynamic state of the aircraft, in particular air speed (throttle), loading state and aerodynamic configuration (*Garman et al.*, 2008).

alpha The usual procedure to determine the conversion between the vertical pressure difference of the five hole probe and the vertical angle of attack α is the same as to determine the (static) pressure partitioning factor, a straight flight with stepwise increase of TAS (*Lenschow*, 1986, see also Section 4.3.2).

Here we use a modified form of the approach presented by *Bögel and Baumann* (1991). For this method, the aircraft has to perform a series of phygoids

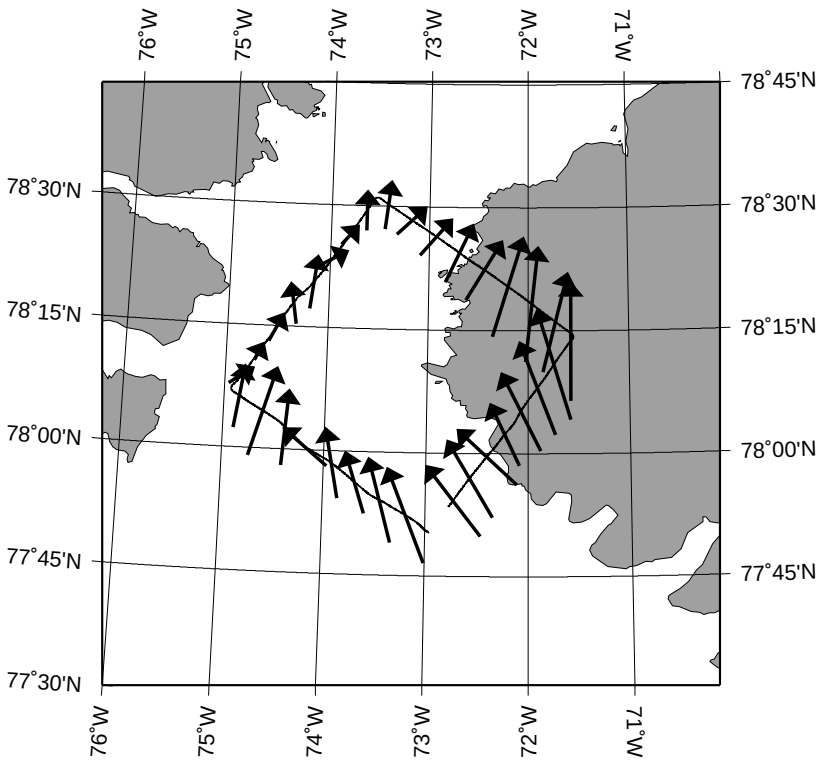

Figure 4.6: Horizontal wind measured during on the main flight pattern – a horizontal box – of the calibration flight. Note the inhomogeneity.

(i.e. pitch angle variations) in an area with zero vertical wind (w = 0). During IKAPOS, an amplitude of $\pm 10^\circ$ was used.

From the pressure difference q_{alpi} the local angle of attack α_L is determined using the manufacturer wind tunnel calibration. Angle of attack α is then calculated by a linear equation

$$\alpha = \alpha_1 \cdot \alpha_L + \alpha_0 \quad . \tag{4.4}$$

If the vertical wind is assumed to be zero (w = 0), the vertical component of the TAS vector ($w_{\text{TAS}} = \sin\alpha \cdot v_{\text{TAS}}$) equals the vertical speed of the aircraft w_{plane}. The latter is calculated primarily from the INS vertical acceleration, as described in *Drüe* (2001), following the method of *Matejka and Lewis* (1997). To allow for internal lags of data processing, a time shift dt_{INS} of the INS vertical acceleration is introduced. Finally, the RMS of the difference ($w_{\text{plane}} - \sin\alpha \cdot v_{\text{TAS}}$) is minimized by synchronous variation of α_0, α_1, and dt_{INS} .

During IKAPOS, four series of phygoids were performed, which yield

$$\alpha_0 = -2.068^\circ \pm 0.193^\circ \tag{4.5}$$

$$\alpha_1 = 0.960^\circ \pm 0.021^\circ \tag{4.6}$$

$$dt_{\text{INS}} = (0.103 \pm 0.005)\text{s} \tag{4.7}$$

The vertical wind before and after application of the calibration according to (4.5) – (4.7) is shown in Figure 4.5

beta In the literature, three main procedures to determine the conversion between the horizontal pressure difference at the tip of the five hole probe into the

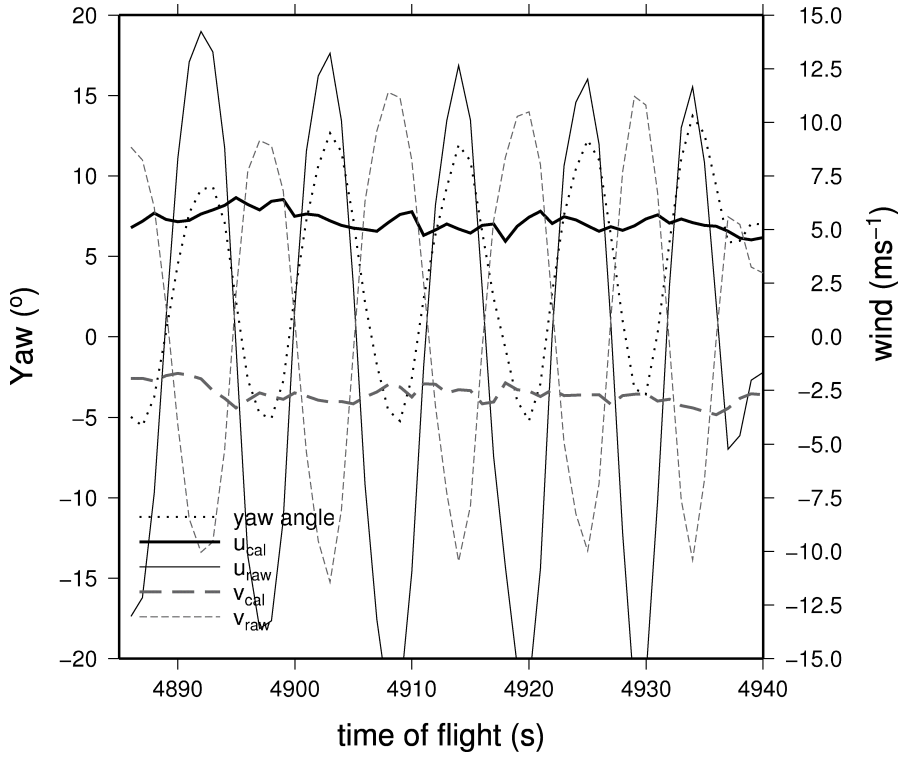

Figure 4.7: Horizontal wind (right axis, northward wind gray, eastward wind black) assuming a sensitivity of unity (thin) and after calibration (thick). Yaw angle (left axis) is shown as dotted line.

horizontal angle of attack β are found, which all assume a linear relationship

$$\beta = \beta_0 + \beta_L \cdot \beta_1 \qquad : \tag{4.8}$$

Either go-and-return maneuvers on a horizontal trajectory are performed and the coefficients are adjusted to minimize the horizontal wind difference before and after the turn (*Lenschow*, 1986). Or the aircraft flies along horizontal box patterns, with one side parallel and one side perpendicular to the mean wind direction, and the coefficients are adjusted to minimize the variance of the horizontal wind (*Cremer*, 2008). Or the aircraft performs yawing oscillations, similar to the procedure used for α, allowing a time shift and minimizing the difference between the indicated air speed and ground speed (*Bögel and Baumann*, 1991).

During the calibration flight, the wind field in the area turned out to be rather inhomogeneous (Figure 4.6). Hence none of the above techniques could be applied and a split technique was used:

The sensitivity β_1 and time shift dt_{INS} were determined from the yawing maneuvers performed on every side of the box shown in Figure 4.6 (see Figure 4.7). For this procedure, both prescribing offset β_0 as zero and including β_0 in the variation process yielded almost the same results.

The offset β_0 was determined from a two perpendicular go-and-return maneuvers (see Figure 4.8). To check plausibility of this result, the same procedure was applied to the corners of the box pattern shown in Figure 4.6, which yielded another value (β_1 = 0.97) within the error range of (4.10) but with much greater uncertainty.

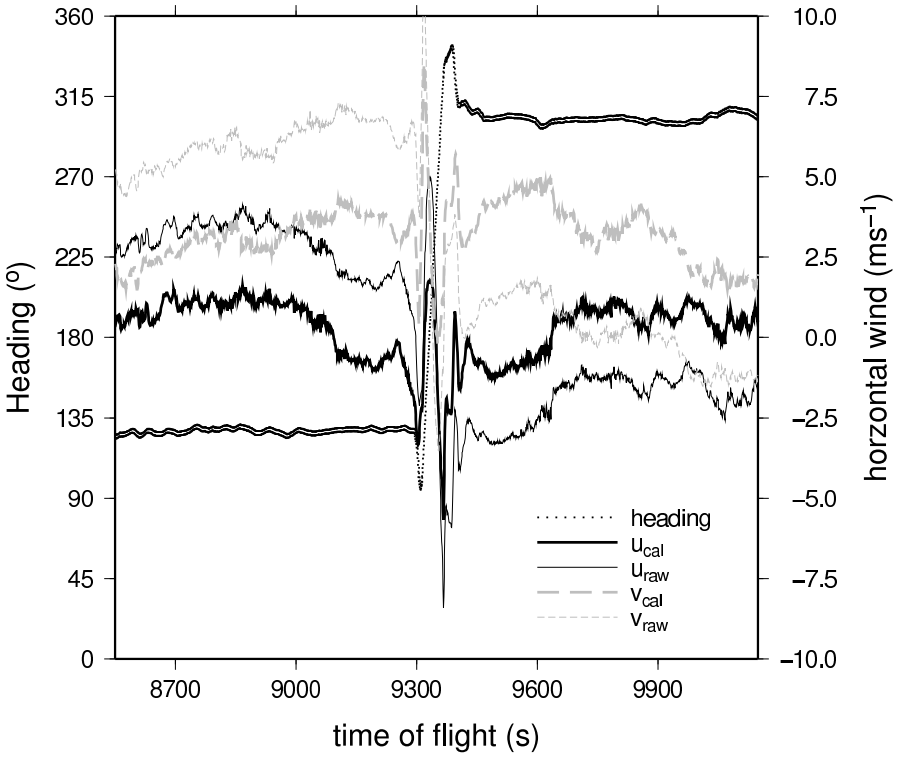

Figure 4.8: Horizontal wind (right axis, northward wind gray, eastward wind black) assuming zero offset (thin) and after offset calibration (thick). True heading (left axis) is shown as dotted line.

To summarize, the split technique yields

$$\beta_0 = 0.898^\circ \pm 0.035^\circ \quad (4.9)$$

$$\beta_1 = 0.957^\circ \pm 0.013^\circ \quad (4.10)$$

$$dt_{\mathrm{INS}} \approx 0.10\mathrm{s} \quad . \quad (4.11)$$

4.3.4 Reverse-flow sensor

response time The nose boom of POLAR 5 carries two temperature sensors, one standard Rosemount 102BV sensor in a Rosemount 102-B, configuration b, deicable housing[1], called “TE”. The other sensor apparently is another Rosemount 102BV sensor which sits in a Rosemount 102-E, configuration b, non-deicable housing[2]. This second sensor is called “TRvF“, because on the predecessor of the nose boom – the METEOPOD on POLAR 2/4 (*Vörsmann et al.*, 1989) – a reverse flow sensor took this position. The idea of both is to supplement measurements of the standard Rosemount sensor by a faster sensor, that is possibly less accurate with respect to the mean temperature (*Inverarity*, 2000).

The lag of temperature sensors in housings usually behaves like a so-called 2-component system (*Inverarity*, 2000), which is depicted in Figure 4.9. Such a

[1]model 102-EJ2BB
[2]model 102-E4AL

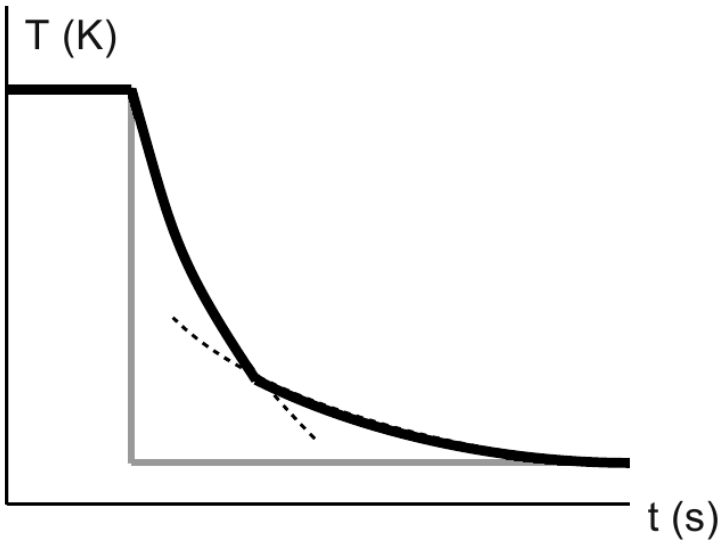

Figure 4.9: Schematic reaction of the temperature T (versus time t) indicated by a two-component system (black) upon an instantaneous temperature change (gray)

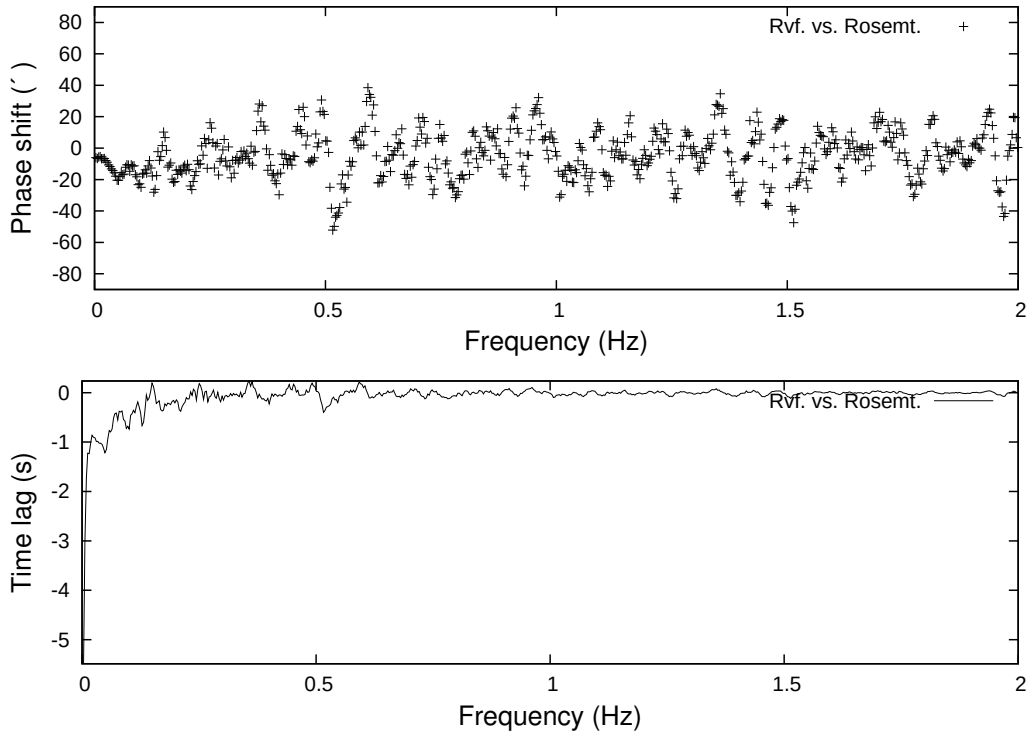

Figure 4.10: Phase spectrum (upper panel) and frequency-dependent lag (lower panel) between the temperature indicated by sensor TRvf versus sensor TE (see text).

system has two response times. On a short timescale, (e.g. $< 1\,s$) it behaves like having a response time τ_2, while on a longer timescale (e.g. $> 1\,s$) it behaves like having a response time τ_1. For the non-deicable Rosemount 102-E2AL configuration b housing, *Spyers-Durand and Baumgartner* (1983) found $\tau_1 = 0.17\,s$ and $\tau_2 = 45\,ms$, respectively.

If these values are known, the time constant of another sensor can be determined by fitting the phase spectrum of two timeseries recorded by both sensors:

$$\Delta\tau = \frac{\Phi(f)}{2\pi f} \quad , \tag{4.12}$$

where $\Phi(f)$ is the phase difference of both timeseries at frequency f and $\Delta\tau$ the difference of the response times.

It turned out that for TRvF versus TE, the phase is not a function of frequency and the time shift of both signals is around zero, for all frequencies above 0.2 Hz. Below 0.1 Hz, the mean response time difference is -0.64 s. Assuming a slower (housing) response time of 1.15 s for TE (*Inverarity*, 2000) yield for TRVF

$$\tau_1 \approx 0.98\,s \quad . \tag{4.13}$$

For the faster response time, it has to be assumed that

$$\tau_2 \approx \tau_1(102E2AL) = 0.045\,s \quad , \tag{4.14}$$

which means that TRvF and TE respond in the same way to temperature variations on a scale below 1 s duration.

recovery factor In order to use TRvF as fast temperature, the recovery factor r of the housing in use has to be known. The air at the sensor location is adiabatically heated by incomplete deceleration. The heating is

$$\Delta T_i \;=\; T_i - T_s \;=\; r\,\frac{\overline{v_0}}{2c_p} \quad , \tag{4.15}$$

where ΔT_i is the adiabatic heating, where T_i is the indicated temperature, where T_s is the static temperature, $\overline{v_0}$ the mean speed of the air flow and c_p the specific heat capacity of air. If the total temperature T_t ($= T_i$ for $r = 1$) and static temperature T_s are known from another sensor, TE in this case, r can be calculated as the ratio

$$r \;=\; \frac{T_t - T_s}{T_{Rvfi} - T_s} \quad . \tag{4.16}$$

For the data taken on the box pattern (Figure 4.6) during the calibration flight, the mean ratio is

$$r = 0.883 \pm 0.005 \quad . \tag{4.17}$$

The above method does not account for a possible calibration offset of the two sensors employed. To allow for such an offset, the recovery factor can be determined from linear regression of $T_t - T_{Rvfi}$ versus $T_t - T_s$ (see Figure 4.11). Unfortunately, this procedure yields a large uncertainty due to the poor resolution of temperature data (see section 4.2.3). Averaging the values determined for

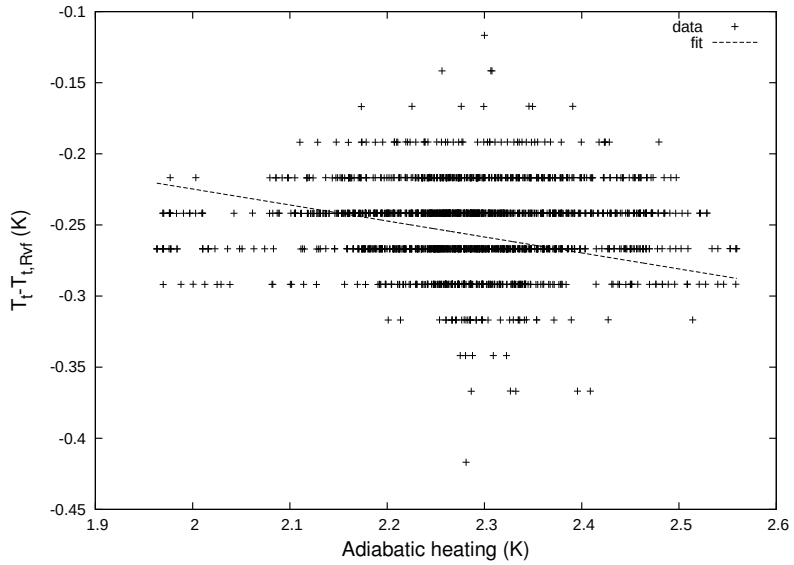

Figure 4.11: Linear regression of the adiabatic heating indicated by sensor RvF versus the adiabatic heating corresponding to full deceleration of air.

each of the four sides of the box pattern (Figure 4.6) during the calibration flight yields

$$r = 0.899 \pm 0.027 \quad , \tag{4.18}$$

which agrees with the result above, but is less well defined. A reprocessing of onboard database might yield one more digit of temperature resolution, but could not yet be done.

4.3.5 Pyranometer misalignment

The alignment of the hemispheric radiation sensors can change slightly with every removal and installation cycle, due to minor mechanical changes such as interchanging washers between the mounting bolts. Hence, minimal angular changes are expected to occur from mission to mission.

The misalignment for a mission can be determined by in-flight calibration, using the modified method of *Freese* (1999), as described in *Drüe* (2001). This method applies a low-pass filter to the data and then determines global radiation K_{down} by linear regression of the indicated global radiation $K_{\text{down i}}$ versus the dimensionless incidence coefficient c representing the sun's zenith angle in the aircraft reference frame. The mechanical offsets are then varied until the variance of the corrected K_{down} gets minimized.

This procedure was applied to two full circles performed during the calibration flight (see Figure 4.12), which yields

$$\text{pitch} \quad \Delta\theta = -1.22^\circ \tag{4.19}$$

$$\text{roll} \quad \Delta\phi = -0.918^\circ \tag{4.20}$$

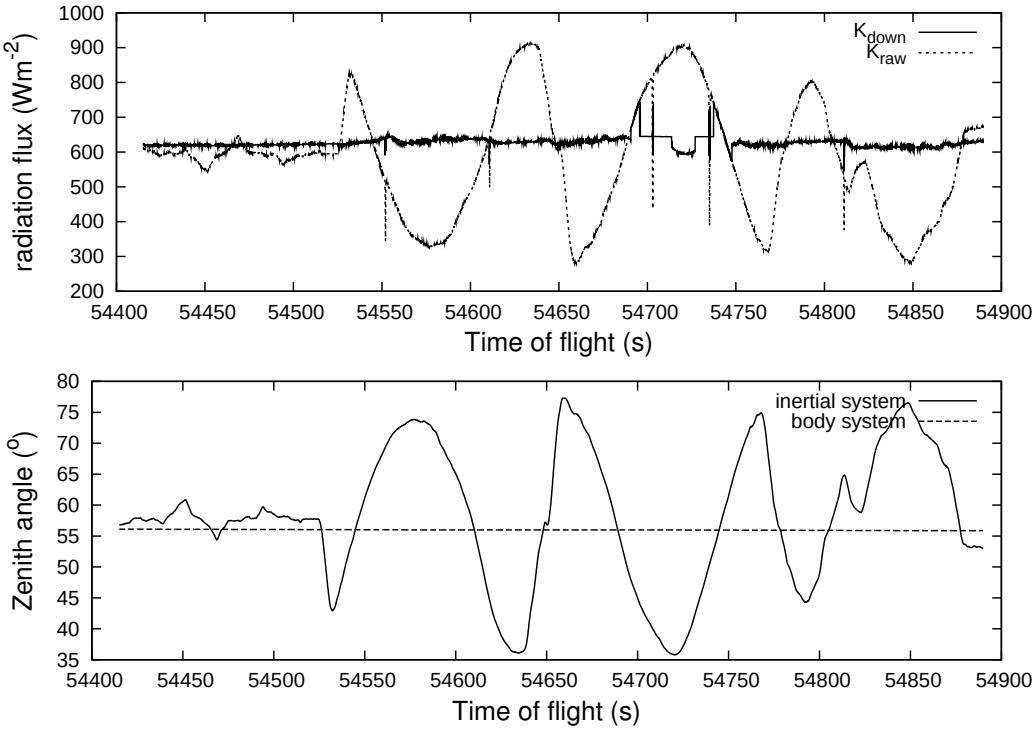

Figure 4.12: Solar radiation recorded during two full circles flown as part of the IKAPOS calibration flight. Uncorrected (dashed) and corrected (solid) shortwave downward radiation flux (upper panel) and solar zenith angle (lower panel) seen from the pyranometer (solid) and in the geodetic system.

4.4 Comparison to manufacturer calibration

Upon delivery, the manufacturer of the nose boom, MessWERK GmbH, performed an extensive verification of wind measurements taken by the nose boom (*Cremer*, 2008).

Unfortunately, this report expresses the empirical relationships determined by in-flight calibration using formulations that partly differ from the formulas used in common literature (*Lenschow*, 1986; *Vörsmann et al.*, 1989; *Bögel and Baumann*, 1991; *Khelif et al.*, 1999; *Strunin and Hiyama*, 2004, to name a few). Hence this calibration does not yield coefficients that can be used in our existing software package. The formulation also hinders comparison with other calibrations presented in literature.

Furthermore, the coefficients for the local angle-of-attack corrections are determined by quasi-static maneuvers, that allow to determine the angular offset with very small uncertainty. On the other hand, the attitude angle variation is small compared to dynamic maneuvers and this method does not allow for time shifts of the timeseries (*Bögel and Baumann*, 1991). Hence, the method used by *Cremer* (2008) is not optimized for turbulence measurements.

4.4.1 static pressure

The correction formula for the pressure partitioning (see Section 4.3.2) used by *Cremer* (2008) is

$$p_s = K_{1,p} q_{ci} + K_{0,p} + p_{si} + \zeta(\alpha, \beta, p_s) \quad (4.21)$$

$$q_c = K_{1,q} q_{ci} + K_{0,q} - \zeta(\alpha, \beta, p_s) \quad , \quad (4.22)$$

where $K_{0/1,p/q}$ are empirical coefficients and ζ is a function that is not needed, if the true air calculation includes horizontal and vertical angle of attack, as it is the case in our data processing.

Comparing 4.21 to 4.1 yields

$$E = -\frac{K_{0,p}}{q_{ci}} - K_{1,p} \quad (4.23)$$

The values $K_{0,p}$ = 0.27 hPa and $K_{1,p}$ = 1.063 yield E = 0.08. This value seems to be quite different from the value (E = 0.1969) determined in this study. But this difference corresponds to a difference of the static pressure calibration offset – including sensor and position errors as well as dynamic pressure field deformation – of roughly only 0.25 hPa. Interestingly, if $K_{0,p}$ is assumed to be 0.027 (i.e. the decimal is shifted by one digit), (4.23) yields E = 0.193, which perfectly matches the value of $E = 0.1969 \pm 0.0058$, determined in this study

4.4.2 alpha

For the correction of local angle of attack α *Cremer* (2008) uses

$$\alpha = \frac{q_\alpha}{q_{ci} K_{1,\alpha}} + K_{0,\alpha} \quad , \quad (4.24)$$

with $K_{0,\alpha} = -1.15^\circ$ and $K_{1,\alpha} = 0.087$.

Other literature (e.g. *Lenschow*, 1986) uses a formulation equivalent to our equation (4.4):

$$\alpha = \frac{q_\alpha}{q_{\mathrm{ci}}} \frac{\alpha_1}{K_1} + \alpha_0 \quad , \tag{4.25}$$

where $K_1 = 0.079$ is a wind manufacturer-supplied value from wind-tunnel calibration of the five-hole probe, valid for around 130 kn (typical measurement speed).

The values determined by *Cremer* (2008) hence correspond to $\alpha_1 = 0.908^\circ$, which differs by about 5% from our value ($\alpha_1 = 0.960^\circ \pm 0.021^\circ$). The smaller value of *Cremer* (2008) presumably reflects the neglected influence time shift between INS and the pressure sensors.

The value $K_{0,\alpha} = -1.15^\circ$ differs significantly from our value ($\alpha_0 = -2.06^\circ$). A difference of almost one degree seem surprising at the first glance, but this offset includes mechanical tolerances in the nose boom mounting, the INS mounting as well as pressure sensor temporal behavior and aging.

The nose boom sensor head has a mounting base of 210 mm which makes it an unlikely source of 1 ° misalignment. Since the tolerance for a regular 4-mm washer is 0.2 mm (ISO 4759, class A), the resulting reproducibility of the nose boom orientation is on the order of 0.2 °. The same applies to the INS inertial reference system, a Honeywell Laserref V, that has an outside dimension of 6.5" (16 cm). The mean orientation tolerance of the INS is 0.1 ° (*Honeywell*, 2004). The pressure offsets indicated by the pressure transducers were determined in a laboratory calibration by the manufacturer of the nose boom and turned out to be on the order of 0.05 hPa (at least if more than 40 min after powering them on have passed). Assuming a differential pressure of 5 hPa, this uncertainty roughly equals 0.5°. Hence, the sum of all such uncertainties may sum up to a mission-to-mission change of the offset of α on the order of almost 1 °. It should be noted, that variations of this order were common with the METEOPOD used under POLAR 2, too.

4.4.3 beta

Analogous to the previous section, *Cremer* (2008) uses

$$\beta = \frac{q_\beta}{q_{\mathrm{ci}} K_{1,\beta}} + K_{0,\beta} + K_{2,\beta} q_{\mathrm{ci}} \quad , \tag{4.26}$$

whereas others like *Lenschow* (e.g. 1986) use

$$\beta = \frac{q_{\mathrm{beta}}}{q_{\mathrm{ci}}} \frac{\beta_1}{K_1} + \beta_0 \quad . \tag{4.27}$$

Assuming a typical measurement speed of 130 kn, the values $K_{0,\beta} = -0.6^\circ$, $K_{1,\beta} = 0.088^\circ$, and $K_{2,\beta} = 0.025^\circ$ reported by *Cremer* (2008) correspond to $\beta_0 = -0.15^\circ$ and $\beta_1 = 0.898^\circ$.

The difference of offset β_0 between *Cremer* (2008) and this study is on the same order as for α_0. The magnitude of β_1 is the same for *Cremer* (2008) and this study. The sign however is opposite, which is hard to explain by any uncertainties. It appears more likely that during the last assembly of the nose boom sensor, the hoses connecting the left and right hole of the five-hole probe to the respective pressure sensor were interchanged.

4.4.4 Angular rates

The calibration report by *Cremer* (2008) states that no significant correlation between vertical wind and pitch rate could be found although wind was not corrected for the probe movement due to aircraft body rotations. But it has to noted that no time shift of INS versus nose boom measurements was introduced.

However, a distance of 5 m between the mounting position of the INS inertial reference system and the five-hole probe provides a large cantilever. During the calibration flight, the 90% percentile of the pitching rate was $0.54^{\circ}s^{-1}$, corresponding to about $0.05ms^{-1}$ vertical movement. Values for the other axes are similar. In consequence this means that for 10% of all data points, the wind error by neglecting the rotation of the aircraft body exceeds $0.1ms^{-1}$. A value of this order shouldn't be neglected in turbulence calculations.

In the present study, a dependency – although not significant – could be found, if the time lag determined in Section 4.3.3 was used.

Chapter 5

First results

5.1 Weather conditions at Qaanaaq

To give an overview of the weather conditions at Qaanaaq during the IKAPOS experimental phase, Figure 5.1 shows the record of the weather station NAQ (Qaanaaq airport, see Figure 2.7 for the position).

The first week of the experimental phase (08 to 16 June 2010) was generally characterized by relative low pressure. From 08 to 12 June it was accompanied by deep to mid-high clouds and surface fog. From 12 June the situation changed – hardly no clouds were present, the visibility was not limited – so that the first research flights could be performed. The air temperature ranged from -1 °C to 5 °C and wind speed was mostly lower than 5 m s^{-1}.

The wind direction at Qaanaaq is strongly influenced by the topography of the east-west orientated Murchison Sound (see Figure 2.3). During the experimental phase, westerly winds were dominant. Often, these winds were associated with moist air coming from the nearby NOW region. In particular, western Murchison Sound was characterized frequently by surface fog prohibiting a take-off of POLAR 5.

On 17 June surface fog was present almost the whole day. However, for a short time period of improved visibility a flight could be performed. During high pressure conditions the temperature did not exceed 3 °C.

During daytime of the following two days (18 and 19 June) advection of relative warm air was associated with wind speed up to 8 m s^{-1}. The temperature increased to a maximum of 12 °C – the highest value throughout the experimental phase. Mainly cirrus clouds were observed during low pressure conditions.

With increasing pressure the cloud base level decreased on 20 June. After a relative pressure minimum and surface fog on 21 June the next two days (22 to 23 June) pressure and temperature were rising up to 1019 hPa and 10 °C, respectively. The last two research flights took place in that period.

From 24 June to the end of the campaign (26 June) surface fog prevailed (Figure 5.2). A high pressure system was associated with relatively low temperatures (maximum 2 °C). On 27 June the synoptic conditions changed: Lower pressure, higher temperatures and no fog. The return flight to Kangerlussuaq could be performed.

To summarize, from 08 to 27 June 2010 Qaanaaq airport was generally characterized by moderate westerly winds, which caused surface fog associated with

relative cold air (on approximately 9 days). Figure 5.2 gives an impression of fog conditions at Qaanaaq.

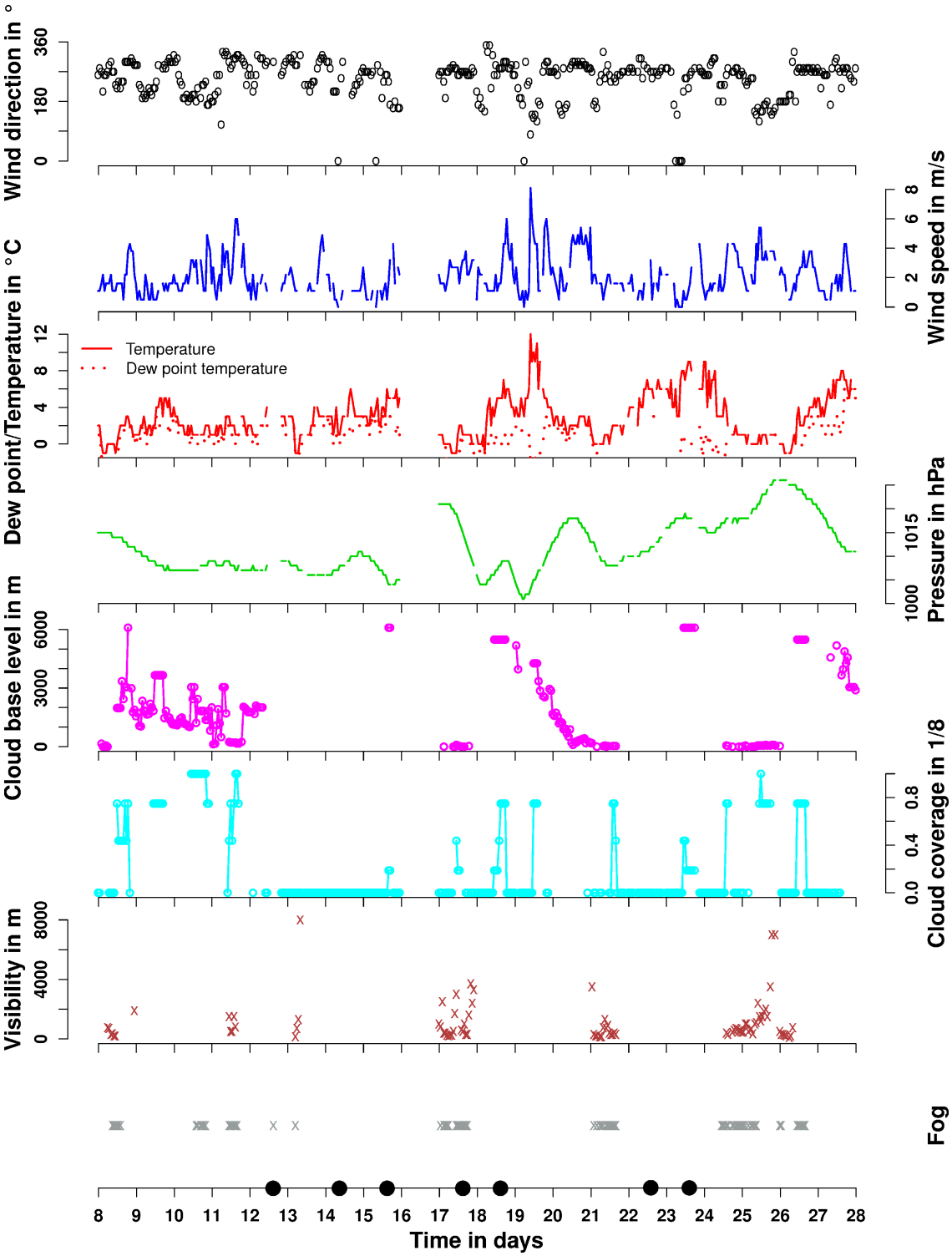

Figure 5.1: Weather conditions (hourly data) at Qaanaaq (IATA airport code: NAQ, ICAO airport code: BGQQ) throughout the IKAPOS experimental period from 08 to 28 June 2010. Flight missions are marked by circles on the time axis.

Figure 5.2: Example of fog at Qaanaaq. (a) View over the fjord with fog in the background at 9 UTC on 24 June 2010. (b) View over the fjord with fog drifting in at 12 UTC on 24 June 2010. The fog stayed until 26 June 2010.

5.2 Katabatic wind flight missions

5.2.1 14 June 2010

In the early morning of 14 June 2010 the first KA flight took place during conditions of weak synoptic forcing. The different structures of the ABL over the Humboldt Glacier and over sea-ice in front of the glacier are illustrated by the two aircraft temps shown in Figure 5.3. Quantities filtered to 15 seconds means are shown. In general, the SBL which drives the katabatic flow is present, but it is weak. However, compared to the potential surface temperature of around 1.8 °C the temperature is about 3 K higher at approximately 40 m AGL (the lowest flight level). At this level downslope southerly winds show a maximum speed of around 8 m s^{-1}. Above, the wind speed decreases quickly to 1 m s^{-1} (at 120 m AGL). In front of the glacier the atmospheric conditions change abruptly (see also Figure 5.4). Over sea-ice relatively cold air – the potential temperature is -2 °C at the lowest flight level – comes from easterly direction with a wind speed of around 3 m s^{-1}. In contrast to the ABL over the glacier the wind profile shows constant wind in the lowest 200 m over sea-ice. As a consequence of the nearby open water and higher absolute temperatures the specific humidity of 3.5 g kg^{-1} is by 1 g kg^{-1} higher than over the glacier. At the lowest flight level, wind and temperature show a marked change at the glacier front.

Overall, this flight represents a weak katabatic SBL under weak synoptic forcing. Due to weakly pronounced daily cycle a strong SBL can hardly develop. In addition, it is too early in the morning to expect appreciable ice melting keeping the lower atmosphere cool. Only few melt ponds could be observed on the glacier, indicating that surface melting was not very pronounced.

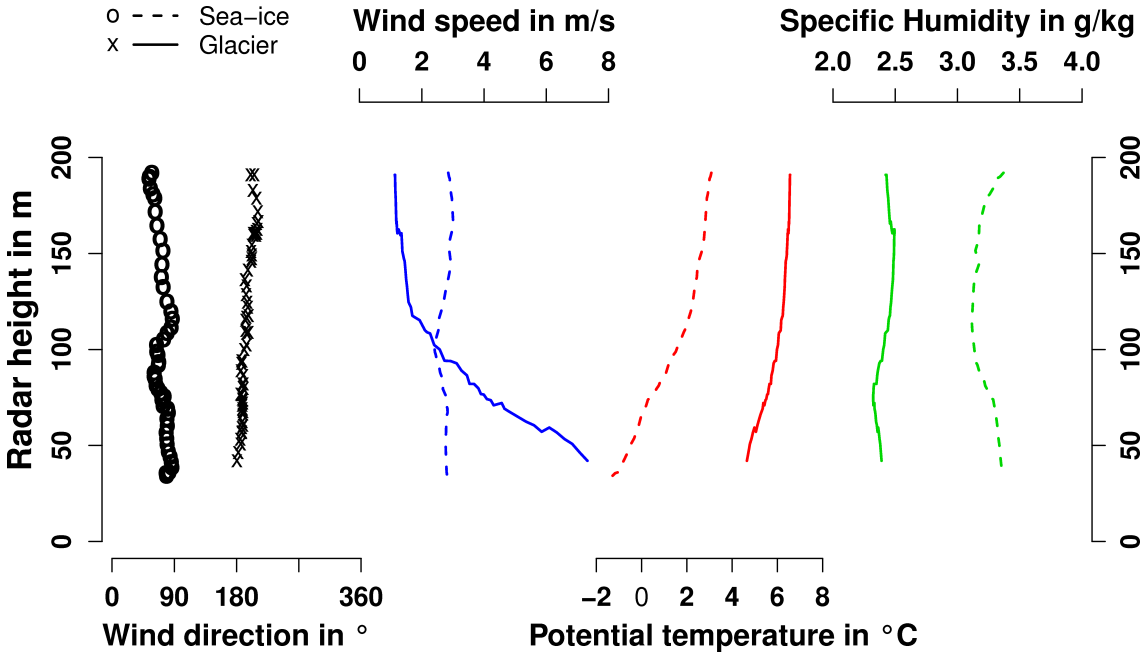

Figure 5.3: Vertical profiles of low-pass filtered mean quantities for 14 June 2010, 0830 UTC over Humboldt Glacier at point B and 0845 UTC over sea-ice in front of the glacier at point A (for positions see Section 3.4).

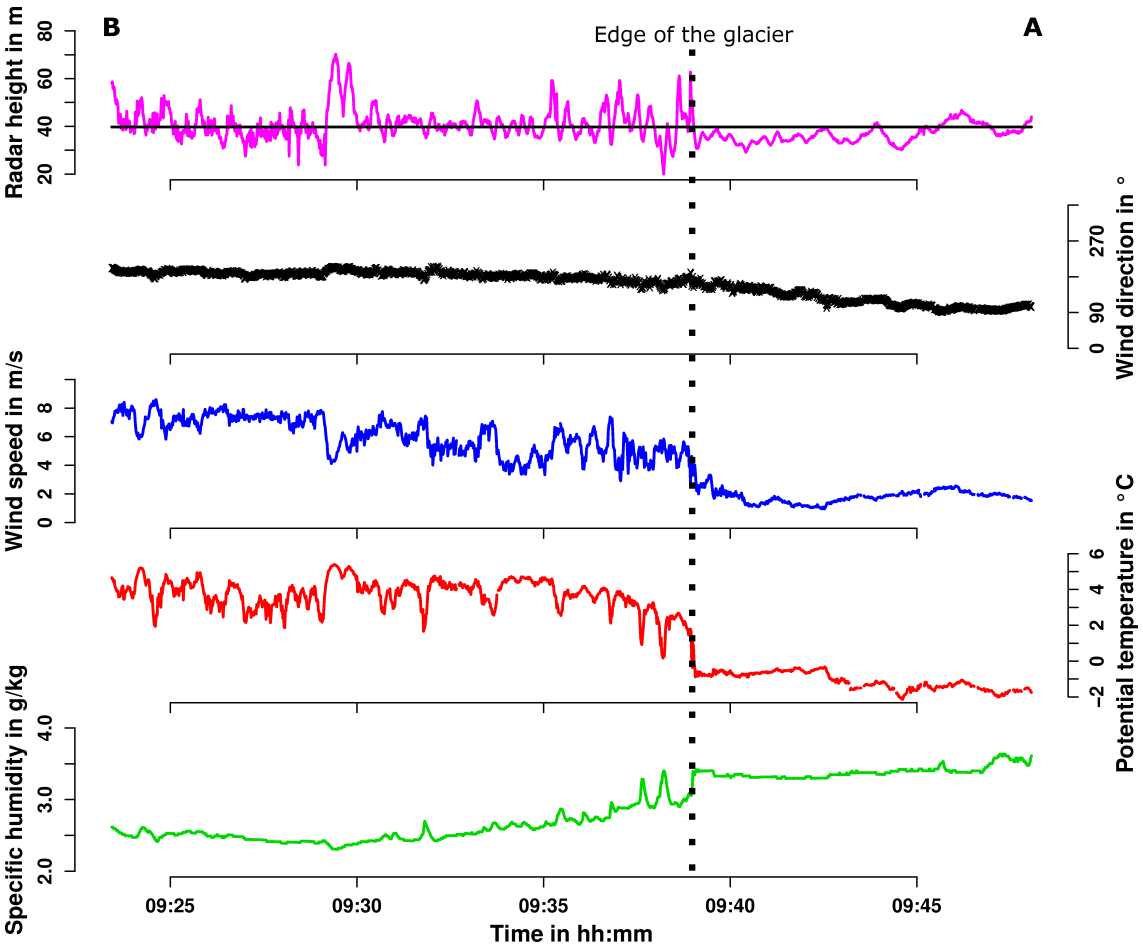

Figure 5.4: Horizontal profiles of quantities sampled at 1 Hz for 14 June 2010 for radar height, wind direction, wind speed, potential temperature and specific humidity. The aircraft leg started over Humboldt Glacier (point B) and ended over the sea-ice in front of the glacier (point A, for positions see Section 3.4). The edge of the glacier is indicated. The horizontal line in the uppermost panel depicts the mean radar height (40 m).

5.2.2 17 June 2010

On 17 June 2010 a flight was performed over the Steenstrup Glacier for a katabatic wind system associated with strong synoptic forcing. Figure 5.5 depicts this situation by showing vertical profiles for one aircraft temp each over the glacier and over the sea-ice in front of the glacier. Over the glacier a wind speed of 14 m s^{-1} is found from 40 m (lowest flight level) to 110 m AGL. Above this layer the downslope (easterly) wind field decreases to 4 m s^{-1} at 300 m. By contrast, over sea-ice in front of the glacier the wind is relatively weak (about 2 to 6 m s^{-1}) and its profile shows small gradients. Here, relatively warm air from northerly direction at the interface of the cold sea-ice causes a well-pronounced surface inversion of approximately 5 K/100 m. However, the potential temperature is clearly lower over sea-ice than over the glacier (see also Figure 5.6) while the absolute temperature is lower over the glacier (not shown). Since the radiation processor failed on this flight, surface temperature could not be measured.

Compared to the case of 14 June the wind speed is considerably higher on 17 June over the Steenstrup Glacier. This reflects the strong impact of synoptic forcing on katabatic flows. As for 14 June, the katabatic wind dissipates within a short distance at the edge of the glacier being associated with large crevasses (Figure 5.6).

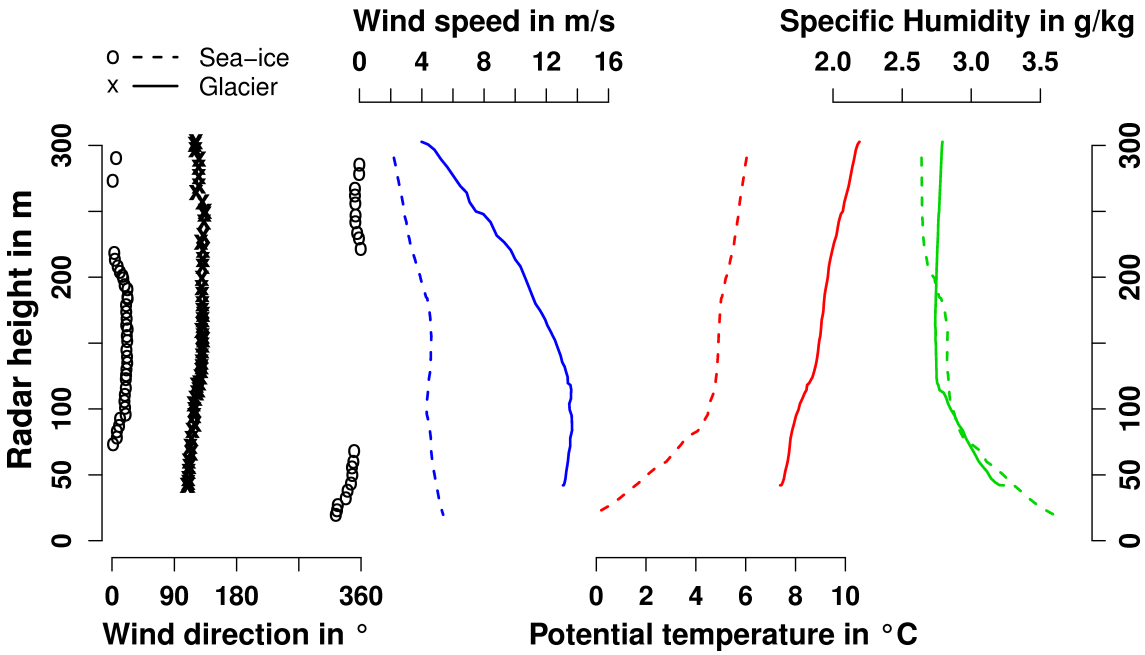

Figure 5.5: Vertical profiles of low-pass filtered mean quantities for 17 June 2010, 1450 UTC over sea-ice in front of Steenstrup Glacier at point A and 1500 UTC over the glacier at point B (for positions see Section 3.5).

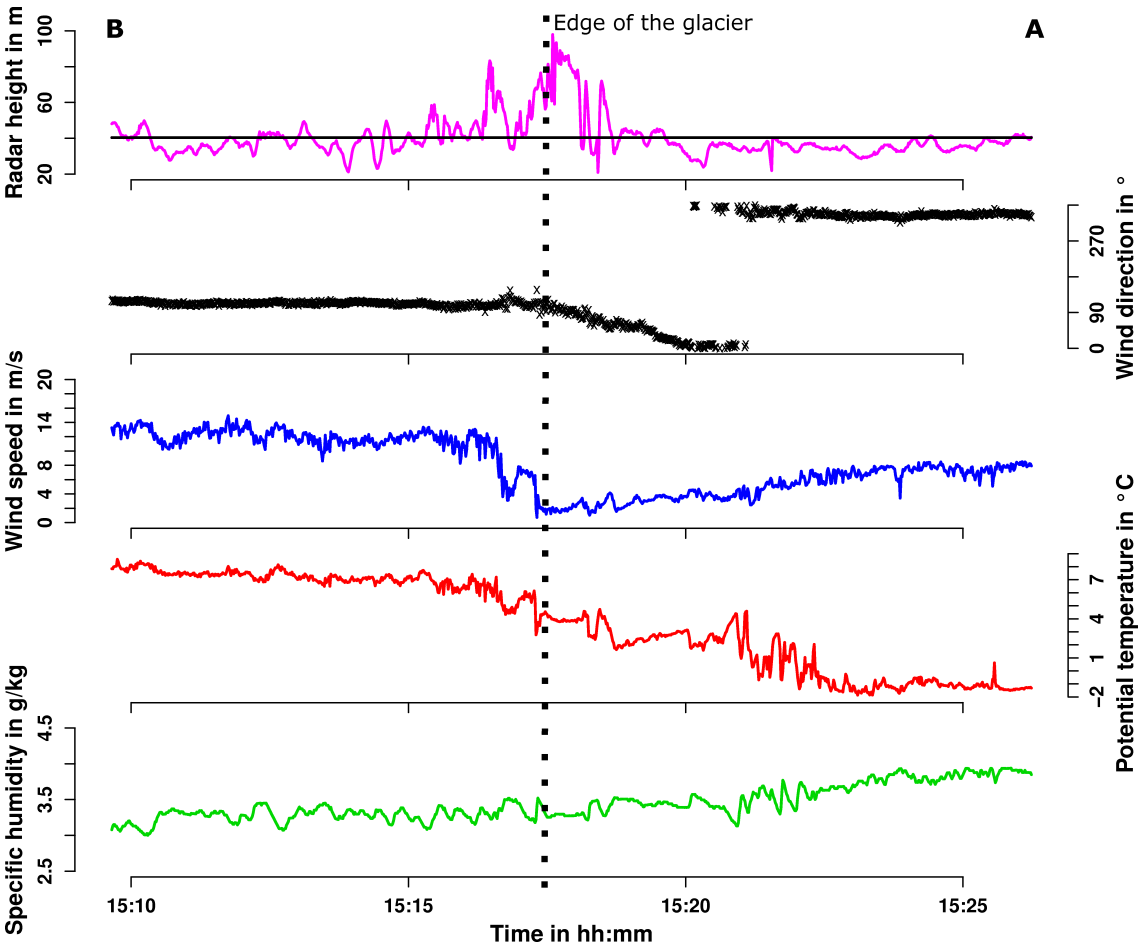

Figure 5.6: As Figure 5.4, but for 17 June 2010. The aircraft leg started over Steenstrup Glacier (point B) and ended over the sea-ice in front of the glacier (point A, for positions see Section 3.5). The edge of the glacier is indicated. The horizontal line in the uppermost panel depicts the mean radar height (40 m).

5.3 NOW flight missions

5.3.1 15 June 2010

On 15 June the first NOW flight took place during relative warm synoptically induced northerly winds. The different structures of the ABL over the northern and north-eastern NOW are presented by the two aircraft temps shown in Figure 5.7. Under the influence of channeling effects over the northern NOW a low-level jet (LLJ) with a wind speed maximum of about 19 m s^{-1} is found (at a height of about 100 m). A temperature gradient of 7 K/100 m reveals pronounced stable conditions below 130 m. By contrast, in the lee area of the eastern NOW the potential temperature and the wind field do not change significantly within heights from 40 to 320 m. In the lee of the steep coast at Smith Sound the wind speed is generally below 6 m s^{-1} (see also Figure 5.8).

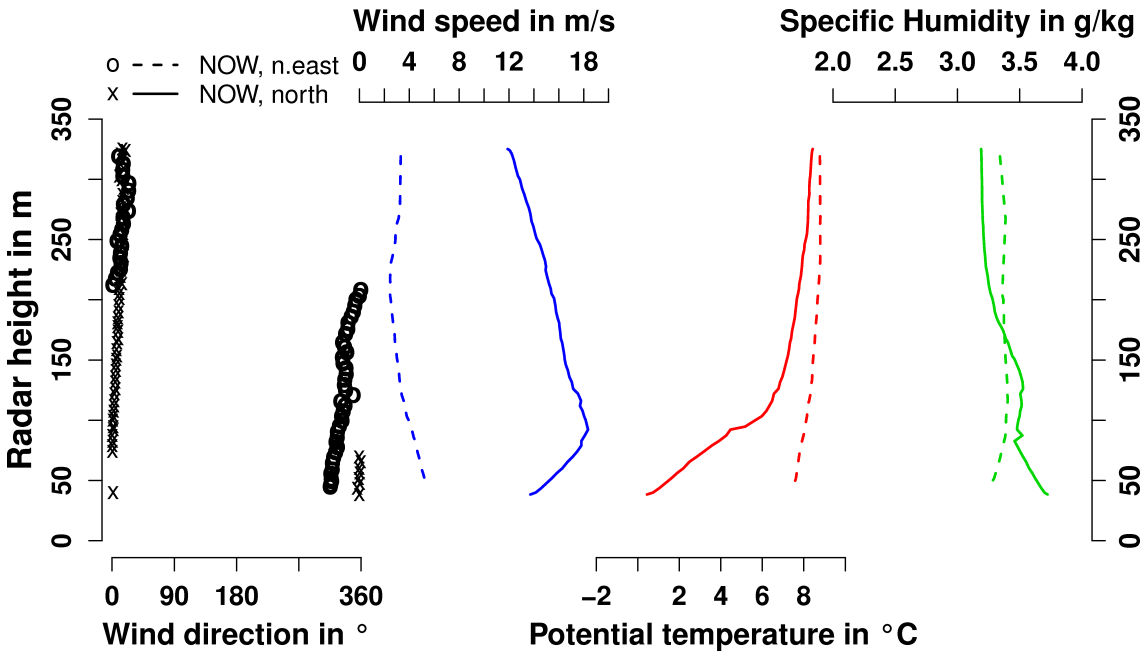

Figure 5.7: Vertical profiles of low-pass filtered mean quantities for 15 June 2010, 1520 UTC at northern NOW (point Q1a) and 1535 UTC at north-eastern NOW (point Q1b, for positions see Section 3.6).

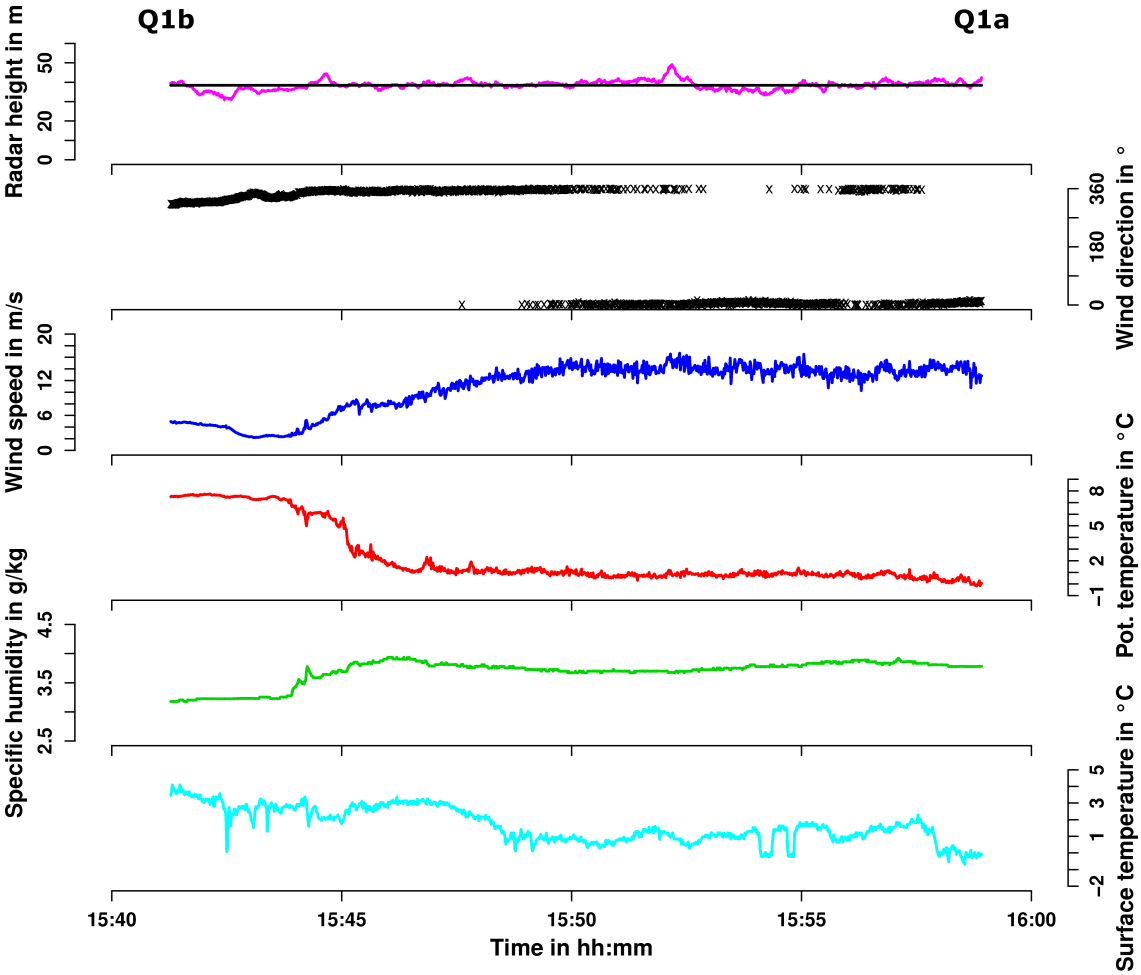

Figure 5.8: As Figure 5.4, but for the cross-profile Q1 for 15 June 2010 (for positions see Section 3.6). Surface temperature is shown in the lowermost panel. The horizontal line in the uppermost panel depicts the mean radar height (39 m).

5.3.2 18 June 2010

In Figure 5.9 three aicraft temps over the northern NOW on 18 June 2010 show a stable but fully turbulent ABL. Interaction processes of relatively warm northerly winds with cold water lead to a surface inversion of about 8 K/100 m. The boundary layer is considerably influenced by channeling effects at Smith Sound (for the position see Figure 2.2). A well-developed LLJ is present with a wind speed maximum of 18 m s^{-1} at a height of 100 m. Above, the wind speed decreases to 3 m s^{-1} and wind direction turns from northerly to southerly direction. The channeling effect of Smith Sound is reflected by the marked increase in wind speed at the centre of the low-level flight leg (Figure 5.10).

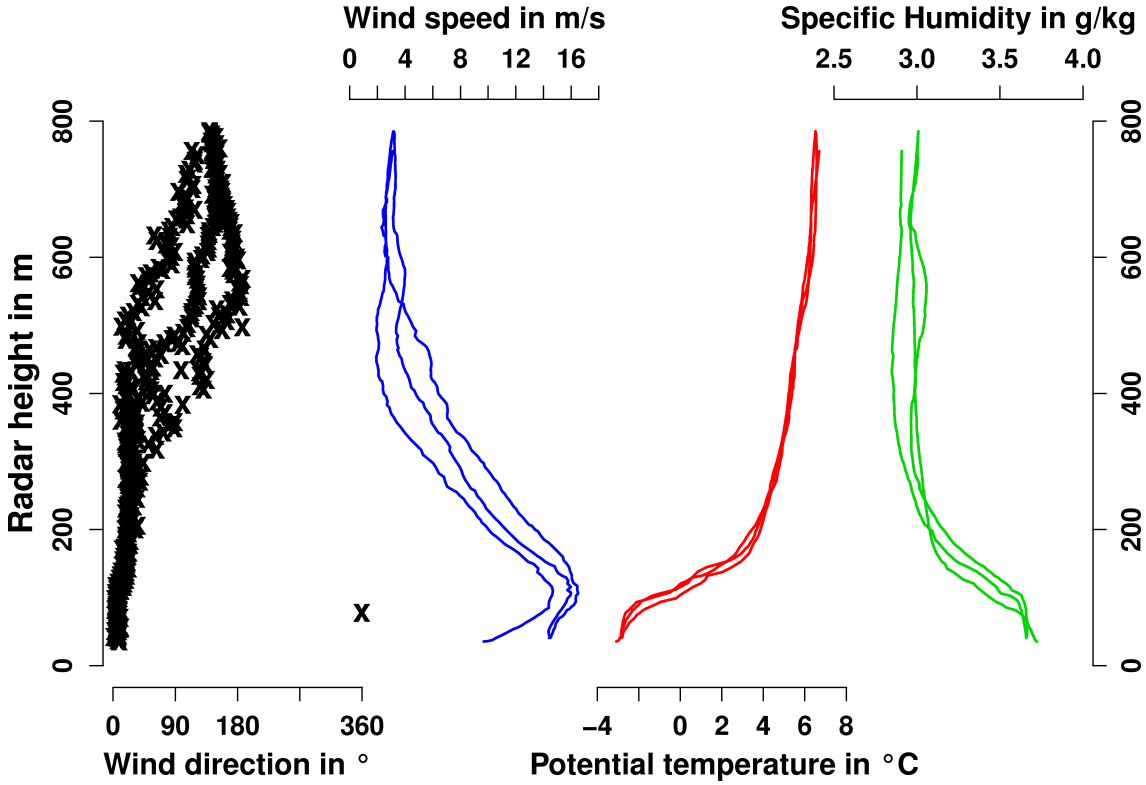

Figure 5.9: Vertical profiles of low-pass filtered mean quantities for 18 June 2010, around 1430 UTC at northern NOW (near point A, for position see Section 3.7).

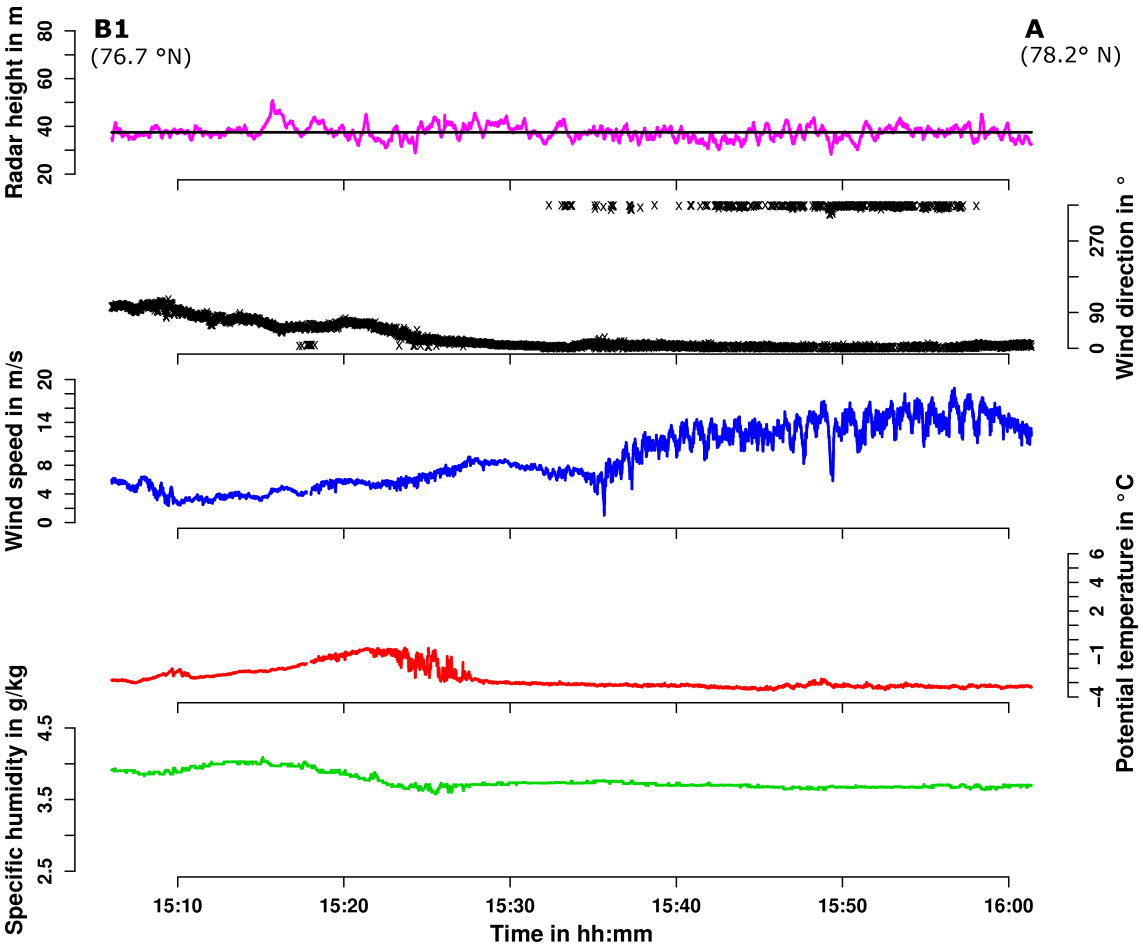

Figure 5.10: As Figure 5.4, but for 18 June 2010. The aircraft leg started at central NOW (point B1) and ended at northern NOW (point A, for positions see Section 3.7). Latitude coordinates are indicated. The horizontal line in the uppermost panel depicts the mean radar height (38 m).

5.3.3 22 June 2010

The third NOW flight is characterized by warm northerly winds, as well. However, compared to the other NOW flights the LLJ is even higher at northern NOW and has a wind speed up to 22 m s^{-1} (Figure 5.11). Due to strong winds and associated mixing, the lowest part of the SBL is only slightly stable. Lee effects at Q1a cause a decrease in wind speed from 14 to 2 m s^{-1} (see also Figure 5.12). In addition, temperature is increased by 2 to 3 °C.

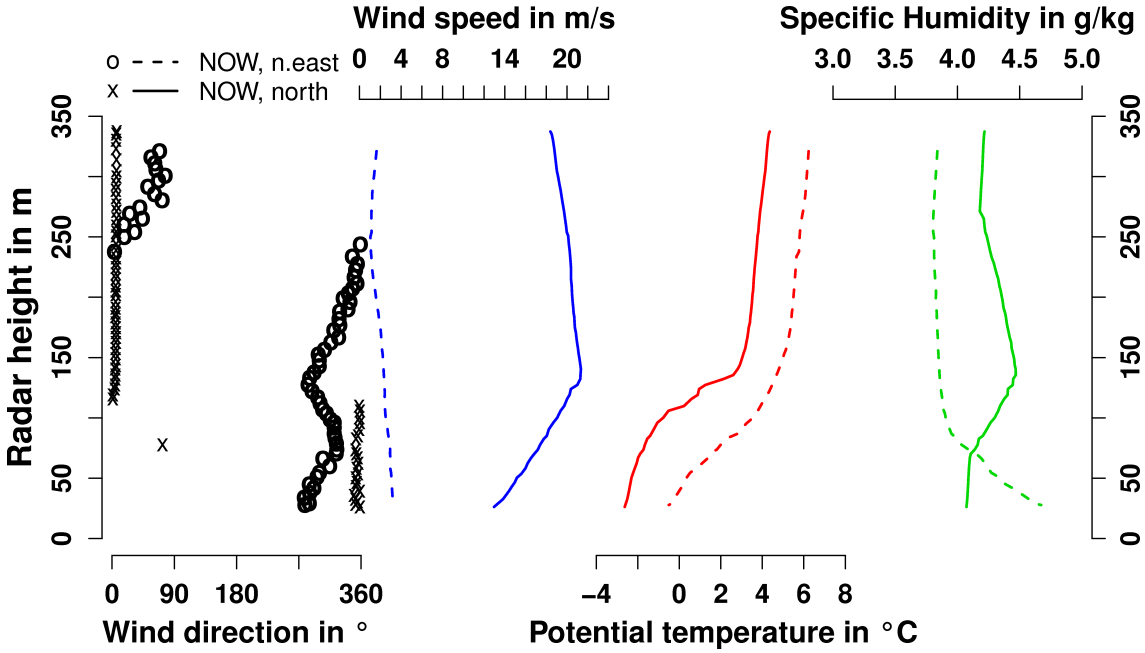

Figure 5.11: Vertical profiles of low-pass filtered mean quantities for 22 June 2010, 1435 UTC at northern NOW (point Q1a) and 1450 UTC at north-eastern NOW (point Q1b, for positions see Section 3.8).

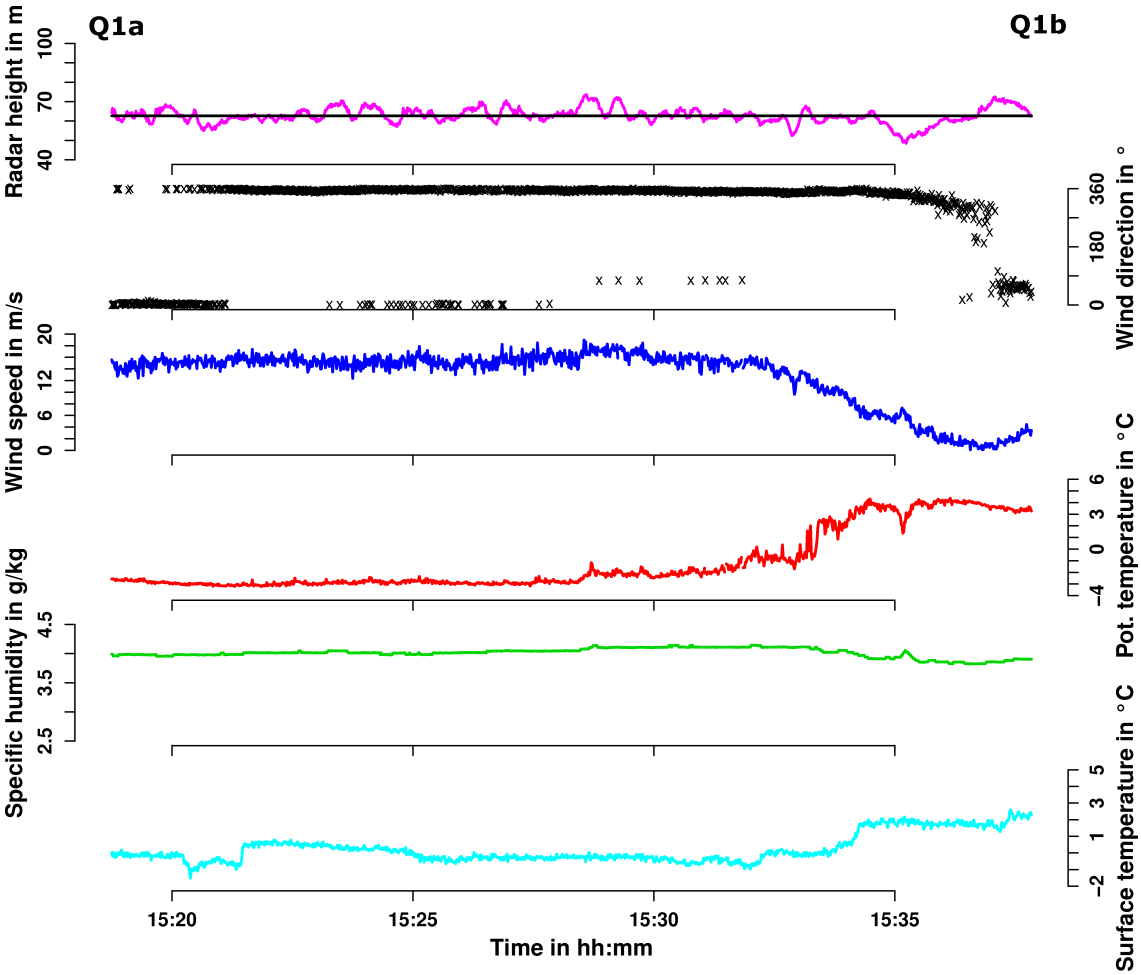

Figure 5.12: As Figure 5.4, but for the cross-profile Q1 for 22 June 2010 (for positions see Section 3.8). Surface temperature is shown in the lowermost panel. The horizontal line in the uppermost panel depicts the mean radar height (63 m).

5.3.4 23 June 2010

On 23 June 2010 the last flight was performed over the NOW and Smith Sound. Figure 5.13 shows vertical profiles of mean quantities for these regions. As during the other NOW flights northern winds channeled by Smith Sound prevail. Directly south of Smith Sound a well-pronounced LLJ associated with a wind speed maximum of 20 m s^{-1} at about 140 m is observed. In contrast, the wind speed is much lower at central NOW (the maximum value is 8 m s^{-1} at 80 m height). In both cases the temperature profile in the SBL is similar. The temperature rises by approximately 10 K within the lowest 150 m flight layer.

In the area north of Smith Sound the wind speed is about 5 m s^{-1} at 65 m height, hence 15 m s^{-1} lower than at the narrow Smith Sound (Figure 5.14) indicating the impact of the channeling effect.

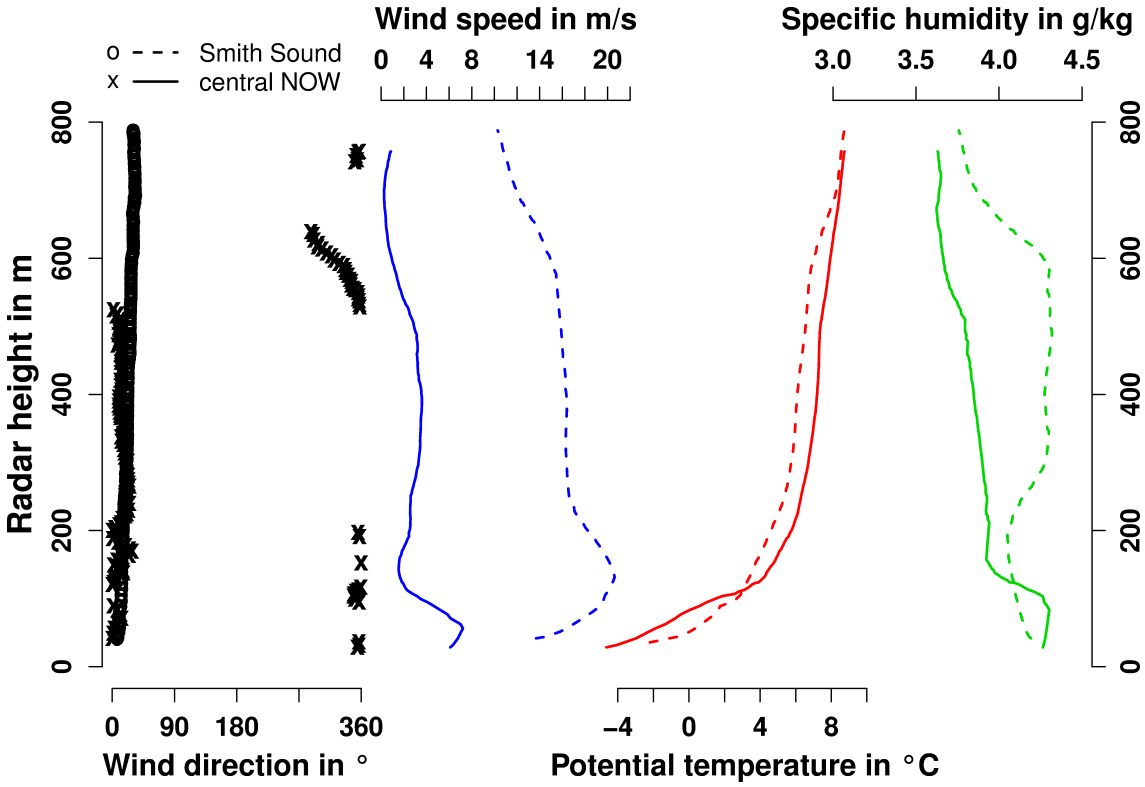

Figure 5.13: Vertical profiles of low-pass filtered mean quantities for 23 June 2010, 1345 UTC at central NOW (point B1) and 1400 UTC south of Smith Sound/at northern NOW (point M1, for positions see Section 3.9).

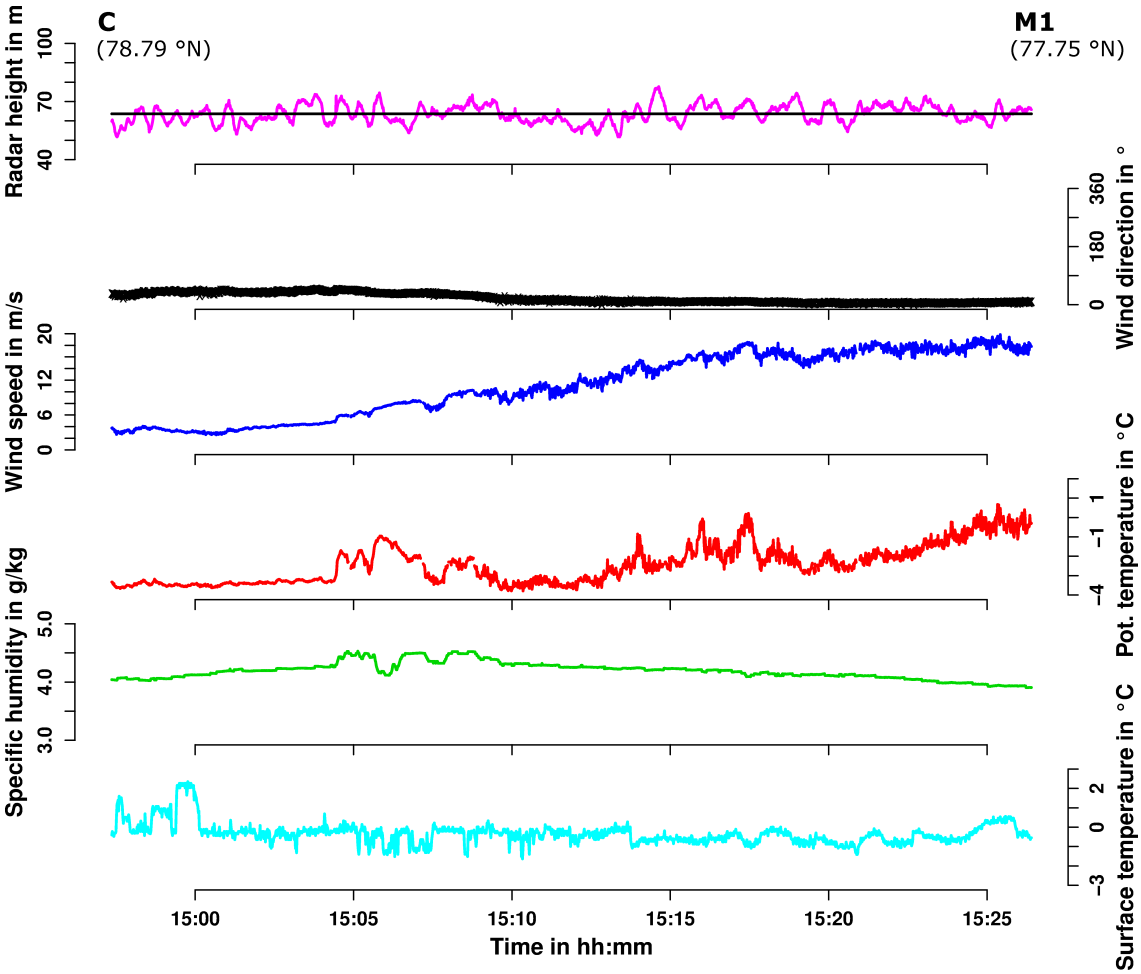

Figure 5.14: As Figure 5.4, but for 23 June 2010. Surface temperature is shown in the lowermost panel. The aircraft leg started north of Smith Sound (point C) and ended south of Smith Sound/at north NOW (point M1, for positions see Section 3.9). Latitude coordinates are indicated. The horizontal line in the uppermost panel depicts the mean radar height (64 m).

Chapter 6

Summary and conclusions

During June 2010, the aircraft-based experiment IKAPOS (**I**nvestigation of **Ka**tabatic winds and **Po**lynyas during **S**ummer) was performed in northwestern Greenland. The main objective was the investigation of the summertime katabatic wind system and of the atmospheric boundary layer (ABL) over the North Water Polynya (NOW).

Katabatic winds play a key role in exchange processes of energy and momentum between the atmosphere and the underlying surface over the ice sheet of Greenland. During summer, cooling of the boundary layer and hence the katabatic forcing is much less than during winter, but strong winds can occur during appropriate synoptic forcing. On the other hand, the NOW represents one of the largest polynyas of the Arctic, and air-sea interaction over the NOW has a significant impact on ocean processes, ice formation, gas exchange and biology.

The present study is based on aircraft measurements in the ABL using the research aircraft POLAR 5 of Alfred Wegener Institute (AWI, Bremerhaven). In order to study the turbulence structure and 3D spatial structures of mean quantities POLAR 5 was equipped with a turbulence measurement system collecting data on a nose boom sampling at a rate of 100 Hz. Additional instrumentation includes basic meteorological equipment, radiation and surface temperature sensors, laser altimeters, and photo and video cameras. A comprehensive in-flight calibration has been carried out. This kind of calibration is a necessary part of a flight campaign in order to determine calibration coefficients and sensor time lags depending on the sensor installation for a specific campaign.

For different synoptic situations, four flights over the NOW and one flight each over the Humboldt and the Steenstrup Glaciers were performed. Over the Steenstrup Glacier, synoptically forced katabatic winds with up to 14 m s^{-1} were found while over the Humboldt Glacier the downslope wind was weaker for weak synoptic forcing. The katabatic wind system depends on synoptic forcing and boundary conditions over the ice sheet, and results from the interaction of buoyancy force, Coriolis force and friction. The katabatic wind system for the summertime conditions during IKAPOS was generally not as well-developed as during KABEG in April/May 1997 in the area of southern Greenland during springtime conditions (*Heinemann*, 1999).

Over the NOW, a stable, but fully turbulent ABL was present during conditions

of strong and relatively warm synoptically induced northerly winds. Strong surface inversions were found in the lowest 100 m – 200 m AGL. As a consequence of channeling effects at Smith Sound a well-pronounced low-level jet with wind speed maxima of more than 20 m s^{-1} was detected. This channeling effect leads to an increased wind-induced sea-ice export from the Nares Strait through Smith Sound, which has not been considered in previous studies of NOW formation (*Barber et al.*, 2001a).

Our results are based on 1 Hz data sampled from 100 Hz measurements. A first insight into the structures of the katabatic wind and of the ABL over the NOW for summertime conditions was given, but a detailed investigation using the full dataset for the computation of turbulent fluxes, boundary layer budget etc. will be the next step. The data will be used for verification of model simulations and parameterizations, and studies of local similarity properties of the continuously turbulent SBL over the NOW will be carried out. In addition, the aircraft data of the IKAPOS campaign have a large potential for further investigations of orographically channeled flows.

Appendix A

Abbreviations

Abbreviation	Explanation
3D	three-dimensional
ACIA	Arctic Climate Impact Assessment
AEEC	Airlines Electronic Engineering Committee
AGL	Above Ground Level
AMSR-E	Advanced Microwave Scanning Radiometer for EOS
APM	Alternating Polarisation Medium-resolution
ARINC	Aeronautical Radio Incorporated
ARTIST	Arctic Radiation and Turbulence Interaction Study
ASAR	Advanced Synthetic Aperture Radar
ASCII	American Standard Code for Information Interchange
ASL	Above Sea Level
ATR	Avions de Transport Régional
AWI	Alfred-Wegener-Institut für Polar- und Meeresforschung
AWS	Automatic Weather Station
BT	Turbo Conversions
CAL	Calibration flight
CIRES	Cooperative Institute for Research in Environmental Science
CIS	Canadian Ice Service
COI	Center for Ocean and Ice
DC	Douglas Company
DEM	Digital Elevation Model
DFG	Deutsche Forschungsgemeinschaft
DMI	Danish Meteorological Institute
DWD	Deutscher Wetterdienst
ECMWF	European Centre for Medium-Range Weather Forecasts
ENVISAT	Environmental Satellite
EOS	Earth Observing System
ESA	European Space Agency
ETOPO2v2	2-Minute Gridded Global Relief Data
ETOPO5	5-Minute Gridded Global Relief Data
GC-Net	Greenland Climate Network
GIMEX	Greenland Ice Margin Experiment

GME	Globalmodell des Deutschen Wetterdienstes
GPS	Global Positioning System
IAPP	International Arctic Polynya Programme
IATA	International Air Transport Association
ICAO	International Civil Aviation Organization
IKAPOS	Investigation of Katabatic winds and Polynyas during Summer
INS	Inertial Navigation System
KA1–2	Flight mission 1 and 2 over glaciers
KABEG	Katabatic Wind and Boundary Layer Front Experiment around Greenland
Leg	Constant level run
LLJ	Low-Level Jet
METAR	Meteorological Aerodrome Report
MODIS	Moderate Resolution Imaging Spectroradiometer
N/A	Not Available
NASA	U.S. National Aeronautics and Space Administration
NCEP/DOE	National Centers for Environmental Prediction/Department of Energy
NEEM	North Greenland Eemian Ice Drilling
NEW	Northeast Water Polynya
NGDC	National Geophysical Data Center
NOAA	National Oceanic and Atmospheric Administration
NOW	North Water Polynya
NOW1–4	Flight missions 1 to 4 over the NOW
NRI	Nunavut Research Institute
NSIDC	U.S. National Snow and Ice Data Center
PBL	Planetary Boundary Layer
PMOD/WRC	Physikalisch-Meteorologisches Observatorium Davos/World Radiation Center
SAFIRE	Service des Avions Français Instrumentés pour la recherche en environnement
SBL	Stable Boundary Layer
SSM/I	Special Sensor Microwave/Imager
TAS	True Air Speed
Temp	Vertical flight profile
U.S.	United States of America

Appendix B

References

ACIA (2005), Arctic Climate Impact Assessment 2005, 1042 pp., Cambridge University Press.

AEEC (2001), Mark 33 Digital Information Transfer System (DITS), Part 3 File Data Transfer Techniques, no. 429P3-18 in Arinc Specification, 18 ed., 123 pp., Aeronautical Radio Inc., Annapolis, MD.

Bâcle, J. (2000), The physical oceanography of waters under the North Water Polynya, Master's thesis, Department of Atmospheric and Oceanic Sciences, Centre for Climate and Global Change Research McGill University, Montreal.

Barber, D., and R. Massom (2007), The Role of Sea Ice in Arctic and Antarctic Polynyas, in *Polynyas: Windows to the World*, *Elsevier Oceanography Series*, vol. 74, edited by W. Smith and D. Barber, pp. 1–54, Elsevier, 10.1016/S0422-9894(06)74001-6.

Barber, D. G., J. M. Hanesiak, W. Chan, and J. Piwowar (2001a), Sea-Ice and Meteorological Conditions in Northern Baffin Bay and the North Water Polynya between 1979 and 1996, *Atmosphere-Ocean*, *39*(3), 343–359.

Barber, D. G., R. Marsden, P. Minnett, G. Ingram, and L. Fortier (2001b), Physical processes within the North Water (NOW) polynya, *Atmosphere-Ocean*, *39*(3), 163–166.

Bögel, W., and R. Baumann (1991), Test and Calibration of the DLR Falcon Wind Measuring System by Maneuvers, *Journal of Atmospheric and Oceanic Technology*, *8*(1), 5–18.

Bromwich, D. H., J. J. Cassano, T. Klein, G. Heinemann, K. M. Hines, K. Steffen, and J. E. Box (2001), Mesoscale Modeling of Katabatic Winds over Greenland with the Polar MM5*, *Monthly Weather Review*, *129*(9), 2290–2309.

Cremer, M. (2008), Kalibrierung der Turbulenzmesssonde der Polar 5, mW-AWI-P5-2008-06, messWERK GmbH, Baunschweig.

Drüe, C. (2001), Experimentelle Untersuchung arktischer Grenzschichtfronten an der Meereisgrenze in der Davis-Straße, *Bonner meteorologische Abhandlungen*, vol. 54, 165 pp., Asgard-Verlag, St.-Augustin, Germany.

Dunbar, M. (1973), Ice Regime and Ice Transport in Nares Strait, *Arctic*, *26*(4), 282–291.

Freese, D. (1999), Solare und terrestrische Strahlungswechselwirkung zwischen arktischen Eisflaechen und Wolken, *Reports on Polar Research*, vol. 312, 116 pp., Alfred-Wegener-Institut für Polar- und Meeresforschung, Bremerhaven.

Garman, K., P. Wyss, M. Carlsen, J. Zimmerman, B. Stirm, T. Carney, R. Santini, and P. Shepson (2008), The Contribution of Variability of Lift-induced Upwash to the Uncertainty in Vertical Winds Determined from an Aircraft Platform, *Boundary-Layer Meteorology*, *126*(3), 461–476.

Gordon, A., and J. C. Comiso (1988), Polynyas in the Southern Ocean, *Scientific American*, *256*(6), 70–77.

Hebbinghaus, H., and G. Heinemann (2006), LM simulations of the Greenland boundary layer, comparison with local measurements and SNOWPACK simulations of drifting snow, *Cold Regions Science and Technology*, *46*(1), 36–51.

Heinemann, G. (1998), Katabatic wind and Boundary Layer Front Experiment around Greenland (”KABEG ’97”), *Reports on Polar Research*, vol. 269, 93 pp., Alfred-Wegener-Institut für Polar- und Meeresforschung, Bremerhaven.

Heinemann, G. (1999), The KABEG’97 field experiment: An aircraft-based study of katabatic wind dynamics over the Greenland ice sheet, *Boundary-Layer Meteorology*, *93*, 75–116.

Heinemann, G. (2000), On the streakiness of katabatic wind signatures on high-resolution AVHRR satellite images: Results from the aircraft-based experiment KABEG, *Polarforschung*, *66*(3), 19–30.

Heinemann, G. (2002), Aircraft-Based Measurements Of Turbulence Structures In The Katabatic Flow Over Greenland, *Boundary-Layer Meteorology*, *103*, 49–81.

Heinemann, G. (2003), Forcing and feedback mechanisms between the katabatic wind and sea ice in the coastal areas of polar ice sheets, *The Global Atmosphere and Ocean System*, *9*(4), 169–201.

Heinemann, G., and U. Falk (2002), Surface winds and energy fluxes near the Greenland ice margin under conditions of katabatic winds, *Polarforschung*, *71*(1/2), 15–31.

Honeywell (2004), Laseref V Micro Inertial Reference System, 3 pp., Honeywell International.

Inverarity, G. W. (2000), Correcting Airborne Temperature Data for Lags Introduced by Instruments with Two-Time-Constant Responses, *Journal of Atmospheric and Oceanic Technology*, *17*, 176–184.

Khelif, D., S. P. Burns, and C. A. Friehe (1999), Improved Wind Measurements on research aircraft, *Journal of Atmospheric and Oceanic Technology*, *16*, 860–875.

Klein, T., and G. Heinemann (2002), Interaction of katabatic winds and mesocyclones near the eastern coast of Greenland, *Meteorological Applications*, *9*(4), 407–422.

Kwok, R. (2005), Variability of Nares Strait ice flux, *Geophysical Research Letters*, *32*, L24502.

Kwok, R., L. T. Pedersen, P. Gudmandsen, and S. S. Pang (2010), Large sea ice outflow into the Nares Strait in 2007, *Geophysical Research Letters*, *37*, L03502.

Lenschow, D. H. (1986), Probing the Atmospheric Boundary Layer, 269 pp., American Meteorological Society, Boston.

Matejka, T., and S. A. Lewis (1997), Improving Research Aircraft Navigation by Incorporating INS and GPS Information in a Variational Solution, *Journal of Atmospheric and Oceanic Technology*, *14*, 495–511.

Meesters, A. (1994), Dependence of the energy balance of the Greenland ice sheet on climate change: Influence of katabatic wind and tundra, *Quarterly Journal of the Royal Meteorological Society*, *120*(517), 491–517.

Melling, H., Y. Gratton, and G. Ingram (2001), Ocean circulation within the North Water polynya of Baffin Bay, *Atmosphere-Ocean*, *39*(3), 301–325.

NGDC (1988), ETOPO5, Data Announcement 88-MGG-02, Digital relief of the Surface of the Earth, NOAA, Boulder, CO.

NGDC (2006), ETOPO2v2, Global Gridded 2-minute Database, NOAA, Boulder, CO.

Oerlemans, J., and H. F. Vugts (1993), A Meteorological Experiment in the Melting Zone of the Greenland Ice Sheet, *Bulletin of the American Meteorological Society*, *74*(3), 355–365.

Preußer, A., G. Heinemann, and C. Drüe (2011), Investigation of the dynamics of the North Water polynya for 1996–2010 using satellite data, *European Geosciences Union (EGU), General Assembly, Geophysical Research Abstracts*, *13*(EGU2011-1919).

Putnins, P. (1970), The Climate of Greenland, *S. Orvig, Climates of the Polar Regions*, vol. 14, Elesevier, New York, 3–128.

Rasmussen, L. (1989), Den dag, Angmagssalik naesten blaeste i havet, *Vejret*, *2*, Danish Meteorological Society, 3–14.

Samelson, R. M., and P. L. Barbour (2008), Low-Level Jets, Orographic Effects, and Extreme Events in Nares Strait: A Model-Based Mesoscale Climatology, *Monthly Weather Review*, *136*(12), 4746–4759.

Samelson, R. M., T. Agnew, H. Melling, and A. Munchow (2006), Evidence for atmospheric control of sea-ice motion through Nares Strait, *Geophysical Research Letters*, *33*(2), L02506.

Schneider, W., and G. Budéus (1997), Summary of the Northeast Water Polynya formation and development (Greenland sea), *Journal of Marine Systems*, *10*(1-4), 107–122.

Spreen, G., L. Kaleschke, and G. Heygster (2008), Sea ice remote sensing using AMSR-E 89-GHz channels, *Journal of Geophysical Research*, *13*, C02S03.

Spyers-Durand, P., and D. Baumgartner (1983), In flight estimation of the time response of airborne temperature sensors, in *Proceedings 5. Symposion on Meteorological Observations and Instrumentation, April 11–15, 1983, Toronto, Canada*, edited by A. M. Society, Boston.

Statistics Greenland (2010), Greenland in figures, *7*, 40.

Strunin, M. A., and T. Hiyama (2004), Response properties of atmospheric turbulence measurement instruments using Russian research aircraft, *Hydrological Processes*, *18*(16), 3099–3117.

Tjernström, M., and P. Samuelsson (1995), The Effect of Inertial Navigation System Time Response on Airborne Turbulence Measurements, *Journal of Atmospheric and Oceanic Technology*, *12*, 1196–1213.

van den Broeke, M., P. Duynkerke, and J. Oerlemans (1994), The observed katabatic flow at the edge of the Greenland ice sheet during GIMEX-91, *Global and Planetary Change*, *9*(1-2), 3–15.

Vörsmann, P., B. Henrici, and A. M. Hoff (1989), METEOPOD - ein flugzeuggestütztes Turbulenzmesssystem, *Promet*, *19*, 57–64.

Yao, T., and C. L. Tang (2003), The Formation and Maintenance of the North Water Polynya, *Atmosphere-Ocean*, *41*(3), 187–201.

Appendix C

Public outreach

Informationsdienst Wissenschaft

Pressemitteilung

Trierer Forscher untersuchen Klimaprozesse in der Arktis

Peter Kuntz, Presse- und Öffentlichkeitsarbeit
Universität Trier

05.08.2010 12:21

Universität Trier

Das DFG-Projekt steht unter Leitung von Prof. Günther Heinemann

Mit dem Spezialflugzeug POLAR 5 führten die Trierer Wissenschaftler ihre Messungen in der Arktis durch.
Günther Heinemann

Wissenschaftler der Universität Trier leisten einen bedeutenden Beitrag zum Verständnis des Klimasystems in der Arktis. Dazu wurde eine dreiwöchige Messkampagne im Rahmen des Trierer Projekts IKAPOS unter der Leitung von Prof. Günther Heinemann (Umweltmeteorologie) in Nordgrönland durchgeführt. Mit dem speziell für meteorologische Messungen instrumentierten Forschungsflugzeug „POLAR 5" wurden bei Flügen über Gletschern in Nord- und Westgrönland sowie über Meereis und Ozean im Bereich der Nares-Straße zwischen Kanada und Grönland Messdaten erhoben. Die Expeditionsbasis befand sich im Inuit-Dorf Qaanaaq, in dem 600 Einwohner leben. Hauptziel der Messungen war die quantitative Erfassung von Austauschprozessen zwischen Eis- bzw. Ozeanoberfächen und der Atmosphäre.
Die Messungen dienen zum Verständnis des arktischen Klimasystems und der Klimamodellierung in polaren Regionen. Die Flugzeugmessungen wurden durch das Alfred-Wegener-Institut gefördert, die Auswertungen finden im Rahmen eines Projekts der Deutschen Forschungsgemeinschaft (DFG) statt und werden etwa zwei Jahre dauern.

URL dieser Pressemitteilung: http://idw-online.de/de/news381827
Merkmale dieser Pressemitteilung:
Geowissenschaften, Meer / Klima, Umwelt / Ökologie
überregional

Forschungsprojekte Deutsch

Figure C.1: Press release ”Informationsdienst Wissenschaft”, 05 August 2010.

JuraForum.de > Nachrichten > Wissenschaft > **Trierer Forscher untersuchen Klimaprozesse in der Arktis**

Trierer Forscher untersuchen Klimaprozesse in der Arktis

05.08.2010, 13:00 | Wissenschaft | Autor: idw

Das DFG-Projekt steht unter Leitung von Prof. Günther Heinemann

Wissenschaftler der Universität Trier leisten einen bedeutenden Beitrag zum Verständnis des Klimasystems in der Arktis. Dazu wurde eine dreiwöchige Messkampagne im Rahmen des Trierer Projekts IKAPOS unter der Leitung von Prof. Günther Heinemann (Umweltmeteorologie) in Nordgrönland durchgeführt. Mit dem speziell für meteorologische Messungen instrumentierten Forschungsflugzeug „POLAR 5" wurden bei Flügen über Gletschern in Nord- und Westgrönland sowie über Meereis und Ozean im Bereich der Nares-Straße zwischen Kanada und Grönland Messdaten erhoben. Die Expeditionsbasis befand sich im Inuit-Dorf Qaanaaq, in dem 600 Einwohner leben. Hauptziel der Messungen war die quantitative Erfassung von Austauschprozessen zwischen Eis- bzw. Ozeanoberfächen und der Atmosphäre.
Die Messungen dienen zum Verständnis des arktischen Klimasystems und der Klimamodellierung in polaren Regionen. Die Flugzeugmessungen wurden durch das Alfred-Wegener-Institut gefördert, die Auswertungen finden im Rahmen eines Projekts der Deutschen Forschungsgemeinschaft (DFG) statt und werden etwa zwei Jahre dauern.

Quelle: idw

Figure C.2: ”JURAFORUM.DE”, 05 August 2010.

16 vor - Nachrichten aus Trier

QAANAAQ/TRIER. Wissenschaftler der Uni Trier leisten einen Beitrag zum besseren Verständnis des Klimasystems in der Arktis. Die Forscher begaben sich auf eine Messkampagne nach Nordgrönland.

Die mehrwöchigen Untersuchungen wurden im Rahmen des Trierer Projekts IKAPOS unter der Leitung von Professor Günther Heinemann (Umweltmeteorologie) durchgeführt. Mit dem speziell für meteorologische Messungen ausgerüsteten Forschungsflugzeug "POLAR 5" wurden bei Flügen über Gletschern in Nord- und Westgrönland sowie über Meereis und Ozean im Bereich der Nares-Straße zwischen Kanada und Grönland Messdaten erhoben.

Die Expeditionsbasis befand sich im Inuit-Dorf Qaanaaq, in dem 600 Einwohner leben. Hauptziel der Messungen war die quantitative Erfassung von Austauschprozessen zwischen Eis- beziehungsweise Ozeanoberflächen und der Atmosphäre. Die Messungen dienen zum Verständnis des arktischen Klimasystems und der Klimamodellierung in polaren Regionen. Die Flugzeugmessungen wurden durch das Alfred-Wegener-Institut gefördert, die Auswertungen finden im Rahmen eines Projekts der Deutschen Forschungsgemeinschaft (DFG) statt und werden etwa zwei Jahre dauern.

von 16vor

Figure C.3: ”16vor.de” (news from Trier), 14 August 2010.

Trierer Forscher untersuchen Klimaprozesse in der Arktis

Wissenschaftler der Universität Trier leisten einen Beitrag zum Verständnis des Klimasystems in der Arktis. Dazu wurde eine dreiwöchige Messkampagne im Rahmen des Trierer Projekts IKAPOS unter der Leitung von Professor Günther Heinemann (Umweltmeteorologie) in Nordgrönland vorgenommen.

Trier. (red) Mit dem speziell für meteorologische Messungen instrumentierten Forschungsflugzeug "Polar 5" wurden bei Flügen über Gletschern in Nord- und Westgrönland sowie über Meereis und Ozean im Bereich der Nares-Straße zwischen Kanada und Grönland Messdaten erhoben. Die Expeditionsbasis befand sich im Inuit-Dorf Qaanaaq, in dem 600 Einwohner leben.

Hauptziel der Messungen war die zahlenmäßige Erfassung von meteorologischen Austauschprozessen zwischen Eis- beziehungsweise Ozeanoberflächen und der Erdatmosphäre.

Die Messungen dienen zum Verständnis des arktischen Klimasystems und der Klimamodellierung in polaren Regionen.

Die Flugzeugmessungen wurden durch das Alfred-Wegener-Institut gefördert, die Auswertungen finden im Rahmen eines Projekts der Deutschen Forschungsgemeinschaft (DFG) statt und werden etwa zwei Jahre dauern.

Figure C.4: ”Trierischer Volksfreund” (daily newspaper of Trier), 25 August 2010.

Arktis spiegelt Klimaänderungen

Trierer Forscher untersuchen Prozesse aus dem Spezialflugzeug heraus

Die Arktis gehört zu den besonders sensitiven Regionen im globalen Klimasystem. Klimaänderungen haben sich bereits in der Vergangenheit viel stärker in der Arktis als z.B. in Europa ausgewirkt. Der Rückgang des Meereises in den letzten 20 Jahren mit dem bisherigen Rekordminimum in 2007 ist ein Indikator für diese Änderungen in der Arktis. Klimasimulationen zeigen noch weitaus dramatischere Veränderungen in diesem Jahrhundert auf. So wird z.B. die Erwärmung in der Arktis bis zu viermal so hoch wie in mittleren Breiten ausfallen. Andererseits haben Klimamodelle noch große Defizite bei der Simulation der Wechselwirkung zwischen Atmosphäre, Meereis und Ozean. Daher ist es besonders wichtig, die Klimaprozesse in der Arktis zu verstehen und zu quantifizieren. Wissenschaftler der Universität Trier leisten dazu einen bedeutenden Beitrag.

Im Juni 2010 wurde eine dreiwöchige Messkampagne im Rahmen des Trierer Projekts IKA-POS unter der Leitung von Prof. Günther Heinemann (Umweltmeteorologie) in Nordgrönland durchgeführt. Mit dem speziell für meteorologische Messungen instrumentierten Forschungsflugzeug „POLAR5" wurden bei Flügen über Gletschern in Nord- und Westgrönland sowie über Meereis und Ozean im Bereich der Nares-Straße zwischen Kanada und Grönland Messdaten erhoben. Die Expeditionsbasis befand sich im Inuit-Dorf Qaanaaq, in dem ca. 600 Einwohner leben. Die Flugzeugmessungen wurden durch das Alfred-Wegener-Institut gefördert, die Auswertungen finden im Rahmen eines Projekts der Deutschen Forschungsgemeinschaft (DFG) statt.

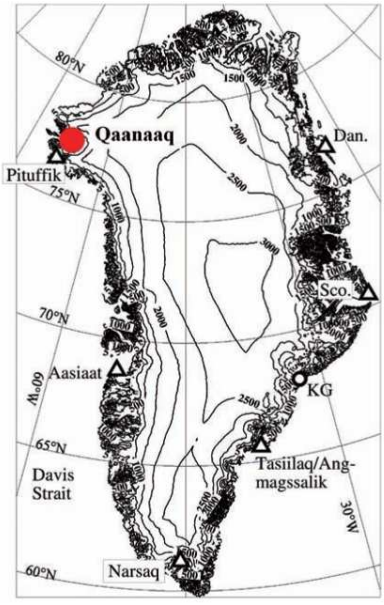

Abbildung 1: Die Topographie von Grönland (Höhenlinien in 500-Meter-Abstand), Qaanaaq ist mit einem roten Punkt markiert (nach Heinemann 2003).

Im Rahmen des von der DFG geförderten Projektes „Experimental study of the interaction of the atmosphere with polynyas/sea ice near Greenland (IKAPOS)" führte Prof. Günther Heinemann mit seinem Doktoranden Thomas Ernsdorf (Fach Umweltmeteorologie der Universität Trier) vom 7. bis 29. Juni 2010 eine Messkampagne in Nordgrönland durch (Abb.1). Das generelle Ziel des Projekts ist die Untersuchung der Prozesse der Wechselwirkung zwischen Atmosphäre, Inlandeis, Meereis und Ozean. Dazu wurden drei Messgebiete ausgewählt (Abb.2): zwei Gletschergebiete (Humboldt-Gletscher an der Nordküste, Steenstrup-Gletscher an der Westküste) und eine Wasserfläche im Meereis des Küstenbereichs von Nordgrönland, der sogenannte North-Water-Polynja (NOW). Diese Polynja bildet sich südlich der Nares-Straße zwischen Kanada und Grönland (Abb.2). Die Erfassung der atmosphärischen Bedingungen über der Polynja ist auch bedeutsam für die ozeanische Konvektion, den Austausch von Spurenstoffen und biologische Prozesse.

Das Experiment IKAPOS wurde mit dem speziell für meteorologische Messungen instrumentierten Forschungsflugzeug „POLAR5" des Alfred-Wegener-Instituts (AWI, Bremerhaven) durchgeführt. POLAR5 ist eine umgebaute DC-3. Dieses eigentlich sehr alte Flugzeug, das in den Zeiten der Berliner Blockade zur Versorgung über die Luftbrücke eingesetzt wurde, ist vor wenigen Jahren vollständig erneuert und mit modernster Elektronik ausgerüstet worden. Zur Untersuchung der atmosphärischen Prozesse in der sogenannten „Grenzschicht", die sich bis in eine Höhe von 100 bis 200 Metern über der Oberfläche erstreckt, sind

Forschungsdossier

39

Figure C.5: "Unijournal" (journal of the University of Trier), no. 3/4, 2010, p. 39.

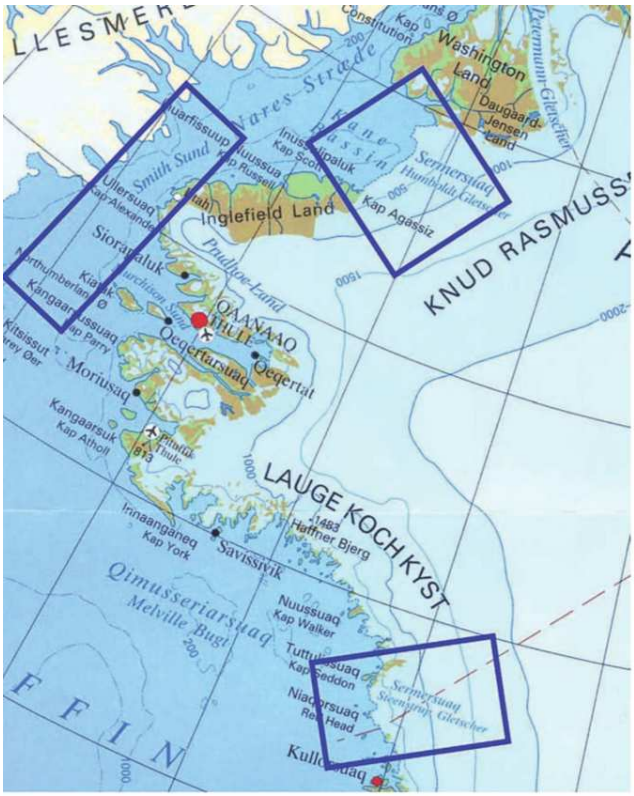

Abbildung 2: Die Lage der Experimentgebiete und der Expeditionsbasis Qaanaaq.

© Heinemann 2009, Karte von Kort & Matrikelstyrelsen, Copenhagen

hochgenaue und zeitlich sehr hoch aufgelöste Messungen nötig.

Hochempfindliche Drucksensoren registrierten den Wind 100 mal pro Sekunde und verrechneten ihn mit der Fluggeschwindigkeit und den Lagewinkeln des Flugzeugs, andere Fühler erfassten zur selben Zeit Höhe, Temperatur, Feuchte und Strahlungsgrößen. Zur Durchführung der Flugmessungen war ein hochspezialisiertes Team aus zwei Piloten, einem Mechaniker und zwei Messtechnikern notwendig, das zusammen mit dem Flugzeug vom AWI für drei Wochen und für maximal 60 Flugstunden zur Verfügung gestellt wurde. Da eine Flugstunde ca. 5000 Euro kostet, musste im Vorfeld von Prof. Heinemann ein Forschungsantrag gestellt werden, der ein Begutachtungsverfahren mit positivem Ergebnis durchlief.

Die Expeditionsbasis war das Inuit-Dorf Qaanaaq, das mit ca. 600 Einwohnern zu der größten Siedlung im Umkreis von fast 1000 Kilometern gehört. Die Menschen leben dort überwiegend von der Jagd auf Wale und Robben. Das Dorf wird einmal pro Jahr im Juli durch ein Schiff mit Lebensmitteln und Geräten versorgt. Während des Aufenthaltes der Trierer Forscher im Juni waren daher viele Lebensmittel, die für uns sonst selbstverständlich sind (wie Milch, Obst, Gemüse), nicht erhältlich. Andererseits war Qaanaaq in einer idealen geographischen Lage, um die Messungen in den drei Messgebieten durchzuführen.

Die Flugbedingungen erwiesen sich als sehr schwierig, da häufig Bodennebel einen Messflug verhinderte. Trotzdem war das Experiment sehr erfolgreich. Es konnten sowohl je ein Flug über den beiden Gletschern als auch sechs Flüge über der NOW-Polynya stattfinden. In Trier werden nun die umfangreichen Messdaten ausgewertet und zusammen mit Satellitendaten zur Validierung von Modellsimulationen verwendet. Abschließende Ergebnisse werden in etwa zwei Jahren vorliegen.

Günther Heinemann
(Umweltmeteorologie, FB VI)

Ein Eisberg in der Nares-Straße.

Forschungsdossier

40

Figure C.6: ”Unijournal” (journal of the University of Trier), no. 3/4, 2010, p. 40.

Mit dem Spezialflugzeug POLAR 5 führten die Trierer Wissenschaftler ihre Messungen in der Arktis durch.

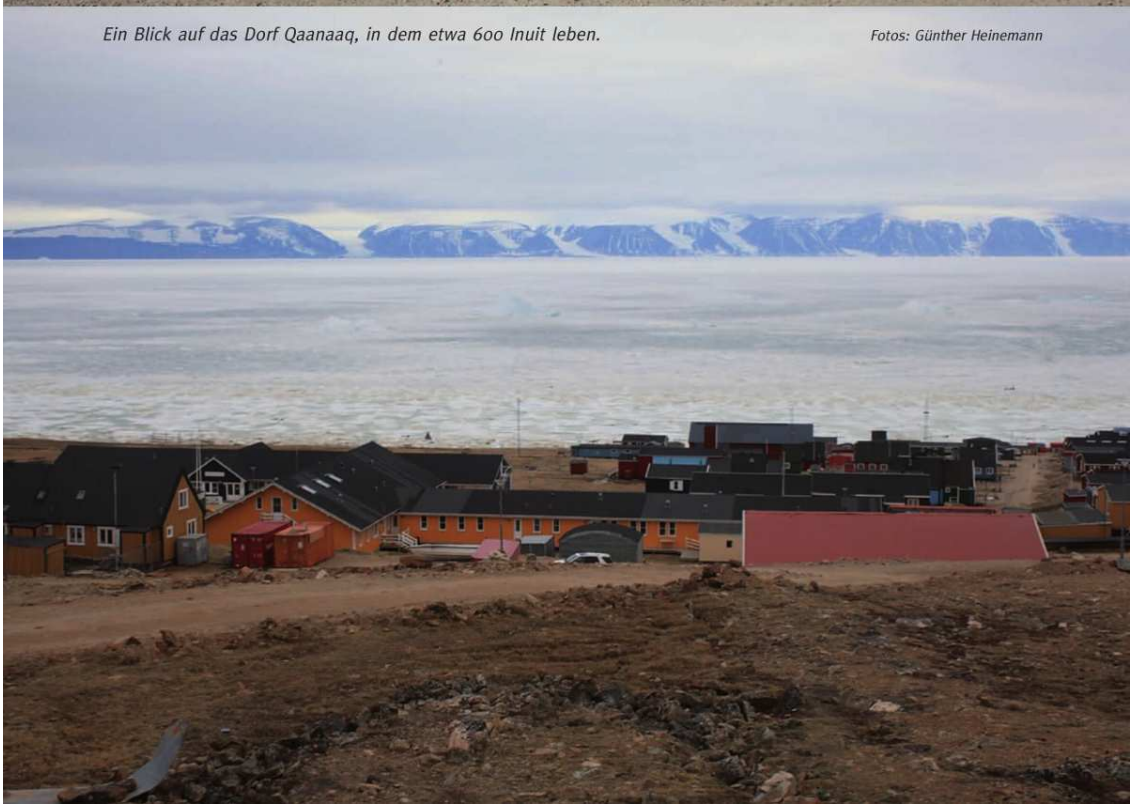

Ein Blick auf das Dorf Qaanaaq, in dem etwa 600 Inuit leben.

Fotos: Günther Heinemann

Figure C.7: ”Unijournal” (journal of the University of Trier), no. 3/4, 2010, p. 41.

Forschung im Kühlschrank der Erde

Mechthild Schneiders

Der Sommer ist die beste Zeit, um ins ewige Eis zu gehen. Dann sind Arktis und Antarktis zugänglicher; es ist hell und vergleichsweise warm. Ideale Umstände für den Trierer Meteorologen Günther Heinemann, das Eis, den Ozean und die Atmosphäre an den Polen zu untersuchen und so den Klimawandel zu verfolgen.

Trier. Idyllisch wirkt der glatte Eisberg im blauen Nordmeer auf dem Foto in Günther Heinemanns Büro in der Universität Trier, klein und dünn. "Der Eisberg ist etwa zehn Meter hoch", erklärt der Umweltmeteorologe. Nur rund zehn Prozent seien sichtbar, der Rest liege unter Wasser. Das mache sie für die Schifffart so gefährlich.

Idyllisch und gleichzeitig gefährlich: ein Eisberg vor Grönland. Foto: Günther Heinemann

Bipolare Forschungen

Eisberge sind alles andere als idyllisch. Wenn sie von den riesigen Eisflächen an Nord- und Südpol abbrechen, können sie bis zu viermal so groß sein wie das Saarland, berichtet der 56-Jährige, der seit 2006 den Lehrstuhl für Umweltmeteorologie in Trier innehat. "In der Arktis zeigen sich besonders große Änderungen beim Meereis, also dem Eis, das durch Gefrieren an der Ozeanoberfläche entsteht." Die Ursache: der Klimawandel. "Klimaänderungen zeichnen sich in der Arktis am stärksten ab." So sei das Meereis im Sommer um mehr als 30 Prozent zurückgegangen. Umso wichtiger, diese Prozesse zu

Figure C.8: ”Trierischer Volksfreund” (daily newspaper of Trier), 09 August 2011, part 1/3.

erfassen, zu erforschen und die Auswirkungen abzuschätzen, sagt Heinemann. Seit 1996/97 ist er schwerpunktmäßig in der Arktisforschung beschäftigt, betreut dort aktuell zwei Projekte. Schwerpunkte sind in Grönland, das er dreimal besuchte, sowie die Laptewsee nördlich des Lenadeltas in Sibirien. "Wir sind eine der wenigen Wissenschaftlergruppen, die dort arbeiten dürfen, und kooperieren mit russischen Arktisforschern", sagt Heinemann. "In der Laptewsee wird am Rand des Schelfmeeres Meereis in offenen oder nur mit dünnem Eis bedeckten Wasserflächen, sogenannten Polynjen, gebildet. Durch den Wind wird es von der Küste weg geweht."An der Kante der Polynjen seien Messstationen eingerichtet, an denen Eiseigenschaften sowie Atmosphäre und Ozean untersucht werden. "Wir arbeiten mit Satelliten. Für die Auswertung dieser Daten ist die Zusammensetzung, die Dichte und der Wassergehalt des Eises wichtig", sagt Heinemann. Dann könne die Verteilung der Eisflächen berechnet werden sowie wo und wie häufig dünnes Eis auftrete.

Der Trierer Meteorologe Günther Heinemann erforscht in der Laptewsee vor Sibirien die Entstehung des Meereises sowie dessen Wechselwirkungen mit Atmosphäre und Ozean. TV-Foto: Mechthild Schneiders

Heinemann forscht seit rund 30 Jahren in den Polarregionen. Seine Liebe zum Eis hat er eher zufällig entdeckt. "Im Rahmen meiner Promotion war ich 1983 in der Antarktis, im deutschen Forschungsbereich, an der Station Neumayer und im südlichen Weddellmeer." Denn 1981 sei Deutschland dem Antarktisvertrag

Figure C.9: ”Trierischer Volksfreund” (daily newspaper of Trier), 09 August 2011, part 2/3.

beigetreten. "Mein damaliger Betreuer hatte einen Forschungsauftrag erhalten und suchte einen Mitarbeiter. Mich hat es sehr gereizt hinzufahren." Bis dahin sei er mit Schnee und Eis wenig vertraut gewesen. "Ich musste mich über alles erkundigen: wie man dort Messstationen baut bis hin zur Kleidung." Nach zwei Besuchen weiß er, in der Kälte zu überleben, und beherrscht die harten Forschungsbedingungen. Seit 2010 ist Heinemann Vorsitzender des deutschen Landesausschusses SCAR (Scientific Committee on Antarctic Research/Wissenschaftliches Komitee für Antarktisforschung) und betreut zwei Projekte in der Antarktis. "Bipolare Forschung ist sinnvoll, weil viele Prozesse vollkommen gleich sind." So seien die Eisbildungsprozesse identisch. "Nur die regionalen Auswirkungen sind unterschiedlich", weiß der Meteorologe. Deshalb sei es interessant, in beide Regionen reinzuschauen. "Es ist eine spannende Frage, wie sich der Klimawandel dort auswirken wird." Der Eisrückgang in den vergangenen 30 Jahren zeige ihn ganz deutlich. "In 40 Jahren wird im Nordmeer das Eis im Sommer ganz weg sein", prognostiziert er. Das habe erhebliche Auswirkungen, etwa auf die Eisbären, die das Eis zum Ausruhen benötigten. "Eis und Wasser haben einen absoluten Reiz, es sind beeindruckende Gegensätze", sagt Heinemann. "Besonders beeindruckend ist, man ist ganz alleine im Eis. Es ist eine absolute Stille, die man sonst nirgends hat, keine Vögel, keine Büsche. Aber es ist auch gefährlich."

EXTRA TRIERER GRÖNLANDEXPEDITION

Günther Heinemanns jüngste Expedition führte ihn im Juni 2010 in den Nordwesten Grönlands, nahe des Inuit-Dorfs Qaanaaq. Dort forschte er mit einem Trierer Doktoranden im Rahmen des Projekts IKAPOS, um Daten für Klimasimulationen zu erhalten, mit denen die Auswirkungen der Klimaänderung dargestellt werden können. Drei Wochen lang haben die Trierer mit dem Forschungsflugzeug Polar5, einer umgebauten DC-3, Messdaten über Gletscher und Meer erhoben. "Meine Spezialität sind Flugzeugmessungen", sagt Heinemann. "Wir untersuchen die Strukturen der unteren Luftschichten im Bereich Meereis, Ozean und Inlandeis sowie deren Wechselwirkungen mit der Atmosphäre." Ergebnisse werden im kommenden Jahr vorliegen.

Figure C.10: ”Trierischer Volksfreund” (daily newspaper of Trier), 09 August 2011, part 3/3.

Die "Berichte zur Polar- und Meeresforschung" (ISSN 1866-3192) werden beginnend mit dem Heft Nr. 569 (2008) ausschließlich elektronisch als Open-Access-Publikation herausgegeben. Ein Verzeichnis aller Hefte einschließlich der Druckausgaben (Heft 377-568) sowie der früheren **"Berichte zur Polarforschung** (Heft 1-376, von 1982 bis 2000) befindet sich im Internet in der Ablage des electronic Information Center des AWI (**ePIC**) unter der URL http://epic.awi.de. Durch Auswahl "Reports on Polar- and Marine Research" auf der rechten Seite des Fensters wird eine Liste der Publikationen in alphabetischer Reihenfolge (nach Autoren) innerhalb der absteigenden chronologischen Reihenfolge der Jahrgänge erzeugt.

To generate a list of all Reports past issues, use the following URL: http://epic.awi.de and select the right frame to browse "Reports on Polar and Marine Research". A chronological list in declining order, author names alphabetical, will be produced, and pdf-icons shown for open access download.

Verzeichnis der zuletzt erschienenen Hefte:

Heft-Nr. 621/2010 — "The Expedition of the Research Vessel 'Polarstern' to the Arctic in 2010 (ARK-XXV/3)", edited by Volkmar Damm

Heft-Nr. 622/2010 — "Environmentally induced responses of *Donax obesulus* and *Mesodesma donacium* (Bivalvia) inhabiting the Humboldt Current System", by Daniel Carstensen

Heft-Nr. 623/2010 — "Research in the Laptev Sea region - Proceedings of the joint Russian-German workshop, November 8-11, 2010, St. Petersburg, Russia", edited by Sebastian Wetterich, Paul Pier Overduin and Irina Fedorova

Heft-Nr. 624/2010 — "The Expedition of the Research Vessel 'Polarstern' to the Arctic in 2010 (ARK-XXV/2)", edited by Thomas Soltwedel

Heft-Nr. 625/2011 — "The Expedition of the Research Vessel 'Polarstern' to the Arctic in 2010 (ARK-XXV/1)", edited by Gereon Budéus

Heft-Nr. 626/2011 — "Towards data assimilation in ice-dynamic models: the (geo)physical basis", by Olaf Eisen

Heft-Nr. 627/2011 — "The Expedition of the Research Vessel 'Polarstern' to the Arctic in 2007 (ARK-XXII/1a-c)", edited by Michael Klages and Jörn Thiede

Heft-Nr. 628/2011 — "The Expedition of the Research Vessel 'Polarstern' to the Antarctic in 2010 (ANT-XXVII/1)", edited by Karl Bumke

Heft-Nr. 629/2011 — "Russian-German Cooperation SYSTEM LAPTEV SEA: The expedition Eastern Laptev Sea - Buor Khaya Peninsula 2010" edited by Sebastian Wetterich, Pier Paul Overduin and Mikhail Grigoriev

Heft-Nr. 630/2011 — "Comparative aerosol studies based on multi-wavelength Raman LIDAR at Ny-Ålesund, Spitsbergen", by Anne Hoffmann

Heft-Nr. 631/2011 — "The Expedition of the Research Vessel 'Polarstern' to the Antarctic in 2010 (ANT-XXVI/4), edited by Arne Körtzinger

Heft-Nr. 632/2011 — "The Expedition of the Research Vessel 'Polarstern' to the polar South Pacific in 2009/2010 (ANT-XXVI/2 - BIPOMAC), edited by Rainer Gersonde

Heft-Nr. 633/2011 — "Investigation of Katabatic winds and Polynyas during Summer – IKAPOS Field Phase Report", by Günther Heinemann, Thomas Ernsdorf and Clemens Drüe"